Geothermics and hydrogeology of the Kenya Rift Valley between Lake Baringo and Lake Turkana

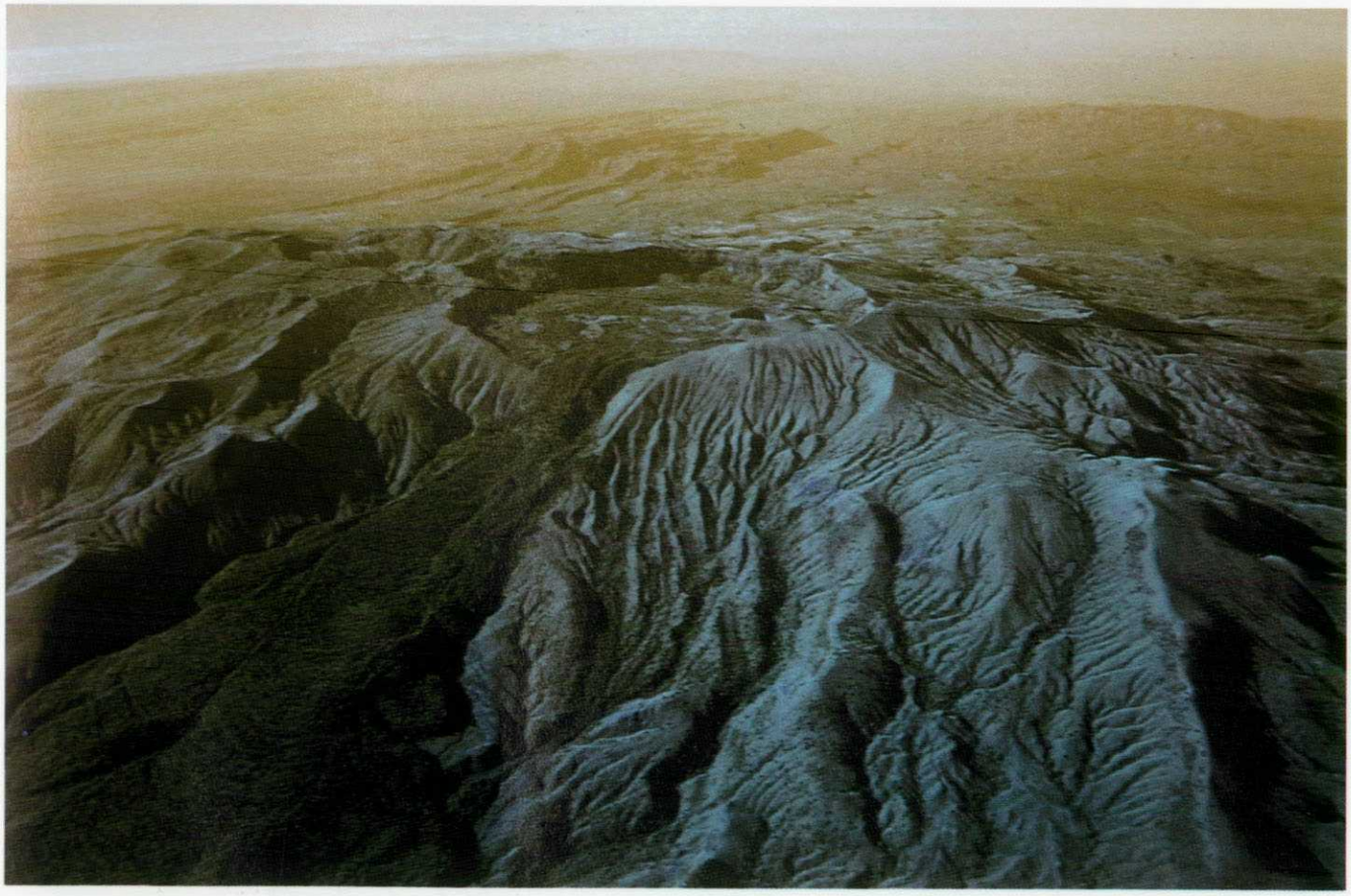

Research Report SD/92/1

Hydrogeology Series

British Geological Survey

BGS Research Report SD/92/1 Geothermics and hydrogeology of the Kenya Rift Valley between Lake Baringo and Lake Turkana

RESEARCH REPORT SD/92/1

Geothermics and hydrogeology of the Kenya Rift Valley between Lake Baringo and Lake Turkana

D J Allen and W G Darling

BRITISH GEOLOGICAL SURVEY

RESEARCH REPORT SD/92/1

Hydrogeology Series

Geothermics and hydrogeology of the Kenya Rift Valley between Lake Baringo and Lake Turkana

D J Allen and W G Darling

This report was prepared for the Overseas Development Administration

Cover illustration

Authors

BGS Keyworth

D J Allen
W G Darling

Geographical index

Kenya

Subject index

Geothermal exploration, hydrogeology

Bibliographic reference

Allen, D J, and Darling, W G. 1992. Geothermics and hydrogeology of the Kenya Rift Valley between Lake Baringo and Lake Turkana. *British Geological Survey Research Report* SD/92/1.

ISBN 0 85272 216 8

Keyworth, Nottingham British Geological Survey 1992

BRITISH GEOLOGICAL SURVEY

The full range of Survey publications is available through the Sales Desks at Keyworth and at Murchison House, Edinburgh, and in the BGS London Information Office in the Natural History Museum Earth Galleries. The adjacent bookshop stocks the more popular books for sale over the counter. Most BGS books and reports are listed in HMSO's Sectional List 45, and can be bought from HMSO and through HMSO agents and retailers. Maps are listed in the BGS Map Catalogue, and can be bought from Ordnance Survey agents as well as from BGS.

The British Geological Survey carries out the geological survey of Great Britain and Northern Ireland (the latter as an agency service for the government of Northern Ireland), and of the surrounding continental shelf, as well as its basic research projects. It also undertakes programmes of British technical aid in geology in developing countries as arranged by the Overseas Development Administration.

The British Geological Survey is a component body of the Natural Environment Research Council.

Keyworth, Nottingham NG12 5GG
☎ 0602-363100 Telex 378173 BGSKEY G
Fax 0602-363200

Murchison House, West Mains Road, Edinburgh EH9 3LA
☎ 031-667 1000 Telex 727343 SEISED G
Fax 031-668 2683

London Information Office at the Natural History Museum Earth Galleries, Exhibition Road, South Kensington, London SW7 2DE
☎ 071-589 4090 Fax 071-584 8270
☎ 071-938 9056/57

19 Grange Terrace, Edinburgh EH9 2LF
☎ 031-667 1000 Telex 727343 SEISED G

St Just, 30 Pennsylvania Road, Exeter EX4 6BX
☎ 0392-78312 Fax 0392-437505

Bryn Eithyn Hall, Llanfarian, Aberystwyth, Dyfed SY23 4BY
☎ 0970-611038 Fax 0970-624822

Windsor Court, Windsor Terrace, Newcastle upon Tyne NE2 4HB
☎ 091-281 7088 Fax 091-281 9016

Geological Survey of Northern Ireland, 20 College Gardens, Belfast BT9 6BS
☎ 0232-666595 Fax 0232-662385

Maclean Building, Crowmarsh Gifford, Wallingford, Oxfordshire OX10 8BB
☎ 0491-38800 Telex 849365 HYDROL G
Fax (0491) 25338

Parent Body

Natural Environment Research Council

Polaris House, North Star Avenue, Swindon, Wiltshire SN2 1EU
☎ 0793-411500 Telex 444293 ENVRE G
Fax 0793-411501

FOREWORD

This report summarises the results of hydrogeological studies carried out by D J Allen and W G Darling of the British Geological Survey as part of Phase II of the British Geothermal Energy Exploration Project. This is a Technical Cooperation project carried out jointly by BGS - under the auspices of the Overseas Development Administration (ODA) of the British Government - and the Ministry of Energy (MERD) of the Government of Kenya.

Phase I of the project was concerned with the southern Kenya Rift, concentrating on the Naivasha region. The object of Phase II was to undertake preliminary geothermal reconnaissance studies of a northern part of the Rift, between Lake Baringo and Emuruangogolak volcano, with particular emphasis on several volcanic centres.

During the project, which was undertaken between 1988 and 1990, field work and hydrogeological data record collection were carried out by D J Allen, W G Darling, P Dunkley and M Smith of BGS, and H Ndambi of MERD.

The work described in this report was carried out on behalf of ODA. The results may be used to aid formulation of Government policy, but do not in themselves represent Government policy. They are presented in a format agreed between ODA and BGS. The views and judgements expressed are those of the British Geological Survey, and do not necessarily represent those of ODA.

SUMMARY

This report presents the results of physical hydrogeological and hydrogeochemical studies in the Kenya Rift Valley as part of Phase II of the British Geothermal Energy Exploration Project.

The objective of these studies was to provide a greater understanding of the location, nature and movement of the thermal waters in the Rift, and of the cooler waters recharging the thermal systems. This information is fundamental to the assessment of the relative merits of different thermal areas for future exploration, and ultimately for exploitation. In the study the physical hydrology and hydrogeology of the project area were investigated to provide basic information concerning regional groundwater occurrence and flow patterns. The chemistries of both thermal and ambient fluids were studied in order to understand the nature and origin of the thermal waters and to further explain groundwater mixing patterns.

The hydrological component of the project broadly covered the region of the Kenya Rift Valley between Lake Baringo in the south and Lake Turkana in the north (Figure 2.1). Of specific geothermal interest are several Quaternary volcanoes in the centre of the Rift; in particular Korosi, Paka, Silali and Emuruangogolak. Very little physical hydrogeological data exist for this arid and sparsely populated study area. This meant that considerably more emphasis had to be placed on surface water and meteorological data than was the case with the Phase I study.

Rainfall data were obtained for a total of 38 stations in the Rift and on its bounding interfluves. Annual rainfall varies considerably in this region, from 200 mm/year in the northern Rift floor, to over 1400 mm/year on the western Rift margins. Evaporation data, collected from 11 stations, indicate potential values ranging from nearly 2000 mm/year on the Rift flanks to 4000 mm/year in the northern central Rift. A recharge model, using daily rainfall and evaporation data from four stations over several years, suggested that despite the large annual excess of potential evaporation over rainfall some recharge occurs, even in the arid Rift floor. Furthermore, the amount of recharge occurring in the vicinity of the central Rift volcanoes is likely to be sufficient to sustain geothermal production.

Lake Baringo is a freshwater body with no surface outlet in an area of very high potential evaporation, suggesting subsurface flow from the lake. Various estimates of subsurface outflow have been made, indicating that values are likely to be of the order of tens of millions of cubic metres per year. Regional groundwater levels show that subsurface flows from the lake are directed northwards, further increasing the recharge potential of geothermal systems in the Rift.

Hydrogeological information in the study area is poor, with only 70 boreholes between Lakes Baringo and Turkana, including the Rift sides. Information from these boreholes has been used to construct a potentiometric map of the region, and to provide some insight into aquifer properties.

Rest water levels in boreholes range up to nearly 150 m below ground level. In the Rift Valley floor of the project area between Korosi and Silali volcanoes water depths vary from around 50 m in the south to about 100 m in the north. This suggests relatively deep rest water levels under the volcanoes, which in turn is likely to affect the nature of any associated thermal systems.

Groundwater flows in the Rift are from areas of recharge on the Rift flanks towards discharge zones on the Rift floor. In addition, axial flows occur from Lake Baringo - in the south of the study area - to the north or north-east, towards a regional depression at Lake Logipi (south of Lake Turkana).

These northerly flows occur mainly to the west of the volcanic centres between Korosi and Emuruangogolak. Groundwater under these volcanoes is therefore likely to be mixture of local infiltration (there may be local recharge mounds under the volcanoes), water from the Rift flanks (mainly the eastern margin) and water from axial flows. The effects of the substantial degree of faulting in the Rift are likely to be twofold; lateral flows will be inhibited and driven deeper, and Rift floor flows will tend to be aligned axially.

The limited borehole data suggest that aquifer types in the study area are similar to those found in the Phase I Project, with fractured volcanics, weathered contacts between different units and sediments predominant. Borehole productivity evidence suggests that the hydraulic properties of aquifers in the project area are in general poor. However the data are sparse, and no data are available for depths greater than 200 m. No reliable predictions can therefore be made for the likely aquifer properties of any thermal systems associated with the volcanoes. However the available evidence suggests that flow in the thermal systems will be due to fracture, rather than intergranular, permeability.

Thermal springs are widespread between Lake Bogoria (south of Lake Baringo) and Lake Turkana. Along the Rift margins springs occur with temperatures up to 48°C and with generally low flows; they do not appear to be associated with high temperature geothermal activity. On the Rift floor groups of springs are found with flows up to 1 cubic metre/sec (at Kapedo), and with temperatures of up to 82°C (at Lorusio). Preliminary gradient estimates from boreholes suggest that thermal waters are widespread, and that other heat sources may exist than those obviously associated with the central Rift volcanoes.

Samples of surface waters, groundwaters and fumarole gases and steam condensates were collected from representative sites within the project area for chemical analysis. This sampling was intended to combine detailed information on the volcanic centres with a more general regional appraisal of hydrogeological and geothermal conditions from a geochemical standpoint.

Lake Baringo is a freshwater lake which fluctuates in size and chemical composition in response to seasonal changes in river and stream input. The fact that Baringo remains fresh is qualitative evidence that the lake is not in a terminal basin and that there must be a sizeable underflow to the north.

Samples from ambient and near-ambient springs and wells indicate that they are mainly fed by meteoric water from the rift flanks or the volcanic centres. Locally they may have high total dissolved solids (TDS) values from dissolution of evaporites, and isotopic compositions indicative of evaporation or mixing with Baringo lakewater.

Thermal springs all have elevated TDS values and an apparent lakewater contribution of between 0% (Lorusio) and 30% (Kapedo). None (with the exception of Ol Kokwe) shows evidence of intimate association with any high-temperature geothermal system, and they probably result from deep circulation or zones of moderately high heat flow situated away from the centres. Lorusio is the highest temperature spring complex (~80°C) and also has the most developed 'magmatic' characteristics.

The chemistry of condensed steam from the four volcanic centres suggests a ranking of fumarole strength in the order Paka > Emuruangogolak > Silali > Korosi, which is largely in accord with the field evidence. Stable isotope ratios in steam indicate that varying amounts of lakewater are being drawn into the hydrothermal systems, though this effect is masked at Korosi by subsurface steam composition, thus confirming the earlier view that fumarolic activity on that centre is weak. Fumarole gas chemistry and isotope ratios indicate that H_2 and ^3He, the strongest magmatic tracers, reach highest percentages on Paka and Silali.

The application of solute geothermometers to the thermal springs of the project area was hampered somewhat by dissolution of evaporites. Nevertheless, only one site (Ol Kokwe) gave unequivocal evidence of temperatures in excess of 150°C, while the other sites gave temperatures around 100°C, which was consistent with chemical evidence of lack of high-temperature water-rock interaction.

Gas geothermometry did not provide particularly consistent results when applied to the fumaroles of the area, but supported in a relative way the ranking of Paka > Silali > Emuruangogolak > Korosi. The new methane/ethane geothermometer developed specifically for the Rift gave similar temperatures (~300°C) for Paka, Silali and Emuruangogolak, but considerably lower temperatures (~200°C) for Korosi.

Finally it can be pointed out that while geochemical indications of high-temperature reservoirs in the project area may be few, there are analagous areas in southern Kenya and Ethiopia (Olkaria, Eburru, Langano) where such reservoirs have been proved. On the other hand there is little evidence that water moves rapidly through these reservoirs, with the implication that permeabilities are likely to be only low.

ACKNOWLEDGEMENTS

The authors wish to express their thanks for the assistance provided by the following: Peter Dunkley and Martin Smith of BGS, MERD staff - in particular Mr J Kinyariro (Project Leader) and Mr H Ndambi, and BHC staff in Nairobi. We are also grateful to the Ministry of Water Development for permission to use hydrological data. Our colleagues at BGS Wallingford are thanked for their assistance with chemical and isotopic analyses, except for helium which was kindly analysed by Erika Griesshaber at the University of Cambridge.

We thank Dr R O Fournier for his comments on the first draft of this report, which is published with the permission of the Director, BGS (NERC).

Contents

List of Figures

7.8 Plot of δ^2H vs $\delta^{18}O$ for selected fumarole steam condensates (values in permil SMOW).

7.9 Plot of $\delta^{13}C_{CO2}$ vs $\delta^{13}C_{CH4}$ for fumarole gases (values in permil PDB).

7.10 Plot of log C_1/C_{2+} alkanes vs $\delta^{13}C_{CH4}$ (values in permil PDB).

7.11 Plot of log C_1/C_{2+} alkanes vs $^3He/^4He$ (values in R_A). Figure includes data from Southern Rift sites.

List of Tables

1. INTRODUCTION

The aim of this study was to investigate the hydrogeology (including physical and chemical hydrology) of a section of the Kenya Rift Valley with particular reference to its geothermal potential. The study concentrated on an area between Lake Baringo in the south and Emuruangogolak Volcano in the north (Figure 2.1), with emphasis on several Quaternary central volcanoes; in particular Korosi, Paka and Silali. In order to place these volcanoes in a regional hydrogeological context, chemical sampling and physical data acquisition was undertaken over a region from Lake Baringo to Lake Turkana, and covering the Rift sides.

As with Phase I of the Project (which investigated a region of the southern Kenya Rift between Lake Magadi and Lake Naivasha) the ultimate objective of this type of study is to obtain a conceptual model of the major hot and cold systems of groundwater flow in the region of interest. Naturally the main task is to investigate the nature of the hot thermal systems which could potentially form producing geothermal fields; however the cold regional systems are also important because they are potential sources of recharge to an exploited field.

The lack of any deep borehole information for the geothermal systems investigated meant that geochemical studies were even more important than they were in Phase I. The main purpose of the geochemical component of the project was to provide information on the nature of the thermal fluids, likely temperatures at depth, mixing processes between different waters and possible areas of upflow. To this end a wide-ranging chemical sampling programme was undertaken - much of it by helicopter-borne survey parties - and samples from a wide range of sources involving lakes, rivers, springs, boreholes and fumaroles were obtained over a large region of the Rift.

The study of the cold water systems normally relies on standard hydrogeological techniques, involving the use of borehole data to provide information concerning aquifer properties and groundwater flows. In the present study however the paucity of borehole data meant that greater reliance had to be placed on indirect methods of assessing groundwater conditions and use was made of available meteorological information to enable some insight to be gained into groundwater recharge. As with Phase I of the project, chemical and isotopic data were important in helping to identify possible recharge areas, mixing patterns and residence times of groundwaters.

It must be stressed that the interpretation of the hydrogeological information contained in this report is not considered to be definitive. In an area of low rainfall, few boreholes, a low water table and no primary geothermal waters present at the surface, interpretations must necessarily be somewhat speculative. Our aim has been to provide a hydrogeological framework which, when combined with the geological studies undertaken by the Project Team will provide guidance for future detailed surveys.

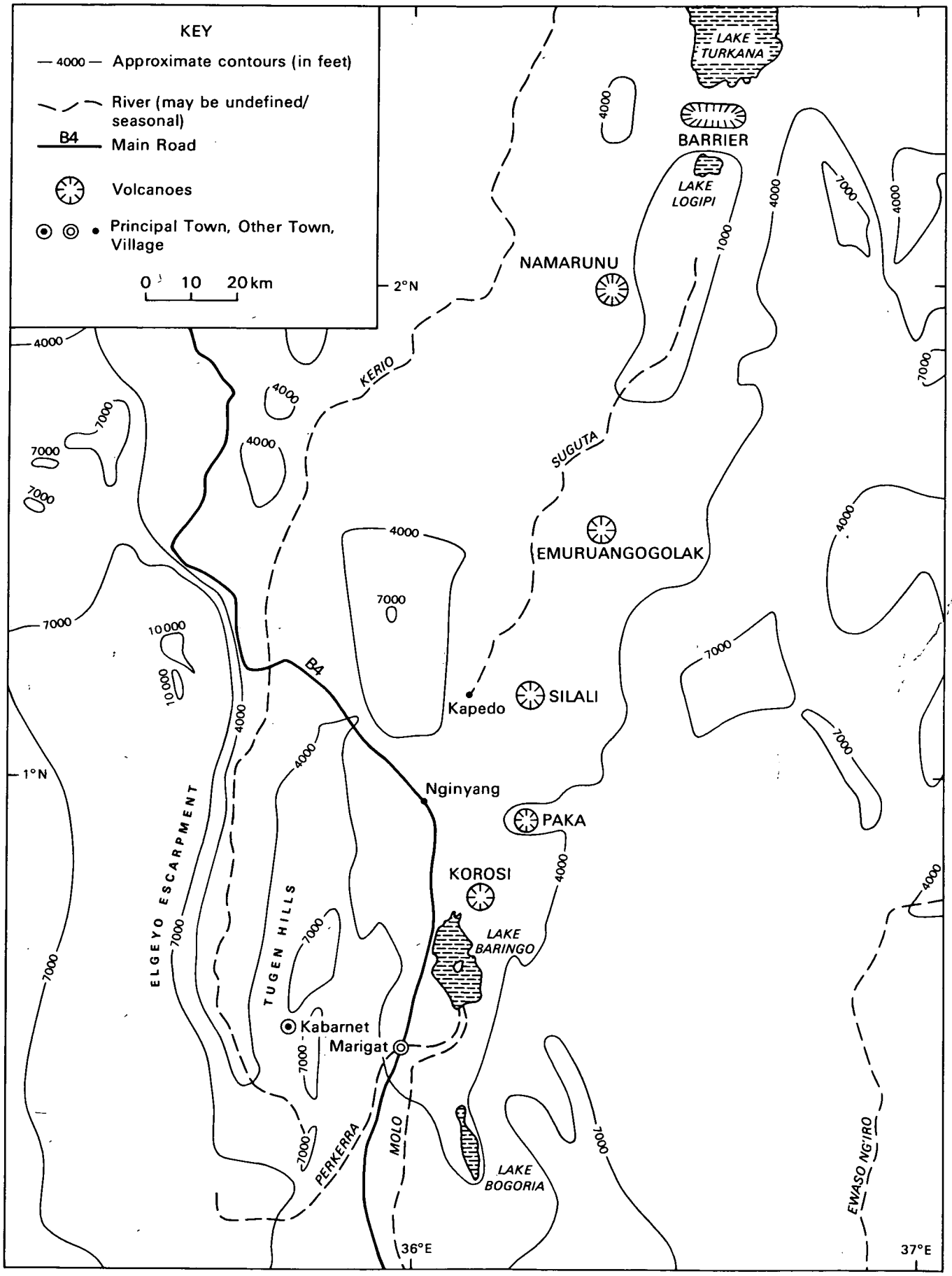

Figure 2.1 Location map

2. PHYSIOGRAPHY AND GEOLOGY

2.1 Physiography

The hydrological component of the Geothermal Project is concerned with the area between Lake Baringo and Lake Turkana which lie within the catchment boundaries defined by the sides of the Rift. The region of investigation therefore lies roughly between latitudes 0°30'N and 3°N and between longitudes 35°30' and 36°30'.

The topography of the area is dominated by the East African Rift Valley, which in the west is bounded by the Elgeyo Escarpment (Figure 2.1) rising to over 3000 m. The Tugen hills rising to almost 2500 m lie between the Elgeyo Escarpment and the floor of the rift and effectively form the western boundary of the southern part of the project area. Further north the Tiati hills and Loriu Plateau separate the Rift Valley floor from the western escarpment. In the east the Rift Valley is bounded by the Laikipia Escarpment at around 2250 m which give way northeastwards to the Loroghi Plateau (200 m) and the Poro Forest (2500 m).

The floor of the rift falls to the north, from an altitude of 970 m at Lake Baringo to 250 m at Lake Logipi, south of Lake Turkana. This slope is interrupted at intervals in the project area by the volcanic piles of Korosi, Paka, Silali and Emuruangogolak. The rift floor also has a westward tilt over much of its length.

The drainage system in the project area consists of numerous seasonal streams which in the south drain to Lake Baringo and in the north drain to marshes in the Suguta Valley via the Suguta River. The Perkerra River, the upper part of the Molo River and the upper Suguta River are perennial.

2.2 Geology

The following brief description of the geology of the study area is paraphrased from Dunkley and Smith (1990).

The Kenya Rift Valley between Lake Baringo and Emuruangogolak volcano can be divided into three physiographic zones which broadly coincide with the main tectonic features of the Rift. These are the inner trough, the eastern margin and the western margin.

The inner trough is a NNE-trending zone of Quaternary volcanism and sedimentation which is bounded to the east and west by escarpments that are controlled by faults and monoclinal warps. In the south of the area the trough is an asymmetrical graben structure - deepest in the west - bounded to the west by major fault-founded escarpments and to the east by a series of smaller faulted escarpments.

Several Quaternary central volcanoes (Ol Kokwe Island, Korosi, Paka, Silali and Emuruangogolak) are located along the axis of the central trough (Figure 2.1). They take the form of large low-angle multi-vent shields, composed predominantly of trachyte and basaltic lavas and pyroclastic deposits, upon which parasitic volcanic cones are superimposed. These volcanoes are the principal focus of geothermal research in the study area.

Between the volcanoes on the floor of the trough are extensive plains which are mainly covered with alluvium laid down by ephemeral rivers and sheet wash. Along the western side of Korosi and Silali, and to the north and south-east of Paka, large tracts of low ground are also underlain by horizontally bedded pumiceous volcaniclastic deposits, which in some cases have been reworked by fluvial and lacustrine processes. Lacustrine sediments related to the former Lake Suguta occur in the Suguta Trough to the north and west of Emuruangogolak. These consist of horizontally bedded diatomites, conglomerates and sandstones.

The eastern margin of the rift is mainly composed of stratified Miocene and Pliocene volcanic deposits. Several high plateaux flank the margins of the rift and are separated from the inner trough by a complex shoulder made up of a series of westerly facing escarpments controlled by a combination of steeply dipping faults (to the south of Silali) and west-facing monoclinal warps (to the north of Silali).

The western margin of the rift in the south of the study area is controlled by the Elgeyo and Saimo fault systems, both of which give rise to impressive east-facing escarpments (the Elgeyo Escarpment and the east side of the Tugen Hills respectively) which expose metamorphic rocks overlain by Neogene volcanics. The displacement of the Elgeyo fault decreases northwards and eventually has no surface expression. From the latitude of Silali northwards the western shoulder of the inner trough is marked by a complex zone of low angle Pliocene volcanoes on a gently easterly dipping plateau of Miocene volcanic rocks. To the north of the study area, in the Namarunu-Barrier region, the Loriu Plateau, underlain by Pliocene and Pleistocene lavas, divides the Suguta and Kerio rivers. The shoulder between the plateau and the inner trough is marked by east-facing fault scarps.

3. RAINFALL AND EVAPORATION

3.1 Rainfall

Rainfall data have been obtained for an area of the Rift Valley between Lake Baringo in the South and Lake Turkana in the north and on the bounding interfluves. Data have been obtained from the Meteorological Office and from the Ministry of Water Development (MWD). The MWD Water Resource Assessment and Planning (WRAP) reports for the Baringo district (WRAP, 1987a), Laikipia area east of Baringo (WRAP, 1987b), and Samburu area south-east of Lake Turkana (WRAP, 1991) have proven to be valuable sources of information. Data used range in quality from contoured values on annual rainfall maps in the WRAP reports to daily rainfall data obtained from MWD records for infiltration analysis (see Section 4).

The distribution of rainfall stations in the Project Area is shown in Figure 3.1. The figure indicates that data availability is much greater in the southern part of the Project Area than in the north, with few stations north of Silali. Daily data are collected at each rainfall station, although gaps in the records of the order of one month are not uncommon. The lengths of records are variable, ranging from around a year, to 68 years (Lodwar). Of the 45 stations examined, 23 have records exceeding 10 years in length, and 33 have records longer than 5 years.

The map of mean annual rainfall (Figure 3.1) has been produced using all the available data. Meteorological data indicate that annual rainfall over the Geothermal Project area varies from less than 200 mm in the arid northern rift floor to over 1400 mm over the Tugen Hills, to the west of Lake Baringo. It is also likely that pockets of high rainfall exist over high, forested ground (e.g. to the south-east and east of Barrier volcano). In the floor of the rift the rainfall ranges from less than 200 mm (Lake Turkana area) to around 650 mm (Lake Baringo area) with perhaps locally elevated values over the central rift volcanoes. The general dependence of rainfall on altitude is shown by Figure 3.2. The figure indicates that the relationship appears to be different for the eastern and western rift margins. The western escarpment - and the floor of the rift - shows a good linear relationship between rainfall and altitude, with annual rainfall increasing by around 60 mm for each 100 m of ascent. The eastern escarpment indicates more variable behaviour, but with a general increase of the order of 20 mm in annual rainfall for every 100 m of ascent. The reason for this difference between the two sides of the rift is unknown. Rainfall values vary considerably from year to year, and it has been suggested (WRAP, 1987a) that the highest variability occurs in the areas of lowest rainfall.

The WRAP work (WRAP, 1987a) concluded that rainfall in the Baringo catchment (i.e. as far north as Korosi) is unpredictable, with values for a given month varying substantially from year to year. Over a long period the study identified two peaks; in August (which in many places was the month of maximum rainfall) and in April. The lowest rainfall was found to occur between December and February, with January being the driest month.

Data collected during the present study show that this interpretation is valid further north, at least as far as Silali. However, to the north-east of Emuruangogolak and around Lake Turkana the August peak occurs later - in November - and September is the driest month.

In the south of the Project Area, in the Baringo catchment, around 70% of the annual rainfall occurs between March and August (WRAP, 1987a). In the northern part of the area the more limited precipitation is concentrated in the peak months with nearly one third of the annual total falling during each of the March/April and November maxima. Rainfall intensity is considered further in Section 4.

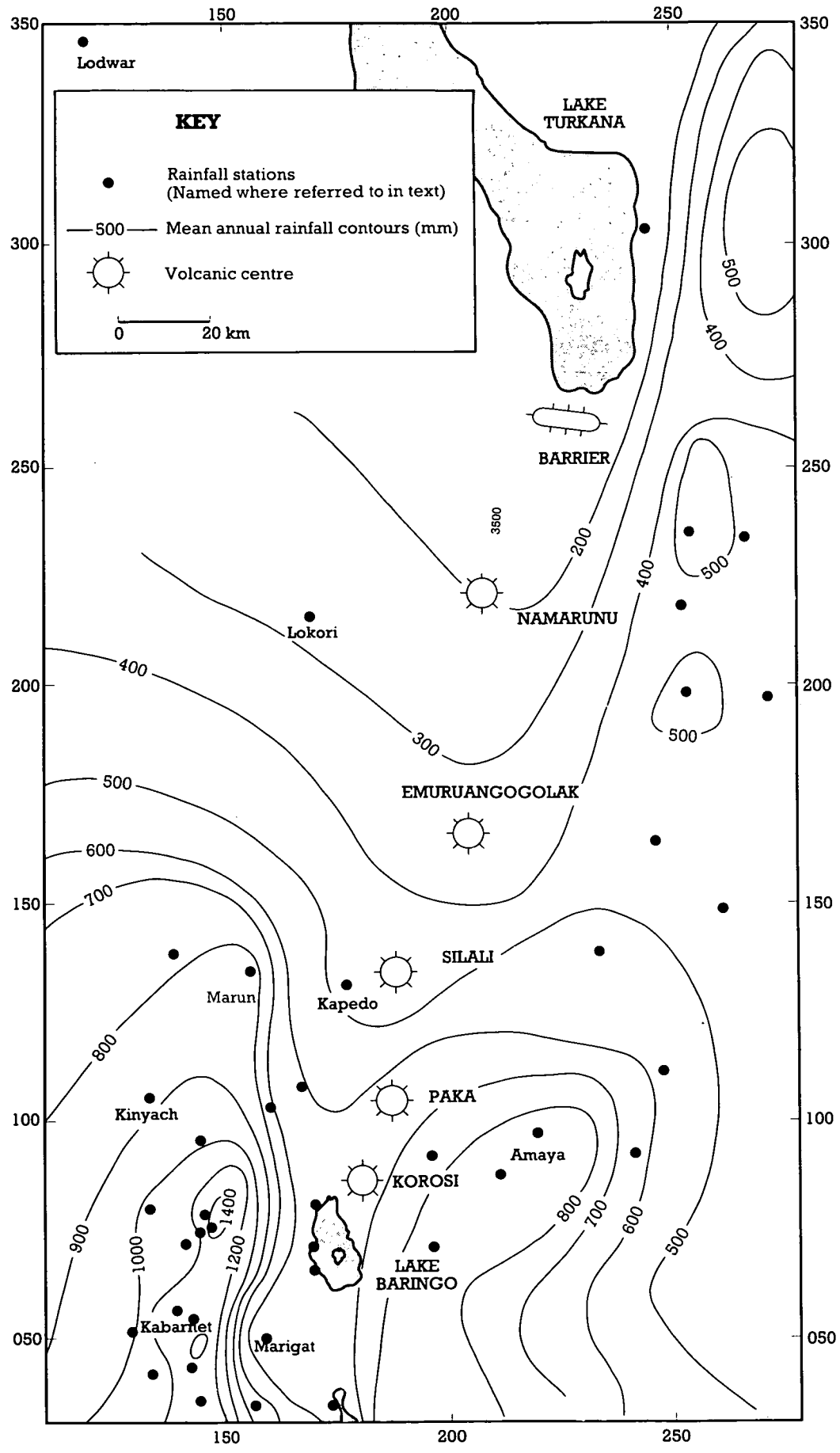

Figure 3.1 Mean annual rainfall in the Baringo–Turkana area

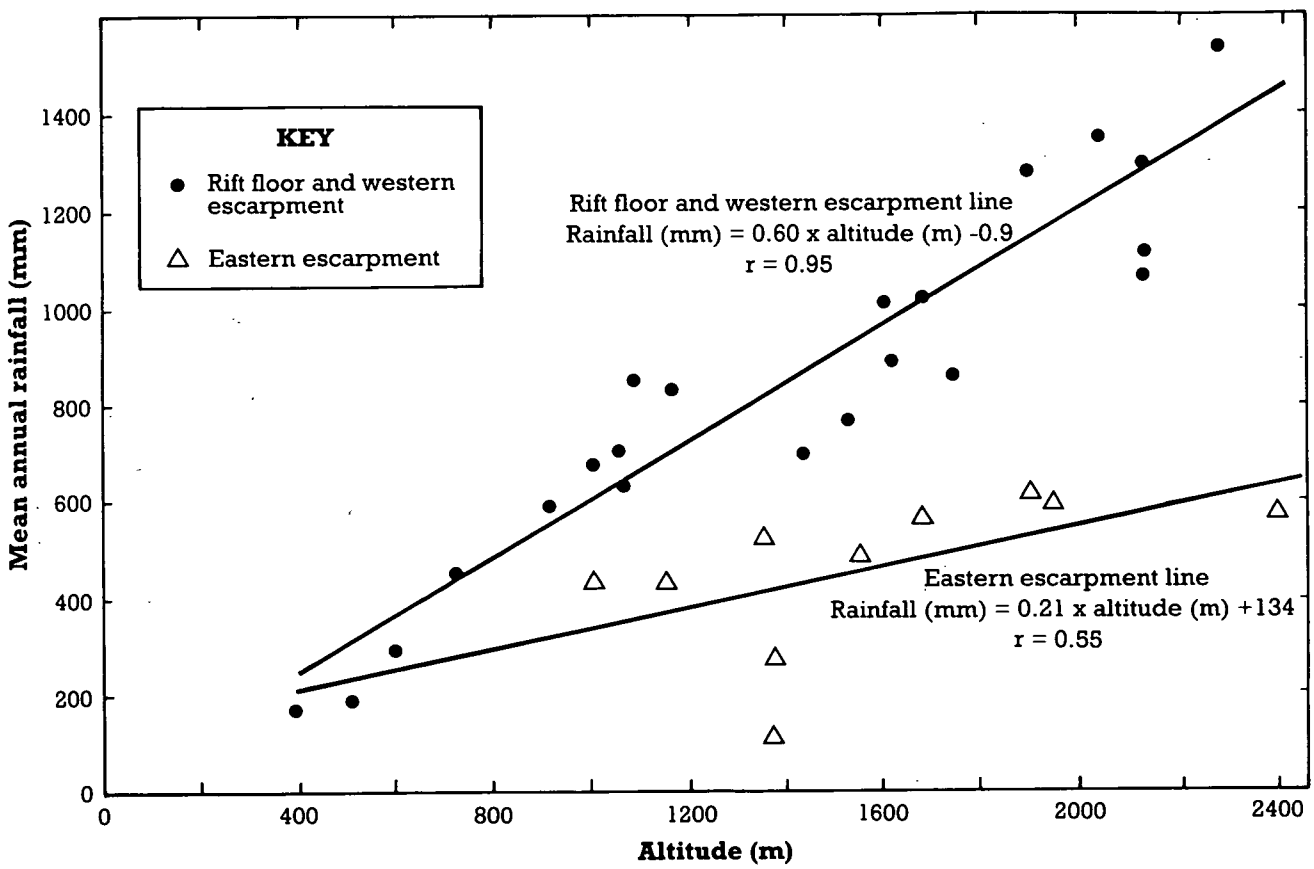

Figure 3.2 Plot of mean annual rainfall versus altitude in the Baringo - Turkana area.

3.2 Evaporation

Potential evaporation data (monthly means) from evaporation pans for 11 stations between Marigat and Lodwar were abstracted from records at the Meteorological Office and Ministry of Water Development. Evaporation station locations are shown on Figure 3.4 (in several cases, where two stations are located near to each other, one general site is shown). For four of these stations (Amaya, Kabarnet, Kapedo and Marigat) daily evaporation data were obtained over several years for comparison with daily rainfall values. In addition data were available for four evaporation stations near the Project Area (WRAP, 1987a).

Mean annual evaporation values vary from 1934 mm at Kabarnet to 3999 mm at Lokori. A major factor influencing evaporation rates is altitude as is shown in Figure 3.3 where a correlation coefficient of -0.95 indicates a very good fit to the data. There are two reasons why potential evaporation rates should be dependent on altitude. Firstly evaporation rates are temperature-dependent and mean annual ground temperatures vary inversely with altitude. A second factor influencing evaporation is the amount of precipitation, and this also tends to be altitude-dependent as discussed in Section 3.1.

Average monthly evaporation rates are found to vary most at high altitudes where seasonal cloud cover is significant and least in the arid low-lying areas of the northern rift floor. For example, at Kabarnet (altitude 1480 m) and Amaya (altitude 1620 m) the ratio of minimum to maximum monthly evaporation rates is approximately 0.5. At Lokori (600 m) and Lodwar (500 m) the ratios are 0.7 and 0.8 respectively, indicating much less seasonal variation in evaporation.

The month of highest evaporation is normally March for most of the evaporation stations, although in some cases (Kapedo, Kinyach, Marigat, Marun) the March peak is slightly exceeded by a January maximum. The months of minimum evaporation occur between May and August, and mainly in June and July. When monthly temperature, evaporation and rainfall data are examined for three stations it is seen that the most influential factor in determining evaporation rates is temperature. Thus the maximum rates of evaporation are found in the hottest months, whether these are months of minimum rainfall or not.

The limited number of evaporation stations in the Project Area means that insufficient data are available to draw a reliable map of potential evaporation. However the good agreement between evaporation rates and altitude means that a map of estimated potential evaporation based on topographic data may be drawn and such a map is shown in Figure 3.4. The figure indicates that potential evaporation rates in the Project Area are high - of the order of 3000 millimetres per year.

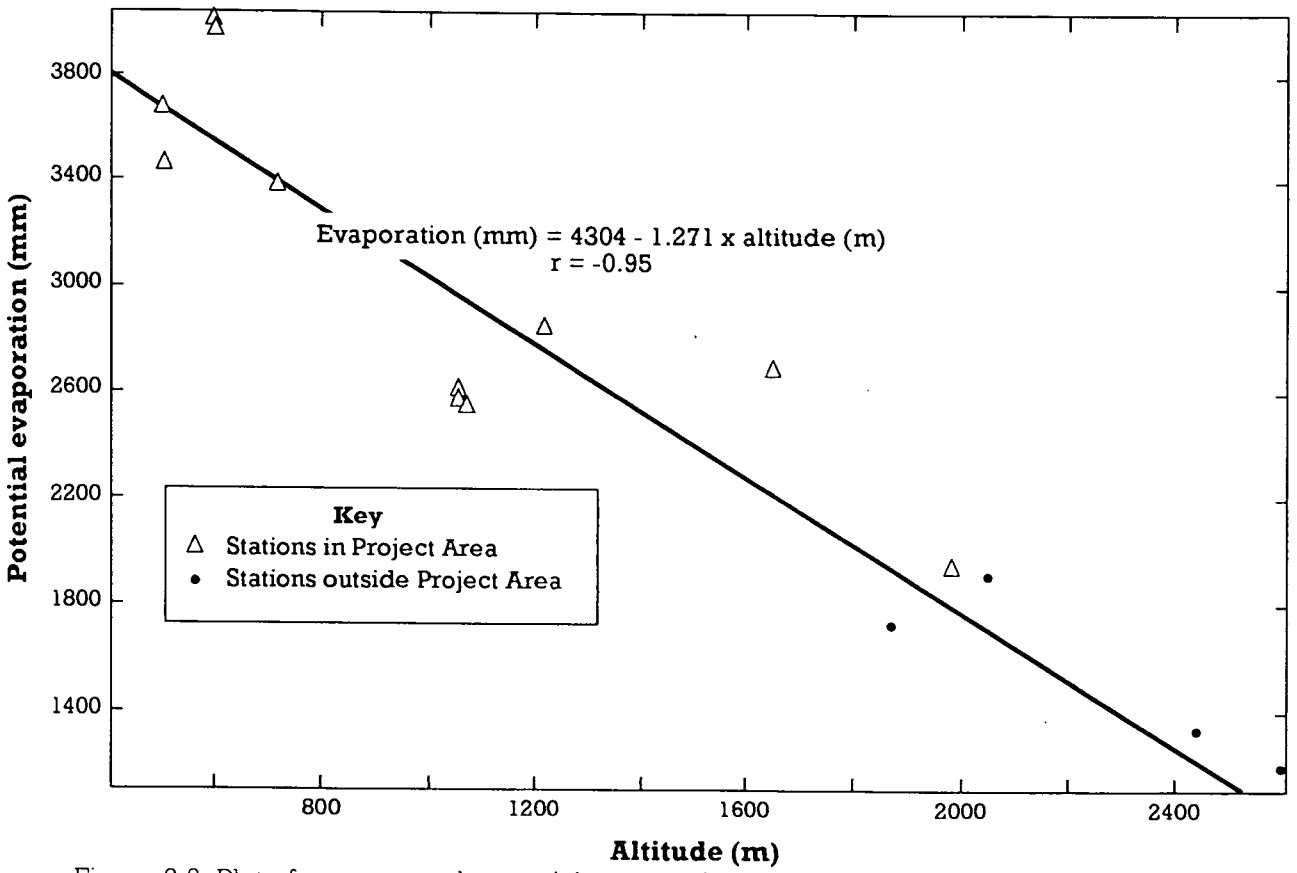

Figure 3.3 Plot of mean annual potential evaporation versus altitude in the Baringo - Turkana area

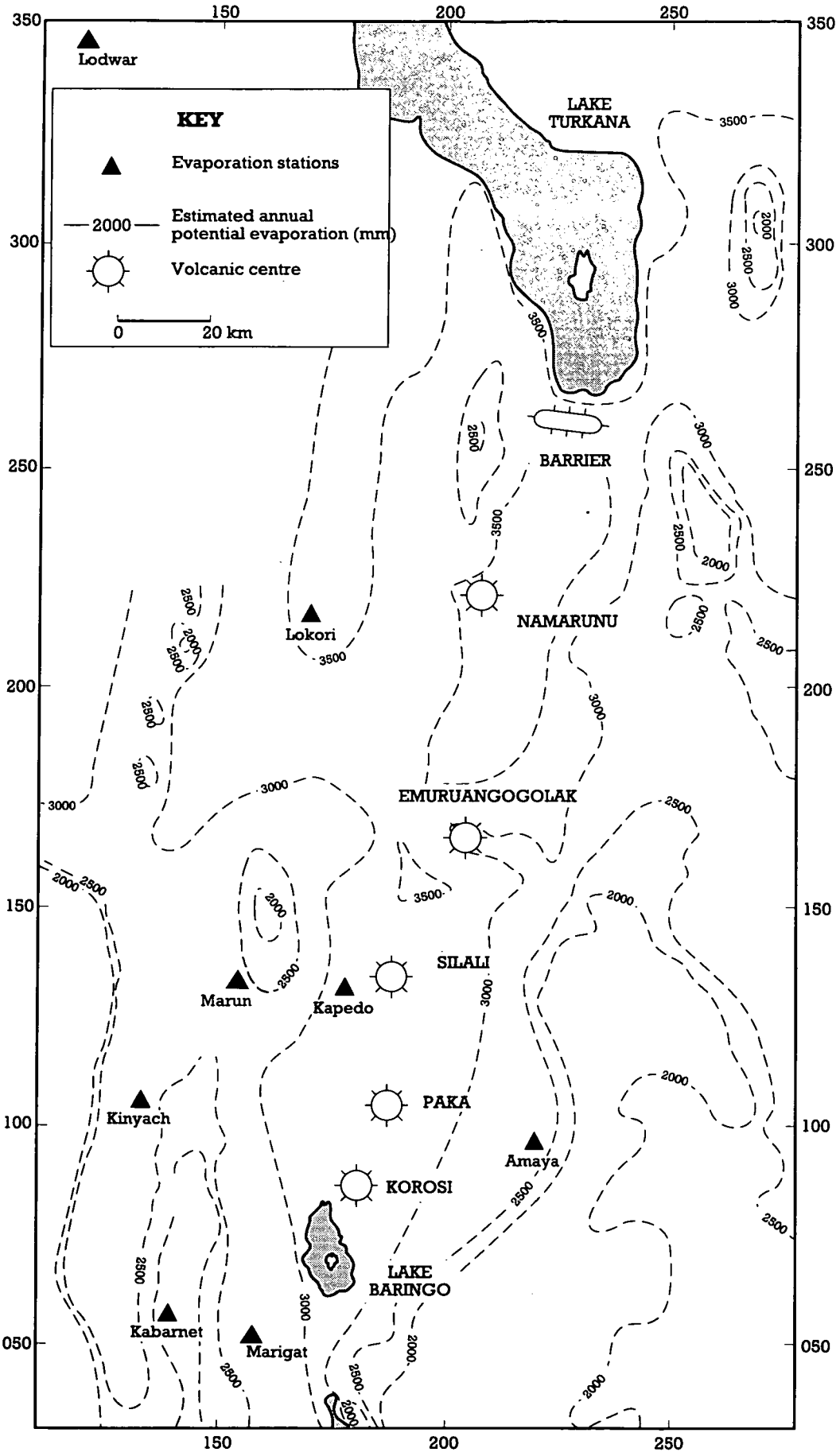

Figure 3.4 Map of estimated annual potential evaporation for the Baringo–Turkana area

4. RECHARGE

4.1 Introduction

The extent of groundwater availability for potential geothermal systems depends primarily on hydrogeological factors such as hydraulic conductivity and storage. However groundwater data are few in the Geothermal Project area and therefore more emphasis is placed on the use of surface water data to estimate natural recharge.

In broad terms, rainfall incident on a catchment which does not evaporate or run off infiltrates the soil, and, if the soil moisture deficit is satisfied, may act as recharge to groundwater aquifers. In a region such as the Rift Valley floor in the Project Area there is little evidence of substantial surface runoff, presumably because the thin volcanic soils are relatively permeable and because of the low incident rainfall, and the assumption is therefore made that rainfall which does not evaporate is potentially available as recharge.

If average annual rates of rainfall are compared with similar values of potential evaporation (Table 4.1) it is seen that in every case - even in the areas of high rainfall bounding the rift - potential evaporation exceeds rainfall. Even if average monthly figures are used (to allow for the concentration of rainfall into particular seasons) rainfall only exceeds evaporation at the Kabarnet site, between April and August with a total annual excess of 254 millimetres.

This type of analysis of potential recharge is however too crude for two reasons. Firstly rainfall over the rift is generally concentrated into short periods of intense precipitation during which precipitation greatly outweighs evaporation, but this difference is lost when considering monthly data, and especially long-term monthly means. Secondly, potential evaporation data only apply to freely evaporating surfaces; actual values in an arid area will be much lower. To address these problems a more sophisticated approach was required, described below.

4.2 The Recharge Model

The first of the above drawbacks may be overcome by using rainfall and evaporation data on a time scale more appropriate to the rainfall patterns. To this end daily rainfall and potential evaporation data were obtained over several years for four meteorological stations at different altitudes around the project area. Basic data concerning the stations are given in Appendix 2. In three cases - Marigat, Kabarnet and Amaya - data were obtained from files held by the Ministry of Water Development. Data for Kapedo were abstracted from files at the Kapedo meteorological station. After checking for errors all data were converted to SI units and stored in a computer database.

The problem of estimating the actual amount of water lost by evapotranspiration was considered by using a computer model developed by Adams (1977). The program is based on a model of soil moisture deficit (SMD) proposed by Penman (1949). Soil moisture deficits occur when evapo-transpiration exceeds precipitation and vegetation has to draw on reserves of moisture in the soil to satisfy transpiration requirements. The SMD must be satisfied before infiltration can commence. When potential evaporation exceeds precipitation over a given period the potential SMD increases by that amount and, up to a point (termed the Root Constant) the actual SMD increases by the same amount. Once the Root Constant value of SMD has been reached it becomes increasingly difficult for evapotranspiration to occur, and therefore subsequent increases in potential SMD (potential evaporation minus precipitation) lead to ever smaller increases in actual SMD. In practical terms this means that even for very arid areas there is an upper limit of SMD, taken to be 3.33 times the Root Constant by Adams (1977), and once this is satisfied infiltration can

Table 4.1 MEAN ANNUAL VALUES OF RAINFALL AND POTENTIAL EVAPORATION IN THE PROJECT AREA

Station	Annual Rainfall (mm)	Potential Evaporation (mm)
Amaya	889	2698
Kabarnet	1357	1934
Kapedo Mission	445	3373
Kinyach Dispensary	875	2534
Lodwar MWD	-	3657
Lodwar Met	182	3488
Lokori MWD	-	3999
Lokori Met	295	3945
Marigat Pekerra MWD	-	2607
Marigat Pekerra Met	637	2559
Marun Mission	820	2824

Table 4.2 LONG-TERM ANNUAL INFILTRATION VALUES PREDICTED BY THE RECHARGE MODEL FOR DIFFERENT ROOT CONSTANT (Rc) VALUES

Met. Station	Altitude (m)	Infiltration (mm) Rc = 50 mm	Rc = 75 mm	Rc = 100 mm	Rc = 150 mm
Kabarnet	1980	447	388	<u>358</u>	<u>321</u>
Amaya	1620	143	<u>101</u>	<u>64</u>	12
Marigat (MWD)	1060	<u>36</u>	<u>21</u>	9	0
Kapedo	720	<u>38</u>	<u>22</u>	13	0

Values underlined are those considered to be most realistic

commence. The relationship between actual SMD and potential SMD used in the program is that proposed by Penman.

The program requires as input data an initial value of SMD, a Root Constant and daily values of rainfall and potential evaporation. The program calculates the actual SMD at the end of each day, the actual amount of evaporation for that day, and the effective precipitation (infiltration) during the day.

Potential drawbacks with the use of the program were that neither initial values of SMD, nor values of Root Constant were available for the four data sets. With regard to initial SMD values it was found by running the program with different values that the model was very insensitive to this parameter. This was to be expected because errors in the initial value of SMD would quickly become negligible in a program using daily data over several years.

A more serious problem is the choice of Root Constant. Since the Root Constant defines the point beyond which increases in potential SMD lead to smaller increases in actual SMD the choice of value for Root Constant must directly affect the amount of rainfall required to reduce the SMD to zero, and thereby allow infiltration to occur. In other words, the higher the Root Constant the lower the calculated infiltration for a given amount of rainfall.

Precise values of Root Constant are unknown in the Rift Valley, but estimated values were obtained from a recent hydrogeological study of the Chyulu Hills in southeastern Kenya in which the Adams model was employed (Wright and Gunston, 1988). In this study light scrub vegetation growing on lavas were allotted a root constant of 50 mm, grassed lavas and pyroclastics were given a value of 100 mm and for pyroclastics under montane rain forest a value of 200 mm was used. On this basis a range of root constants between 50-150 mm were considered appropriate for the four sites examined during the present study, with the lower value considered to represent conditions at Marigat and Kapedo on the floor of the rift, 75 mm representing conditions at Amaya, and 150 mm for Kabarnet on the rift flanks.

4.3 Results of the Recharge Model

The input data for the four sites illustrated the necessity of considering daily rainfall data rather than longer-term averages because of the high intensity of precipitation even in very arid areas. For example at Kapedo, with an annual mean rainfall of only 445 mm, daily totals sometimes exceeded 40 mm and on one occasion (15 July 1988) reached 79 mm, or nearly 18% of the long-term mean on a single day.

Such rainfall patterns for the rift floor stations meant that the model predicted a rapid increase to maximum SMD levels during the long dry periods, followed by occasional reductions in deficit towards zero conditions during periods of heavy rain. Infiltration was therefore predicted only on days when very heavy rain occurred, usually during a sequence of wet days. The same pattern, although more subdued in nature, characterised the Kabarnet station.

Table 4.2 shows the long-term infiltration values obtained from the model for the four stations. Values for the whole range of Root Constants used are given, with the most appropriate values marked.

The table shows the expected result that the SMD model predicts higher values of infiltration for the highest-rainfall station at Kabarnet than would be suggested by taking potential values of evaporation. What is less predictable however is how the low-rainfall stations would behave; Table 4.2 suggests that, for realistic root constant values of 50-75 mm, the model predicts that infiltration does occur for both Kapedo and Marigat, with annual values of the order of 25 mm.

The values of infiltration for the rift valley floor are around 5% of the rainfall figures (rising to about 20% for Kabarnet, but the Kabarnet value is probably too high, because in this area of relatively high precipitation, some runoff is likely to occur). Some support for the 5% figure is provided by WRAP, who calculated from analysis of baseflow hydrographs that average infiltration in the Baringo catchment is of the order of 1.5-3% of precipitation (WRAP, 1987a). It is possible that the calculated infiltration for the rift valley floor is an under-estimate, because the model assumes that recharge cannot occur until the SMD is satisfied. However it is possible that when infiltration occurs in fractured aquifers (such as the fractured volcanics that underlie the rift) - particularly during heavy rainfall - bypass mechanisms may operate and some percolating waters may enter the aquifer directly via open fractures before the SMD is reduced to zero.

Another factor affecting infiltration within the rift valley floor is that the central volcanoes of Korosi, Paka, Silali and Emuruangogolak are likely to receive more rainfall than the surrounding areas because of their altitude. However the excess infiltration which might be expected as a result will be to some extent mitigated by the extra vegetation found on the volcanoes.

These and other considerations (such as errors in the data) mean that the recharge figures for the rift must be viewed with caution; but the value of 25 mm for the rift floor does suggest that an area of the order of 120 km^2 would be required to support a discharge of 3 x 10^6 m^3/year, which is the discharge rate from the Olkaria Geothermal Field in the Central Kenya Rift (Allen et al., 1989). This area is of the same order as the regions occupied by each of the central rift volcanoes and suggests that in the arid rift floor, local recharge mechanisms might be enough to sustain geothermal production, even in the absence of recharge from the rift sides and along its axis.

5. WATER BALANCE

5.1 Introduction

The Soil Moisture Deficit model used in the previous section to estimate recharge considers only the relationship between rainfall and evaporation. In this section the extent to which the analysis can be extended by considering catchment water balance is examined.

In general terms, the water balance equation for a catchment may be written as follows:

$$P = E + R_{out} + G_{out} + \Delta S_{total} \quad \ldots (1)$$

where P = Precipitation
E = Evaporation
R_{out} = Runoff (out of the catchment)
G_{out} = Subsurface flow (out of the catchment)
ΔS_{total} = Change in storage (surface water + groundwater)

The quantity of interest is G_{out} because this determines the theoretical long-term maximum value for groundwater abstraction for all purposes, including geothermal.

5.2 Lake Baringo

5.2.1 Water balance model

The water balance of Lake Baringo, within the Baringo catchment, is best considered separately from the rest of the catchment, because a major factor in its water balance equation - evaporation - can be accurately estimated, since it is equal to the potential value at all times.

The water balance of Lake Baringo was considered in a recent study (WRAP, 1987a), where the following equation was used:

$$P_{Lake} + R_{in(Lake)} = E_{Lake} + G_{out(Lake)} + \Delta S_{Lake} \quad \ldots (2)$$

where P_{Lake} = Precipitation over the lake
$R_{in(Lake)}$ = Runoff into the lake
E_{Lake} = Evaporation from the lake
$G_{out(Lake)}$ = Subsurface flow from the lake
ΔS_{Lake} = Change in lake storage

The WRAP study estimated annual values for precipitation P from those recorded at Marigat and adjusted for those expected over the lake using a rainfall map. Annual values of evaporation E were obtained partly by application of the Penman formula (as used by Woodhead [1968]) and partly from evaporation pan data. The annual change in lake storage ΔS was obtained from lake water level measurements.

Unfortunately, values of river discharge into the lake (R_{in}) are too poorly known to be used in equation (2). Therefore WRAP used a salt balance approach to relate R_{in} to the subsurface outflow from the lake, G_{out}. Thus:

$$R_{in(Lake)} = G_{out(Lake)} \times TDS_{Lake}/TDS_{River} \quad \ldots (3)$$

where TDS_{River} and TDS_{Lake} refer to the total dissolved solid content of river and lake water respectively.

By combining equations (2) and (3) to eliminate R_{in}, and by using the resulting formula to calculate G_{out} on an annual basis, values for G_{out} ranging between 199 and 248 mm were derived. For a mean lake area of 144 km^2 and an average value of G_{out} of 229 mm/year this corresponds to a mean annual subsurface outflow of 33 x 10^6 m^3/year.

5.2.2 Discussion

Any water balance approach to the problem of assessing groundwater recharge is limited by its weakest component. In this case, while factors such as precipitation, evaporation and change in lake storage can be adequately assessed, the difficulty lies in adequately estimating the river and lake chemistry in the relationship between groundwater flow and river runoff (equation 3).

The WRAP study assumed a constant lake chemistry, with a TDS of 550 mg/l. The study noted that the average TDS of influent river water was difficult to determine (mainly because it varied with discharge) but obtained a value of 70 mg/l from available data. The evaporative concentration factor (TDS_{Lake}/TDS_{River}) derived from these data is therefore 7.9.

Subsequent work by BGS as part of the present project has indicated by a chloride balance (Section 7.2) that the evaporative concentration factor may be as low as 2.5, which would suggest a subsurface outflow of 104 x 10^6 m^3 per year from the lake. Also, an estimate of subsurface flow using an isotope balance suggests that flows in excess of 150 x 10^6 m^3/year occur.

In conclusion, while it is difficult to calculate the amount of underflow from Lake Baringo it is apparent that groundwater recharge from the lake with a magnitude of at least several tens of millions of cubic metres per year is occurring. The limited available borehole data show that several such flows will be directed axially northwards along the rift floor (Section 6).

5.3 Baringo Catchment - The Problem of Groundwater Flow Estimation

The water balance equation for the Baringo catchment (not including the lake, which may be considered as a separate, but connected, system) may be written as:

$$P_{Basin} = E_{Basin} + R_{out(Basin)} + G_{out(Basin)} + \Delta S_{total(Basin)} \quad \ldots (4)$$

where the symbols have the same meaning as in equation (1). $R_{out(Basin)}$ is equal to $R_{in(Lake)}$ in equation (2) because no rivers flow out of the catchment. The groundwater inflow from Lake Baringo to the basin is transferred out of the catchment and therefore does not enter into the calculation; also the ΔS (storage) term may be eliminated by considering long periods.

The problem with attempting to use this equation to estimate the groundwater flow term is that it is so small compared with the other terms. The analysis of Section 4 suggested that most rainfall evaporates, at least in the Rift Valley floor. The WRAP study considered that groundwater flow from the whole basin was at least one order of magnitude less than rainfall, evaporation or surface runoff, and in using equation (4) regarded the groundwater flow term as unimportant. WRAP in fact reduced equation (4) to:

$$P_{Basin} = E_{Basin} + R_{in(Lake)} \quad \ldots (5)$$

and found that 95% of the rainfall evaporates, which agreed well with their baseflow hydrograph analysis, and agrees with the results of Section 4.

It is apparent therefore that using a catchment water balance to determine groundwater flows in the Baringo catchment is not possible at present, because the volumes of flow lie well within the likely errors in precipitation, evaporation and runoff data. The position is even more difficult for the catchments further north because data are fewer and uncertainties proportionally greater.

6. HYDROGEOLOGY

6.1 Introduction

For the purposes of this study a section of the Rift Valley was considered between Lake Bogoria to the south and Lake Turkana to the north and extending to the bounding interfluves. Within this region data for a total of 70 boreholes have been obtained, mainly from Ministry of Water Development (MWD) records, with additional information from the WRAP Baringo and Laikipia studies (WRAP, 1987a, 1987b) and from personal communication with a Missionary actively drilling water wells in the Project Area, Mr A Davies.

Spring details were obtained mainly from visits by BGS staff to spring localities. In addition some data were taken from the WRAP study of the Baringo area (WRAP, 1987a).

The borehole data set is much smaller than that obtained for Phase I of the Geothermal Project where nearly 600 boreholes were available. In addition, few of the boreholes are located in the rift floor (Figure 6.1) which is the area of greatest geothermal interest. A further problem is that no boreholes at all are known in the rift north of Silali, although some springs have been located in this region (e.g. Figure 6.2 which shows thermal springs in the area), so groundwater conditions there are not entirely unknown.

Borehole records held by MWD contain details such as borehole location, depth, diameter, casing details and data concerning water strikes and rest levels. Borehole productivity data for old boreholes may be limited to yield but in recent years some water level data during pumping tests have been recorded enabling estimates of transmissivity to be made.

Information about aquifer lithology held by MWD is limited to basic drillers' logs but these indicate that the types of material forming aquifers are the same as for the Phase I Project Area further south; namely fractured volcanics, weathered contacts between different lithological units, and sediments.

It is important to reiterate the point made in the Phase I study (Allen et al., 1989) that the aquifer properties of rocks determined by the analysis of borehole records can only apply to the depths penetrated by the boreholes. Since water boreholes only reach a few hundred metres at most it is not possible to predict the properties of potential geothermal reservoirs at greater depths, except by extrapolation. However the regional flow systems suggested by examination of water level data may persist to substantial depths.

6.2 Water Level Data and Regional Flows

6.2.1 Water Strikes

Borehole depths in the Project Area range up to 286 m, with nine boreholes (13%) exceeding 200 m and 38 boreholes (54%) in the range 100-200 m. The deepest boreholes have been drilled on the rift flanks; boreholes on the rift floor range up to 180 m (C3437-Tangulbei).

Water strike information is available for 66 of the 67 boreholes which found water. Water was encountered in these boreholes at depths ranging from a few metres, to 206 m (C1397 on the eastern rift interfluve). Fifteen boreholes (23%) had water strikes at depths greater than 100 m, the majority of these being on the rift flanks.

Rest water level depths range up to 146 m below ground level (C2434, on the eastern rift interfluve). Most borehole water levels (89%) however are less than 100 m below ground level and a significant proportion (61%) are at depths of less than 50 m.

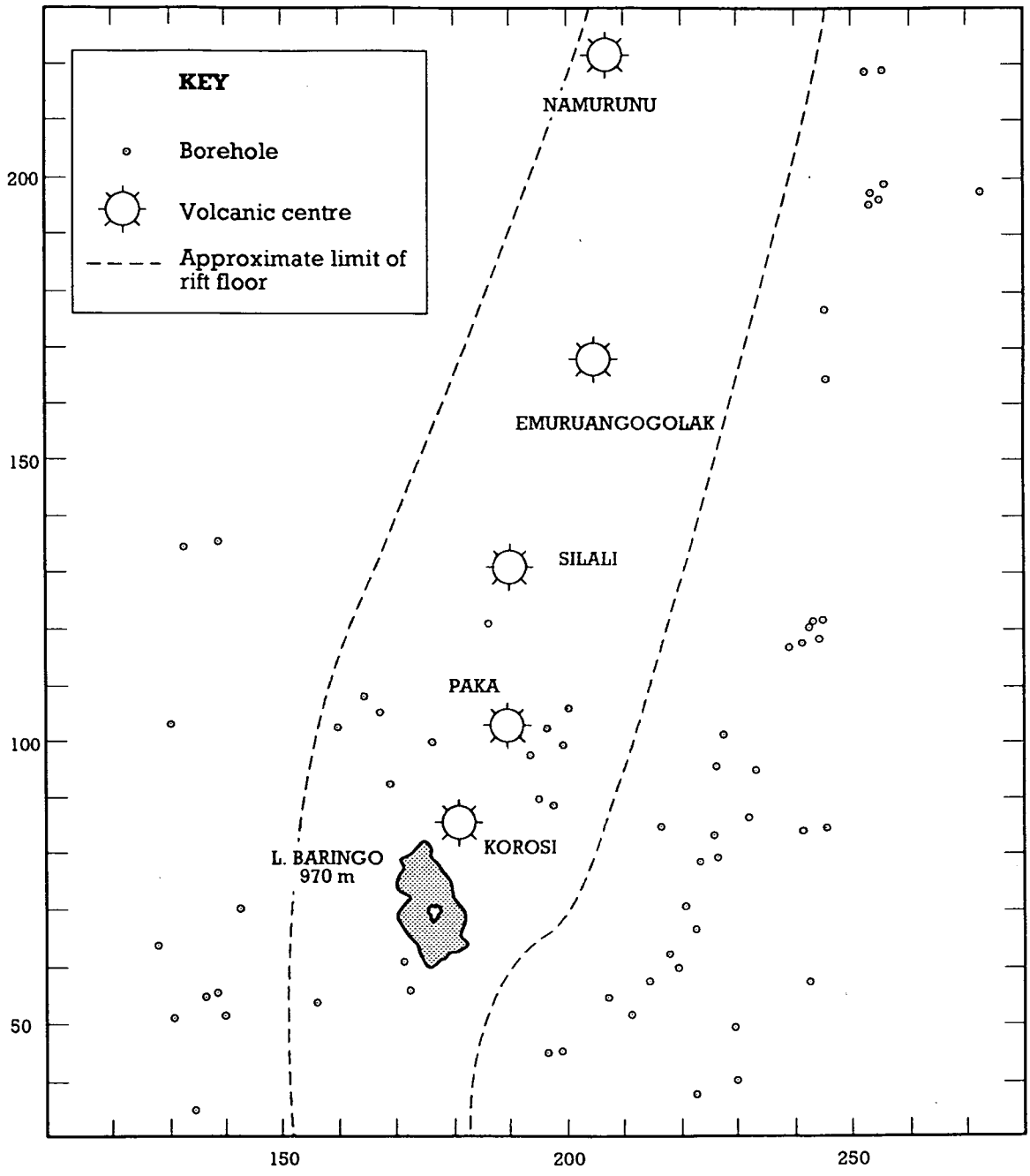

Figure 6.1 Borehole Location Map.

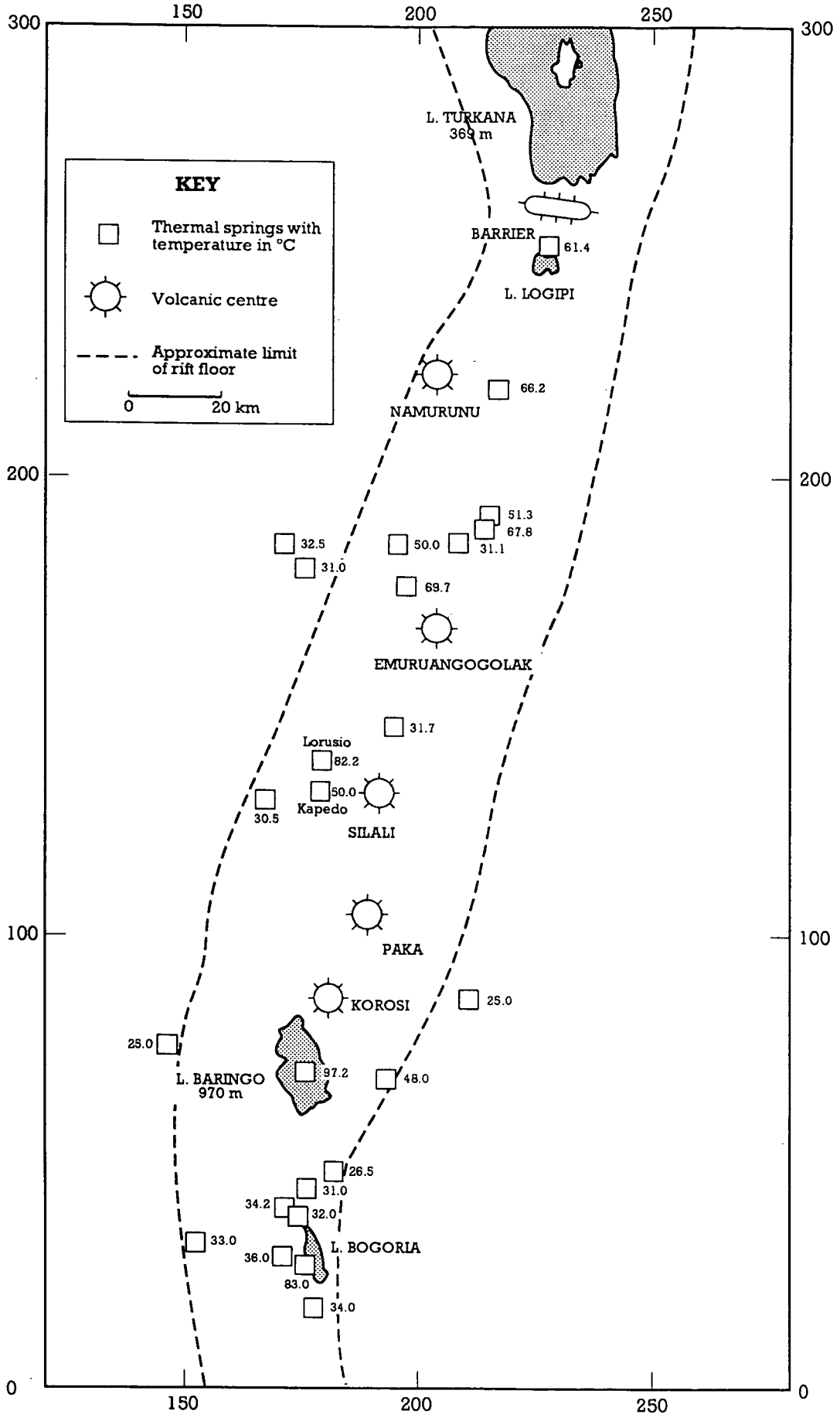

Figure 6.2 Map of Thermal Springs in the Bogoria-Turkana Region of the Rift.

A combination of water strike and water rest level information is available for 63 boreholes. In 55 (87%) of these boreholes the final rest water level was found to be higher than the initial water strike level, suggesting that the aquifer was confined. The incidence of confined conditions is probably not as high as this because if drilling rates are high in aquifers of low permeability then water strikes may not be observed until the borehole has been deepened. However even if only differences between strike level and rest level exceeding 5 m are considered, then 42 (67%) of boreholes for which information is available indicate confined conditions. The greatest rises in water level (of over 50 m) were recorded in boreholes C1397 and C1473 (east of Churo), C7122 at Tangulbei and C4722 at Kabarnet. The Churo and Tangulbei results may be associated with the significant faulting seen in this area. The C4722 figure is suspect, since Kabarnet is in a recharge area where significant artesian heads should be uncommon.

Records for 36 boreholes indicate that multiple aquifers were encountered (the records do not indicate how this was known). In 25 cases the rest water level after the first water strike did not change after subsequent strikes and therefore hydraulic connection between the water-bearing layers can be assumed. In 11 cases the rest water level changed after the second water strike indicating the presence of separate aquifers. These boreholes occur mainly on the eastern flanks of the rift (east of Baringo), and around Kabarnet. There is usually little difference between the rest water levels of the first and subsequent strikes and discrete or perched aquifers do not appear to be common.

6.2.2 The Potentiometric Map

A potentiometric map of the Project Area has been constructed using borehole rest water level data and spring data (Figure 6.3). Where data are scarce contours have been estimated by assuming that the potentiometric surface is a subdued replica of the ground surface. The errors inherent in using water levels measured in different boreholes at different times, or in boreholes where several separate aquifers were encountered are insignificant when the scale and topographic variation of the map necessitate the use of contour intervals of 200 m or more.

In the main Project area the depth to the water table varies from probably less than 50 m below the rift floor near Korosi to around 100 m near Silali. Depths to water under the volcanoes are unknown, although rest water altitudes may be higher than in the surrounding rift floor if recharge mounds exist (see below).

In broad terms groundwater flowlines would be expected to be perpendicular to the groundwater contours shown on the map, with recharge occurring at high groundwater altitudes and discharge at low altitudes. The figure therefore illustrates the areas of groundwater recharge on the east and west flanks of the rift and the zone of discharge along the rift floor. Flows along the rift floor are directed northwards from Lake Bogoria and somewhat east of north from Lake Baringo. This trend is followed as far as Lake Logipi which is in a regional discharge area and has a water surface level at only around 250 m above mean sea level. Lake Turkana, to the north of Lake Logipi, lies at an altitude of nearly 370 m above mean sea level and therefore subsurface drainage from Lake Turkana is directed to the south in this region.

The potentiometric data indicate that the regions around the volcanic centres of Korosi, Paka, Silali and Emuruangogolak appear to be subject to groundwater flows both laterally from the rift flanks and axially from the south. The rift flank component appears to be dominantly from the east for the Paka, Silali and Emuruangogolak areas, and perhaps for Korosi. The rift floor (axial) component is likely to be dominated by Lake Baringo water near Korosi and less so further north and flows mainly on the western side of Korosi, Paka, Silali and Emuruangogolak.

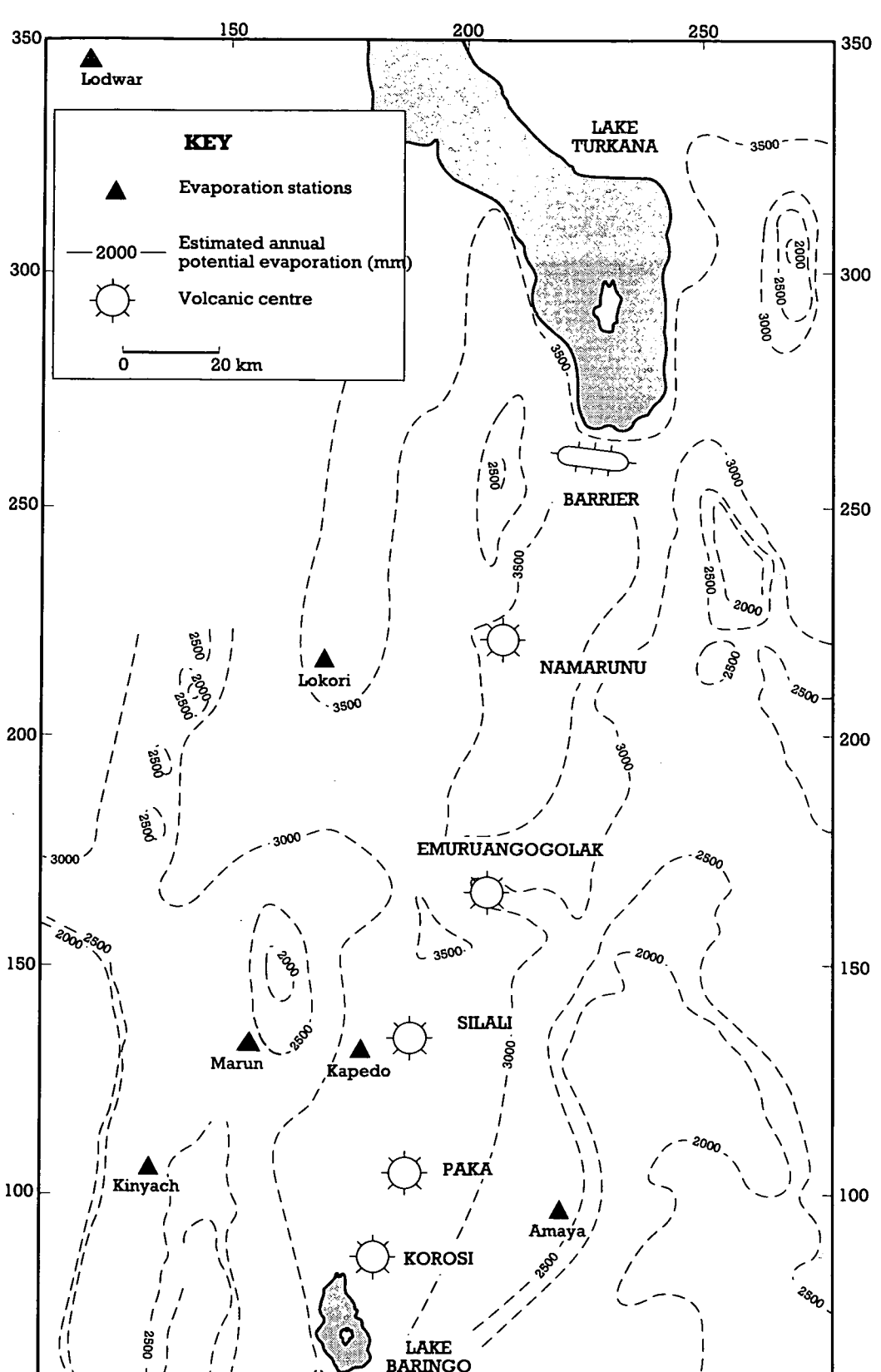

Figure 6.3 Potentiometric map of the North Kenya Rift Valley—Bogoria to Turkana

To the north of the present Project Area the volcanic centre of Namarunu appears to be in an area of easterly groundwater flow, with perhaps an axial component (although in this region it is unlikely that any Baringo water could persist in readily identifiable form). Groundwaters in the area around the Barrier volcano are likely to be dominated by subsurface flow from Lake Turkana.

The above discussion does not necessarily imply that water encountered by drilling directly under the volcanic centres would necessarily be expected to derive from lateral rift wall or axial rift-floor sources, because the volcanoes form substantial topographic hills and may form local recharge mounds. Thus groundwater encountered beneath them to an unknown depth could be purely local in origin (the possibility of local recharge on the rift floor was discussed in Section 4.3).

6.2.3 Effects of Structure on Regional Flows

In the first phase of the Geothermal Project it was considered that faulting in the Rift had a significant affect on regional flows (Allen et al., 1989). Flows across the rift were inhibited by major faults acting as zones of low permeability and in some areas (for example in the region around Mount Suswa) the potentiometric surface was very deep. In addition, flows along the rift were affected by the minor axial faults in the rift floor. These faults were considered to channel flows along the rift axis, either by acting as conduits if they were permeable, or by inhibiting lateral flow if there were of low permeability. In essence therefore the effects of faulting in the Phase I Project Area were considered to cause groundwater flows from the sides of the rift towards the centre to follow longer flow paths reaching greater depths and to align flows within the rift along its axis.

In hydrogeological terms the structure of the present Project Area has similarities with the Phase I Project Area, with significant recent faulting generally trending along the axis of the rift. Therefore the same effects of structure on regional flows might be expected. The general paucity of borehole data makes this supposition difficult to prove or disprove but some support for the inhibition of lateral flows by faults is shown by borehole data in the Baringo-Paka area. This region is heavily faulted (with most fault trends NNW-SSE) and the regional groundwater level gradient is roughly E-W, across the fault trend. Several boreholes in the eastern part of this area show anomalously high hydraulic gradients in an E-W direction. For example, boreholes D1 and D7 are only 6.25 km apart and have an altitude difference of only 55 m, yet the rest water altitude difference between these boreholes is 134 m. Similarly boreholes C3437 and C7122, while only 2.24 km apart and with an altitude difference of only 30 m, have rest water altitudes which differ by 120 m. These figures strongly suggest that hydraulic barriers exist between these borehole pairs and the offset of aquifers by faults is the most likely explanation.

The great depth (>250 m) to the water table, caused by faults impeding lateral flow in the Suswa area, is not seen to the same extent in the present Project Area although water rest levels in excess of 100 m below ground level have been recorded in two boreholes in the rift floor (D1 and C3461). Bearing in mind that the rift floor is theoretically an area of discharge this again implies impedance of lateral flow by faults.

6.3 Aquifer Properties

6.3.1 Introduction

Hydraulic information relevant to the determination of aquifer properties is available in variable amounts for the 70 boreholes in the project area. Most of the boreholes (90%) have some productivity information, however only 45% have data enabling specific capacity to be calculated, and only 25% have enough information for an estimate of transmissivity to be made. The paucity

of transmissivity information (only 18 values in total) means that more reliance must be placed on the less accurate, but more numerous, specific capacity and yield data as a guide to aquifer properties.

6.3.2 Yield

Information about borehole yield was obtained for 63 boreholes. Three of these, or 5%, were dry. Data for the rest, based on pumping test estimates, was obtained from MWD records or from local sources.

Figure 6.4 shows the cumulative relative frequencies of yields (smoothed data) from the 60 production boreholes, and Figure 6.5 illustrates the same data in the form of a relative frequency histogram. Both figures indicate clearly that borehole yields are generally low throughout the project area. Figure 6.4 shows that 50% of boreholes have yields less than 103 m^3/day (1.2 l/s) and 90% have yields less than 400 m^3/day (4.6 l/s). Figure 6.5 shows that the greatest frequency of borehole yields is in the range 40-60 m^3/d (0.5-0.7 l/s).

The few high yielding boreholes shown on Figure 6.5 are C5349 (Tot Bridge), C6363 (Kositei) and D7 (Kokwototo) with yields of 1056 m^3/day (12.2 l/s), 1088 m^3/day (12.6 l/s) and 785 m^3/day (9.1 l/s) respectively.

These yield estimates can only be used as a rough guide to aquifer properties because the values are influenced by factors other than the nature of the aquifer. For example in a productive borehole the yield may be more a function of pump capacity than potential borehole productivity. On the other hand no account is taken of drawdown, and since production tests usually only last 24 hours, the long-term yield may be less than the stated value. However the low value of the majority of 60 borehole yields does suggest that regional permeabilities are low.

6.3.3 Specific Capacity

By using the concept of specific capacity (borehole yield per unit drawdown) for stable drawdown conditions the effects of different pump capacities and variations in drawdown between different boreholes can be eliminated and borehole productivity can be compared on a more equal basis. Specific capacity is not controlled solely by aquifer properties (see below) but it is much more closely related to them than borehole yield alone.

Available data have enabled 32 specific capacity values to be calculated. These are illustrated in a cumulative relative frequency diagram (Figure 6.6) and a relative frequency histogram (Figure 6.7). Figure 6.6 indicates that specific capacity values are generally low, with, on average, 50% of values falling below 4.5 m^3/day/m (0.05 l/s/m) and 90% of values falling below 85 m^3/day/m (1 l/s/m).

Boreholes with specific capacity values greater than 50 m^3/day/m (0.6 l/s/m) are shown in Table 6.1. These boreholes include two of the three high-yielding boreholes mentioned above (borehole D7 has no specific capacity data).

There appears to be no unique reason why these boreholes have specific capacities which are relatively high. The limited lithological data suggest that the three types of aquifer which are commonly found in the rift valley - sediments, weathered material between volcanic deposits, and fractured volcanics - are all represented.

6.3.4 Transmissivity

Pumping test data from which aquifer transmissivity values may be calculated are severely limited in the project area. Conventional pumping tests using

Table 6.1 BOREHOLES WITH SPECIFIC CAPACITY VALUES EXCEEDING 50 m^3/day/m

Borehole	Location	Yield	Specific Capacity m^3/day	Lithology (Driller's Log)
C3055	Mugie Ranch	341	225	Weathered Lava
C4838	Kamnorok	264	68	-
C5349	Tot Bridge	1056	106	Sand
C5487	Kinyach	480	51	-
C6363	Kositei	1089	79	Fractured Phonolite
D1	Katangora	115	152	Weathered Basalt

Table 6.2 TRANSMISSIVITY AND SPECIFIC CAPACITY VALUES FOR BOREHOLES IN THE PROJECT AREA

Borehole	Transmissivity m^2/day	Specific Capacity m^3/day/m
C1833	0.1	0.8
C3470	4.0	3.5
C3506	8.0	16.1
C3833	0.3	0.5
C3855	0.1	0.4
C3868	5.4	4.3
C3869	0.3	0.6
C4722	25.2	31.2
C4780	4.2	19.7
C4838	22.1	68.0
C5170	36.3	28.2
C5349	95.5	105.6
C5370	2.5	5.3
C5487	11.7	51.4
C6362	1.5	1.6
C6363	76.6	79.1
C6364	6.6	9.2
C6365	2.4	3.0

Table 6.3 TRANSMISSIVITY DATA ESTIMATED FROM SPECIFIC CAPACITY VALUES

Borehole	Specific Capacity $m^3/day/m$	Estimated Transmissivity m^2/day
C1018	4.83	2.3
C1785	1.55	0.6
C1882	1.48	0.6
C1896	5.59	2.7
C2345	18.14	10.8
C2434	1.97	0.8
C2844	8.91	4.7
C2847	0.48	0.2
C2972	0.23	0.1
C3055	224.68	208
C3119	1.39	0.5
C3456	0.64	0.2
C3461	3.99	1.8
D1	151.58	131

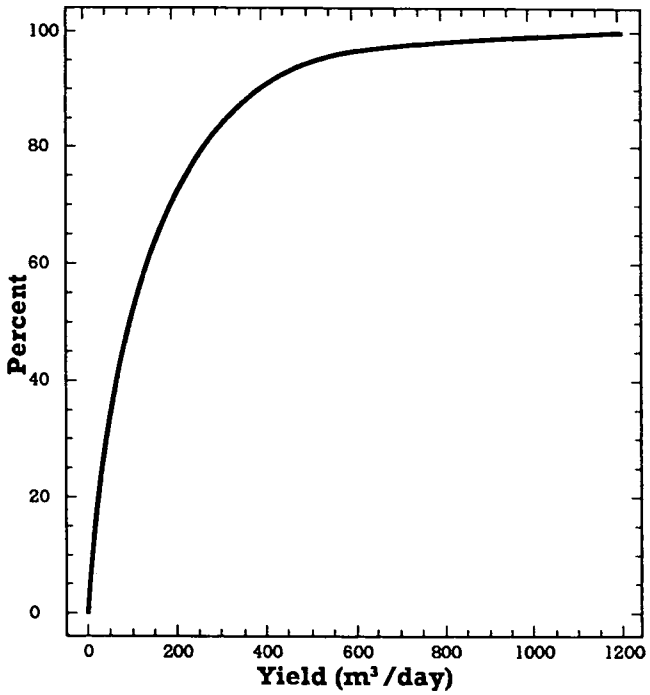

Figure 6.4 Cumulative relative frequency plot of borehole yields

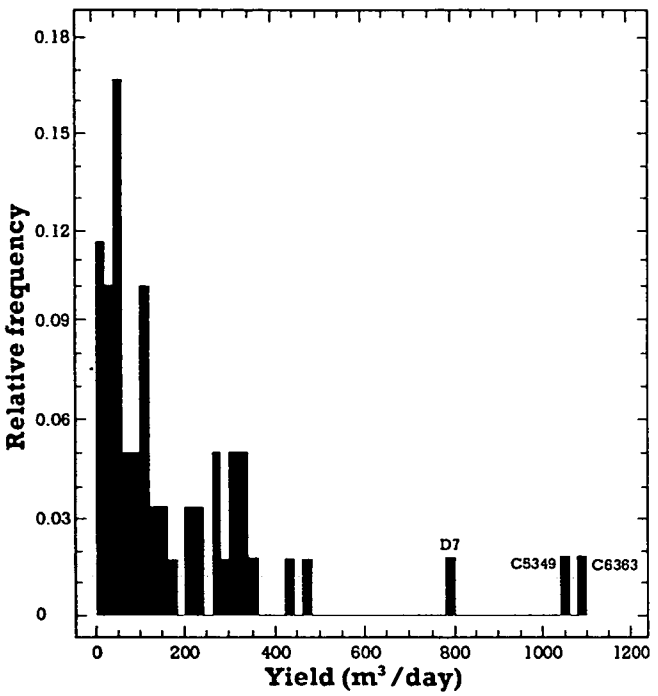

Figure 6.5 Relative frequency histogram of borehole yields

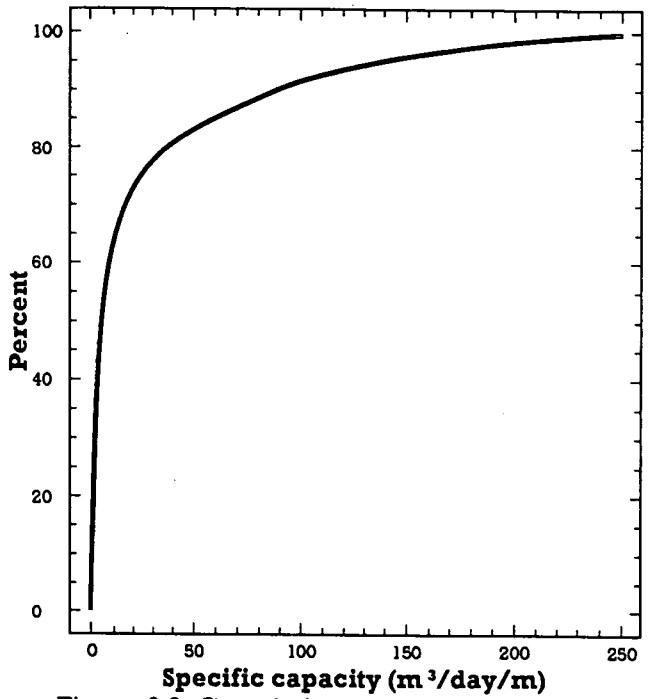

Figure 6.6 Cumulative relative frequency plot of borehole specific capacities

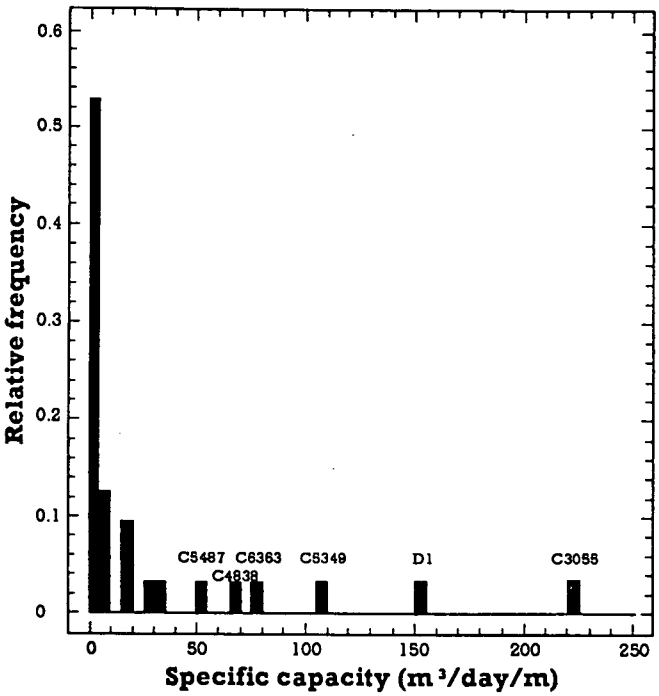

Figure 6.7 Relative frequency histogram of borehole specfic capacities

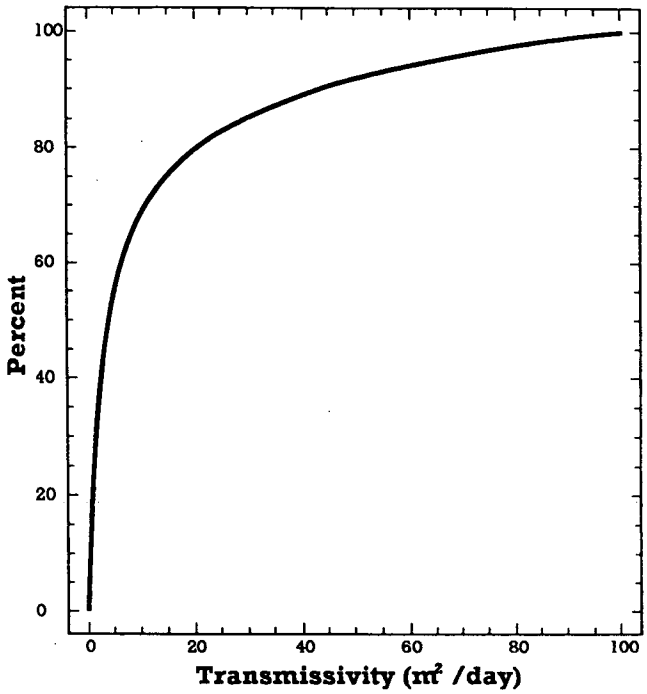

Figure 6.8 Cumulative relative frequency plot of borehole transmissivity

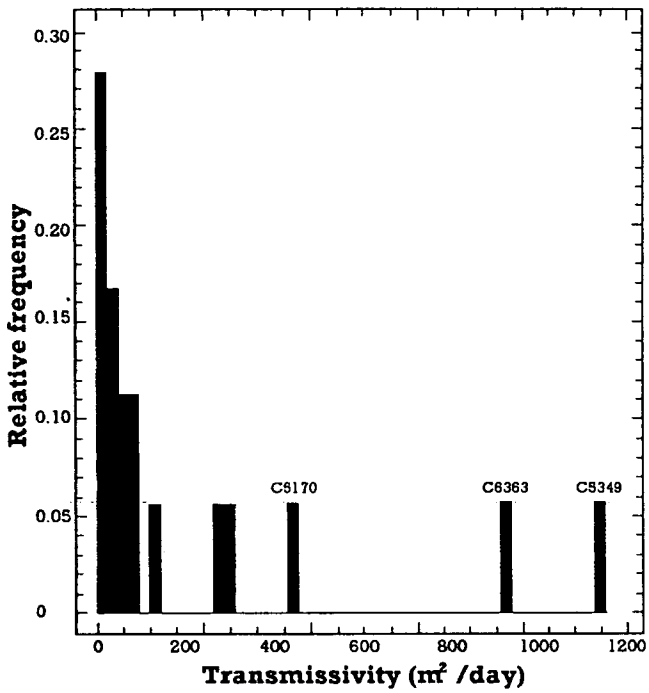

Figure 6.9 Relative frequency histogram of borehole transmissivity

observation boreholes are non-existent and fully-monitored production well drawdowns and recoveries are rare.

The available data (in decreasing order of transmissivity data quality) comprise eighteen estimates of transmissivity; three from tests carried out by WRAP, six from tests with data and analyses recorded in MWD records and noted by WRAP, and nine from tests where some recovery data exist on file at MWD which were analysed by BGS.

Transmissivity values were obtained from drawdown data in some tests, from recovery data in others, and from both in a few cases (in the latter instance an average value has been used).

Table 6.2 shows the transmissivity values obtained and the specific capacity value for the same borehole. Figure 6.8 and 6.9 illustrate the frequency distribution of the transmissivity data.

Although values of transmissivity range up to nearly 100 m^2/day Figure 6.8 shows that 75% of all values are less than 17 m^2/day, and 50% of values are less than 4.8 m^2/day. Figure 6.9 indicates that the greatest frequency of borehole transmissivities lies in the range 0-2 m^2/day and although the average value of the data set is 17 m^2/day this is weighed by a few relatively high values, particularly those of C5349 (Tot Bridge) and C6363 (Kositei).

If the transmissivity and specific capacity values from Table 6.2 are plotted (Figure 6.10) it is seen that the data conform to the line:

$$T = 0.358S_c^{1.175} \quad \ldots (6)$$

with a correlation coefficient r of 0.93, suggesting a good fit to the data. The theoretically-based Thiem equation (Thiem, 1906) which was used in the Phase I study does not fit these data, for unknown reasons.

The good fit of the empirical equation (Equation 6) to the data suggests that there is some validity in using the equation to predict transmissivity values where only specific capacity data exist; thus enabling the transmissivity data set to be enlarged to 32 values.

The resulting additional data are shown in Table 6.3 and have been used with the data in Table 6.2 to produce Figures 6.11 and 6.12. The results suggests that the borehole transmissivities are on average even lower than were indicated by the original transmissivity data, with 50% of values having transmissivities less than 2.6 m^2/day (Figure 6.11). This is reflected in the relative frequency histogram (Figure 6.12) which shows an increased proportion of low transmissivity values.

Boreholes with high predicted transmissivities are C3055 (Mugie Ranch) and D1 (Katangora) which means that only four boreholes of the 32 for which data are available have calculated or predicted transmissivity values in excess of 50 m^2/day.

6.3.5 Discussion

The implication of the above analysis is that aquifer transmissivities in the study area are generally low (and it should be noted that transmissivity values derived from pumping test data include both matrix and fissure contributions to flow). This in turn suggests that, in the absence of other factors the permeability at depth in geothermal reservoirs is also likely to be low - because in general terms permeability tends to decrease with depth as a result of diagenesis and fissure closure caused by overburden stress.

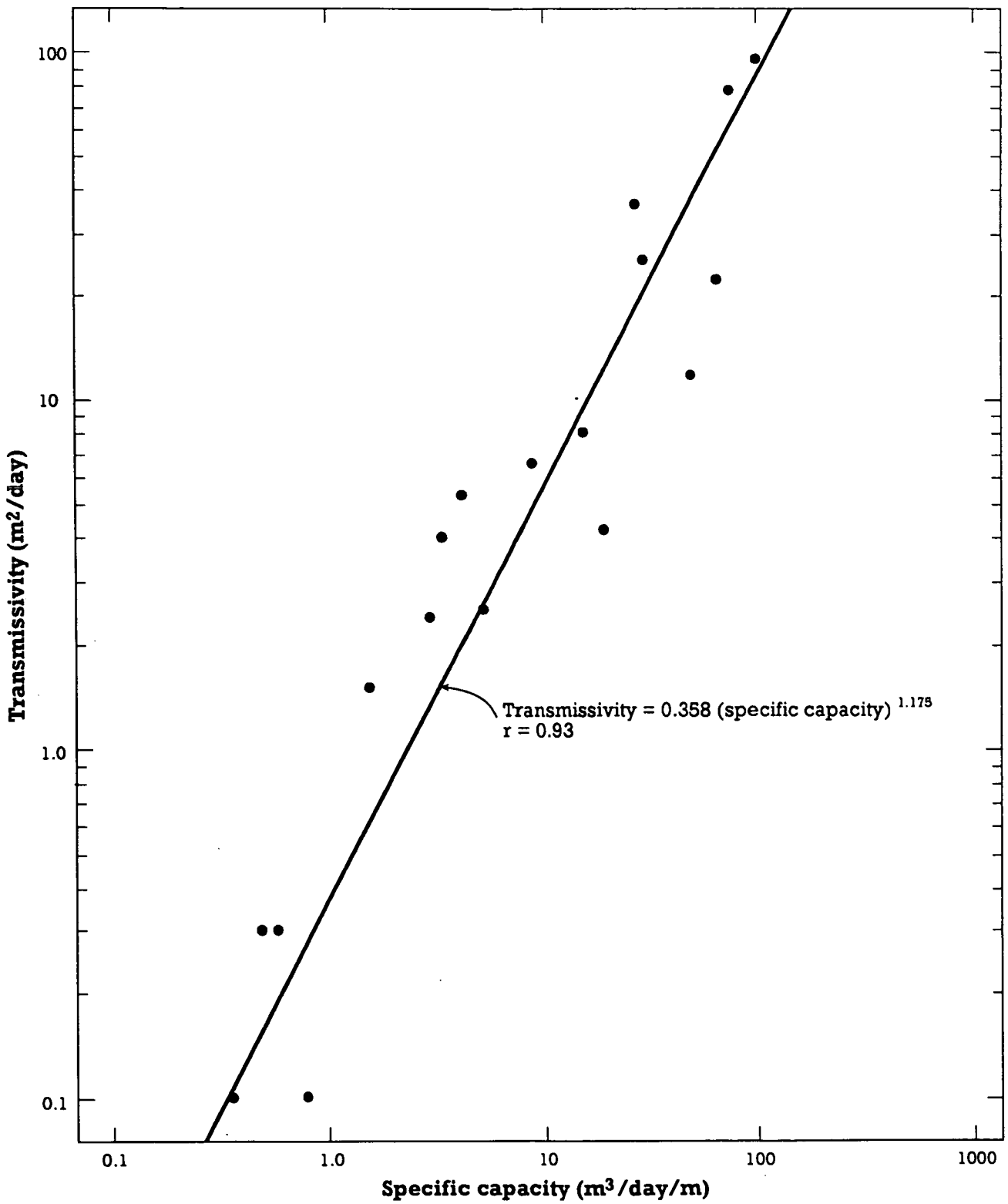

Figure 6.10 Plot of Transmissivity versus Specific Capacity.

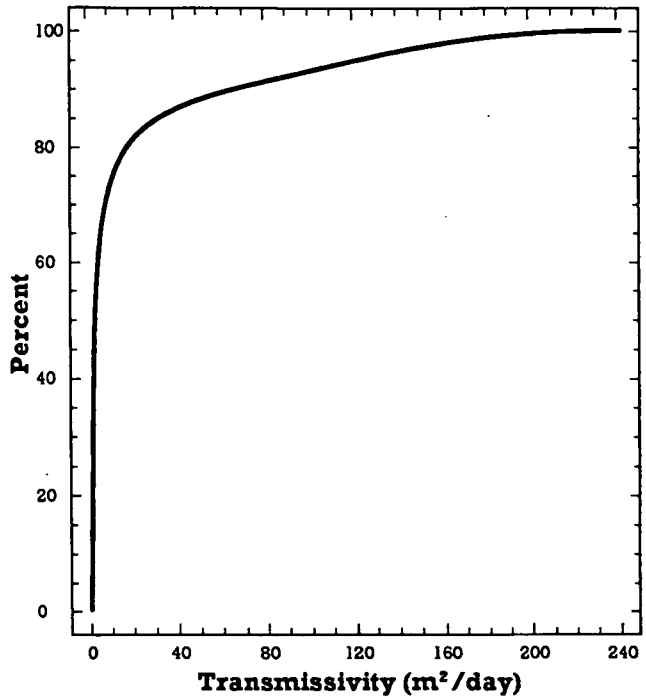

Figure 6.11 Cumulative relative frequency plot of borehole transmissivities

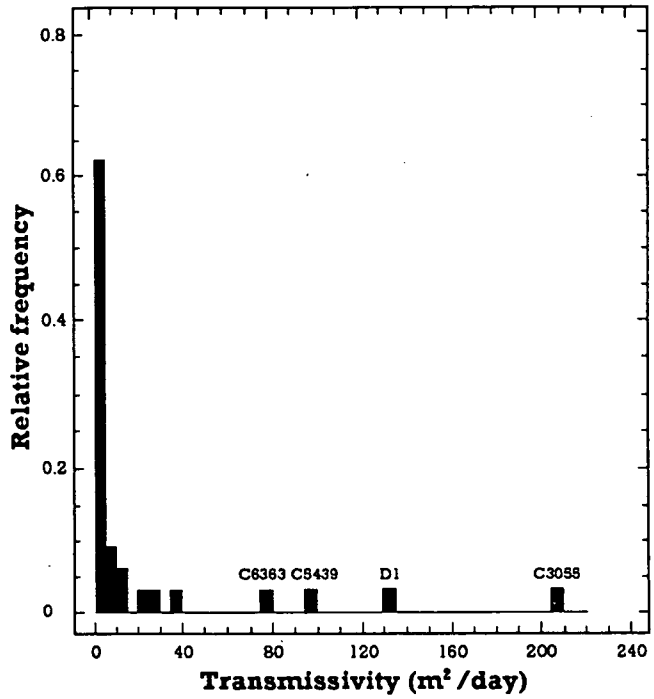

Figure 6.12 Relative frequency histogram of borehole transmissivities estimated from specific capacity data

However, for various reasons the borehole data need to be treated with caution. Firstly, the data set is extremely small for such a large and hydrogeologically complex area and no data at all are available for the potential geothermal target areas. Secondly the borehole values only relate to the depth penetrated, which is much shallower than any geothermal aquifer. Thirdly, the volume of aquifer affected by a borehole productivity test lasting only a day or so is very small; it is therefore possible that the permeability enhancement caused by the considerable faulting of the rift is rarely seen in borehole pumping test data.

A more regional view of aquifer transmissivity may be gained by examination of the subsurface flow from Lake Baringo. In theory, if the volume of flow, the hydraulic gradient, and the cross-sectional area are known, then the average aquifer permeability can be calculated.

Assuming a hydraulic gradient of 0.01, a width of 15 km and a flow from the lake of 100 x 10^6 m^3/year (an average of the three estimates given in Section 5.2), the transmissivity is calculated to be 1800 m^2/day.

This figure is substantially greater than the 17 m^2/day average value estimated for boreholes (Section 6.3.4). However, the boreholes only partially penetrate the aquifers and the average depth of penetration (taken crudely to be the depth between first water strike and the bottom of the borehole) is 74 metres for the 18 boreholes for which transmissivity data are available. this would imply a full aquifer thickness of nearly 8 km to give the transmissivity figure estimated from lake discharge. Such a figure is unrealistically high by a factor of about four - which in turn suggests that the borehole transmissivity values underestimate regional values.

Naturally the above analysis is very simplistic - with the data available it cannot be otherwise. In particular the flow quantity from the lake may be less - if the WRAP estimate is correct. On the other hand the estimate does not include the (unknown) northward rift floor flows other than lake discharge. All that can be concluded is that there is some evidence that regional transmissivities are somewhat larger than those suggested by borehole data alone.

6.4 Thermal Springs and Boreholes

6.4.1 Thermal Springs

The following discussion is concerned only with the physical aspects of the various warm and hot springs encountered in the Project Area.

Thermal springs are widespread between Lake Bogoria and Lake Turkana (Figure 6.2, which shows all known springs above an ambient 25°C). Fumarole condensates are not shown on the map which is restricted to thermal springs which are in direct hydraulic contact with local groundwater. (Thus seeps on the summits of volcanoes are not shown).

The thermal springs in the Project Area fall into two main groups. Along the rift margins springs occur with temperatures of up to 48°C and with generally low flows. These springs do not appear to be associated with high temperature geothermal activity characterised by fumaroles or altered ground and they probably result from deep circulation of rift-wall waters through marginal faults. They are therefore unlikely to be important in a geothermal context.

The second main group of springs comprises those on the rift floor, which have a wide range of flows (up to 1 m^3/s) at Kapedo) and temperatures (up to 82.2°C at Lorusio) and are often relatively close to major recent volcanic centres.

As discussed in Section 6.2 the main direction of subsurface flow under the rift floor is along the axis of the rift from south to north, reversing north

of Lake Logipi and modified by lateral flows from the river flanks and from local recharge mounds under the central volcanoes. Any explanation for the origin of the springs must therefore be set in this context.

The springs discharging on the north shores of Lake Logipi almost certainly have their origins to the north, where groundwater is driven southwards by the potentiometric head gradient of 0.08 m/m which exists between Lake Turkana and Lake Logipi. It is likely that this water from Lake Turkana will have mixed to some extent with rift-wall waters and perhaps locally-infiltrated water and will have been heated during its passage through the young volcanics of the Barrier volcano.

Further south, the hot spring to the east of Namarunu volcano (Figure 6.2) may be associated with high heat flow beneath the volcano which is situated close to the western rift flank in an eastward-trending groundwater flow field.

Between Emuruangogolak and Namarunu several thermal springs have been located with measured temperatures of between 31°C and 70°C. From the orientation of the potentiometric surface in this area it is most probable that these springs represent flow from Emuruangogolak: in a similar way the spring south of Emuruangogolak probably originates from Silali. However neither of these springs appears to be connected with the hydrothermal systems beneath these volcanoes (see 7.4 below).

The Lorusio and Kapedo spring systems near Silali volcano are the hottest and most productive respectively, in the Project Area. At Lorusio the springs discharge at temperatures up to 82°C in a series of seeps and pools 1.5 km to the west of the Suguta River at the base of the Tiati hills on the western margin of the rift. The source of the springwaters is not apparent from the potentiometric map (Figure 6.3) because the springs lie in an area where easterly groundwater flows from the western rift margins, westerly and northerly outflows from Silali and northerly axial rift flows all converge.

If the Lorusio springs had been cold, then on a local scale their position near the foot of the western rift escarpment and at a higher elevation that the Suguta river would undoubtedly indicate an origin to the west. However the high temperature of the springs and their proximity to Silali, the most obvious heat source in the area, and the fact that the potentiometric surface may be complex in an area where groundwaters exist at different temperatures and salinities (causing density variations) suggests that the connection between Lorusio and Silali cannot be discounted, though the waters do not have high-temperature chemical characteristics (see 7.4 below).

The Kapedo hot springs, approximately 9 km to the south of the Lorusio system discharge at 50°C from fissured basalts to the south and east of Kapedo village and the total flow of around 1 m^3/s constitutes the baseflow of the Suguta River. If a mean annual surface temperature of 25°C at Kapedo is assumed this implies a heat flow from the springs of 100 MW, suggesting a significant heat source.

In a regional sense the Kapedo springs lie in an area of converging western rift, rift axis and Silali outflow waters and on this scale the source of the springwaters is not apparent. The WRAP study of the Baringo catchment (WRAP, 1987a) suggested that because the spring flow, at around 30 x 10 m^3/year, is similar to their estimate for the subsurface outflow from Lake Baringo then the lake could provide the source of the springs. This idea has the attraction that it appears to explain how the Kapedo springs have such a large discharge in an otherwise arid area. In the sense that the Baringo outflow is substantial and directed northwards and that some of the outflow presumably does emerge at Kapedo this explanation is partly correct. However as the potentiometric map (Figure 6.3) indicates, all groundwater flows from Baringo to the south of Silali including rift flank lateral flows and locally recharge waters are directed northwards, and much of this water which does not

evaporate may move through the Kapedo area. It is likely that the channelling of groundwaters from a variety of sources gives rise to the Kapedo springs and that the component from Baringo, 50 km to the south, is unlikely to be large. Stable isotope results suggest that it cannot exceed 30% (7.4 below).

If the average recharge in the floor of the rift is taken to be of the order of 25 mm/year (Section 4) then the area required to support the Kapedo spring discharge would be around 1300 km^2 or a region of around 35 km square. This is smaller than the area of the rift floor between Baringo and Kapedo and provides further evidence that subsurface flow from Baringo is unlikely to be the only or even the major component of the spring discharge.

On a local scale, the position of the main springs on the western margin of Silali volcano (and the fact that smaller thermal springs occur a few kilometres to the northeast on the eastern bank of the Suguta River) suggests that Silali provides the source of the heat and perhaps for a significant proportion of the water, for the springs. (Recharge of groundwater into Silali is likely to be higher than that in the rift floor, because of its elevation). It is possible that the heat output of the springs could be provided by regional groundwater flows causing a convective movement of heat to the Kapedo area, but Silali is a much more obvious heat source.

In conclusion, the most likely explanation for the source of the Kapedo springs from a physical hydrological standpoint is as a mixture of outflow from the Silali volcano recharge mound with groundwaters flowing axially northwards along the rift, the axial waters themselves being a mixture of rift floor groundwater, rift wall groundwaters and Baringo lakewater. The heat source is most likely to be Silali itself with possibly a contribution from deeply circulating hot waters from the rift floor. There is little evidence, however, that high temperature waters are contributing to the springs (see 7.4 below).

6.4.2 Thermal Boreholes

The average annual ground surface temperature in the floor of the rift in the Project Area is estimated to be 25°C using temperature data from Marigat. Measured water discharge temperatures from boreholes are often higher than this and sometimes significantly so (e.g. boreholes C6362 and C6365 with discharge temperatures of 45°C).

Anomalously high borehole discharge temperatures do not in themselves imply either high geothermal gradients or high heat flows. However in the absence of borehole temperature logs such data may be used as a preliminary guide to geothermal gradients if the producing aquifer level is known.

Unfortunately aquifer level data are rarely available for the Rift Valley boreholes, but a range of estimates may be made by assuming that all production occurs either where water was first struck during drilling (leading to a maximum estimate of geothermal gradient) or from the bottom of the borehole (giving a minimum value). The true value of geothermal gradient should therefore lie within this range.

Table 6.4 gives details of estimates obtained by this method for boreholes with discharge temperatures in excess of 25°C. Twelve out of the fifteen boreholes with anomalous temperatures lie in the rift floor. The three exceptions occur on the eastern rift flanks (boreholes C3855 and C4417 at Baragoi and C3833, southwest of Maralal) and none indicate particularly strong thermal anomalies.

Two of the thermal boreholes in the rift - C6362 and C6365 - lie outside the present Project Area between Lake Bogoria and Lake Baringo. The boreholes partly penetrate a thick series of fluvio-lacustrine sediments between the two lakes. Temperature logs were run in these boreholes by WRAP (WRAP, 1987a) which indicated a high temperature gradient between the surface and the water table below which a lower but still anomalously high temperature gradient was

Table 6.4 THERMAL BOREHOLE TEMPERATURES AND GEOTHERMAL GRADIENT ESTIMATES

Borehole Number	Location	Discharge Temperature (°C)	Estimated Geothermal Gradient (°C/km)	
			Minimum	*Maximum*
C3437	Tangulbei	30.2	28	49
C3466	Nyunyau	'Hot'	-	-
C3470	Chemolingot	37.7	108	347
C3833	Sirata Oirobi	27	16	53
C3855	Baragoi	26	-	-
C3868	Nginyang	32.2	92	817
C4417	Baragoi	29	33	121
C6362	Salabani	45	220*	775*
C6363	Kositei	36.2	105	116
C6364	Chesirimion	34	75	85
C6365	Ngambo	45	185*	425*
D1	Katangora	36	69	87
D4a	Orus handpump	28	-	-
D4b	Orus solar	28	-	-
D7	Kokwototo	28	-	-

* values obtained from borehole temperature log

encountered to the bottom of the borehole (60 m in each case). These values were used as the maximum and minimum figures in Table 6.4. The explanation for the change in gradient at the water table is presumably that the thermal conductivity of the unsaturated material is lower than in the saturated sediments. The source of the thermal water is unknown but is likely to be to the south or southwest judging by the potentiometric gradients.

The ten remaining thermal boreholes all lie in the Rift Valley floor between Korosi and Silali. Borehole locations, discharge temperatures and estimated geothermal gradients are shown on Figure 6.13. The figure shows that thermal waters are widespread in the area. The highest borehole temperatures are found in the Nginyang-Kositei area (C3470, C3868, C6363) and to the southwest of Paka, although the variation in temperatures is not large. Estimates of geothermal gradients are highest for the Nginyang-Kositei boreholes, with values in excess of 100°C/km suggested.

When these figures are considered with the potentiometric surface in the region it is apparent that groundwater in the Nginyang-Kositei area probably originates to the southwest, rather than in the known geothermal centres of Korosi or Paka. Whether this suggests an as yet unknown geothermal source or is simply a reflection of the widespread nature of the thermal waters in the Rift Valley coupled with the lack of borehole data is unknown.

The boreholes around the 1200 m potentiometric contour level east of Paka intercept water flowing from the eastern rift margin and have less elevated temperatures than the boreholes further west. Borehole D1, closer to the heat source of Paka is warmer and shows a more elevated gradient. It may receive both heat and water fluxes from the volcano because although nominally at a higher potentiometric elevation than the Paka area, it is close to the likely Paka recharge mound.

Heat flow values have been estimated at three borehole sites in the project area (Morgan, 1973). Two of the values were considered relatively reliable; 89.6 mW/m^2 at Chemolingot (C3470?) and 111 mW/m^2 at a site between Paka and Silali. These values, at around twice the world mean, are an extra indication of the widespread nature of the thermal anomalies.

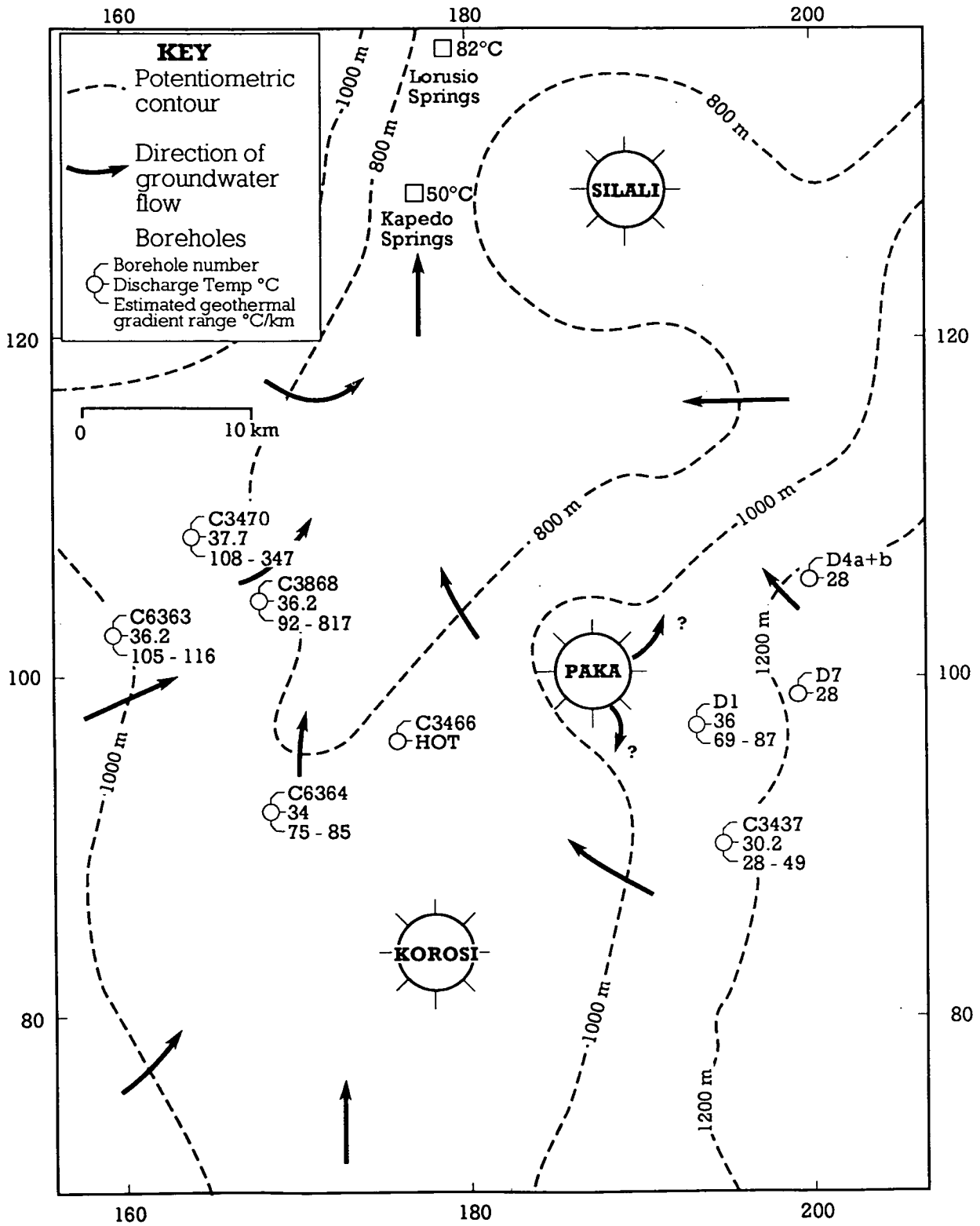

Figure 6.13 Thermal Data for Boreholes in the Korosi-Silali Region

7. FLUID GEOCHEMISTRY

7.1 Introduction

Samples of surface waters (rivers and lakes), groundwaters (thermal and ambient) and fumarole gases and steam condensates were collected from representative sources mainly within the project area (Figure 7.1a-c, Appendix 7). The coverage of sampling was intended to combine detailed information on the volcanic centres with a more general regional appraisal of hydrogeological conditions. Standard chemical, isotopic and gas analytical techniques were employed on samples as appropriate (fuller information on sampling and analysis is given in Allen et al, 1989 and Darling and Talbot, 1991). The results (Tables 7.1 to 7.6) are now considered.

7.2 Surface Waters

These may be conveniently split into two groups: lake and river waters in the Baringo catchment area (and also the seasonal Lake Tilam between Korosi and Paka), and those rivers draining northwards towards the Suguta Valley.

7.2.1 Surface Waters of the Baringo Catchment

These comprise rivers and streams draining the east and west rift flanks, together with Lake Baringo and the seasonal Lake Tilam. Many of the rivers carried a heavy sediment load but most were filterable for chemical analysis. Rivers from the western flanks had total dissolved solids (TDS) contents of 93-250 mgl^{-1}, while rivers from the eastern flanks were higher at 218-655 mgl^{-1} (Table 7.1). The isotopic results do not suggest that evaporation had significantly affected any of the river water compositions, except perhaps for the Mukutan river (147) to the southeast of Baringo. Comparison of the average Cl^- content (unweighted) of rivers feeding Lake Baringo suggests an evaporative concentration factor of some 2.5 times. However, measurement of lake chemistry in 1986 during the dry season (Allen et al., 1989) showed the TDS to be 1½ times higher than in 1988 or 1989, while in 1991 the lake appeared to be returning to a composition similar to that of five years before. Clearly the lake, which is only a few metres deep in most places, is subject to considerable seasonal fluctuations in terms of solute load. There is little evidence that the thermal springs of Ol Kokwe Island exert much influence on lakewater chemistry.

Although chemistry was not measured on the seasonal Lake Tilam (151) between Korosi and Paka, an SEC (specific electrical conductivity) measurement gave a result of 100 mS, suggesting that the TDS would be <150 mgl^{-1}. Despite local legends about an underground source to the lake, such a low TDS is characteristics of surface water and is well below the TDS at Chesirimion (132), the nearest borehole. There is therefore no evidence that Tilam is other than exclusively rain-fed.

Stable isotope measurements on the surface waters present a fairly coherent data set. The δ-crossplot in Figure 7.2 shows the river data together with all other water data, and with one exception (Mukutan, 147) the rivers group into separate eastern and western groups. Since the catchment altitudes on both sides of the Rift in the Baringo area appear to be similar, the difference in isotope values may be attributable to movement of rain-bearing clouds from east to west. The river isotope values are also in good agreement with ambient spring and well waters, demonstrating that they share a similar source on the rift flanks.

7.2.2 Surface Waters North of the Baringo Catchment

Within the project area proper there are only rivers and streams, all of which eventually soak into the arid rift floor either within or to the north of the area in the Suguta Valley. The increasing temperature and aridity of this

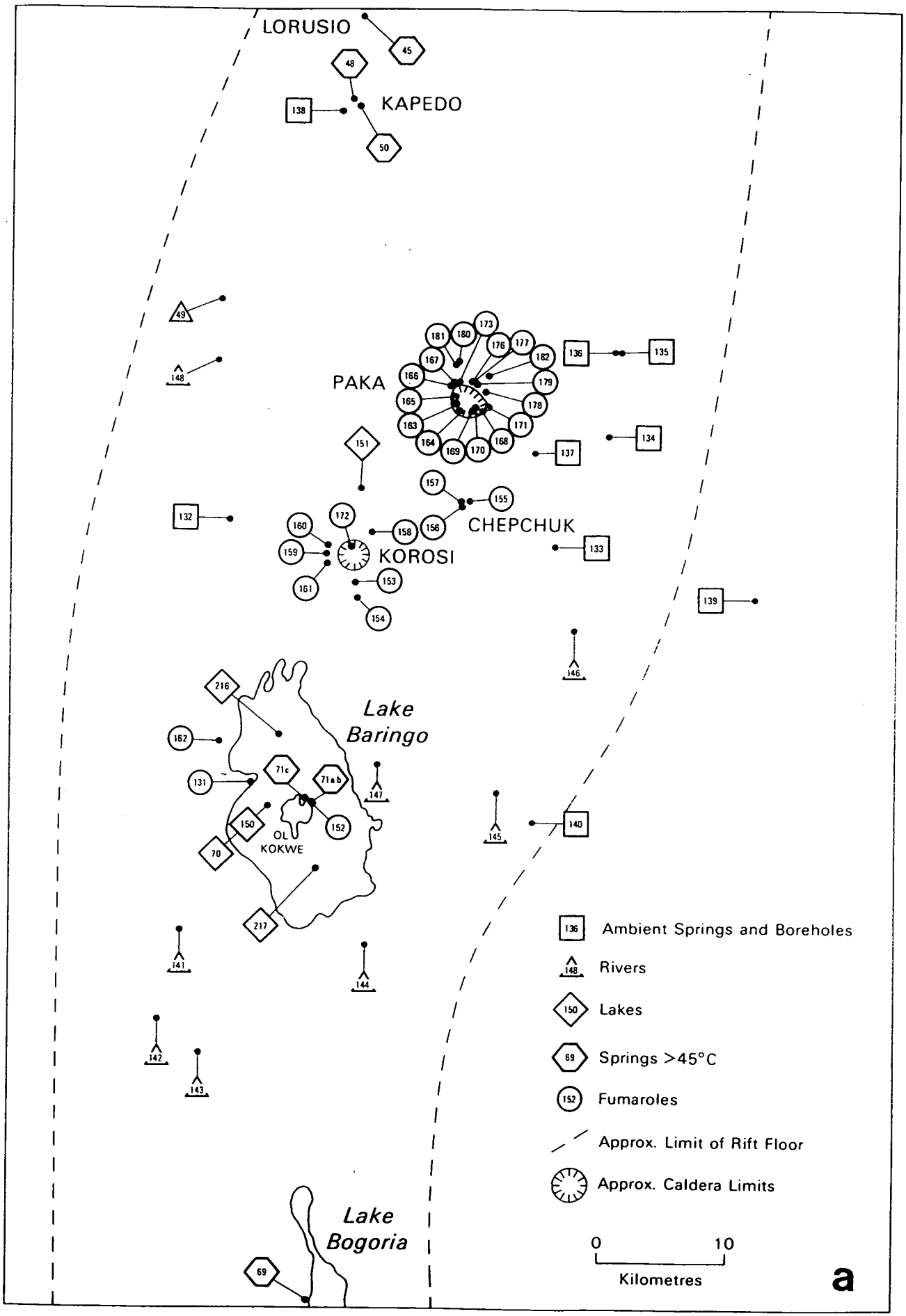

7.1(a)-(c) Map showing location of samples and sample type.

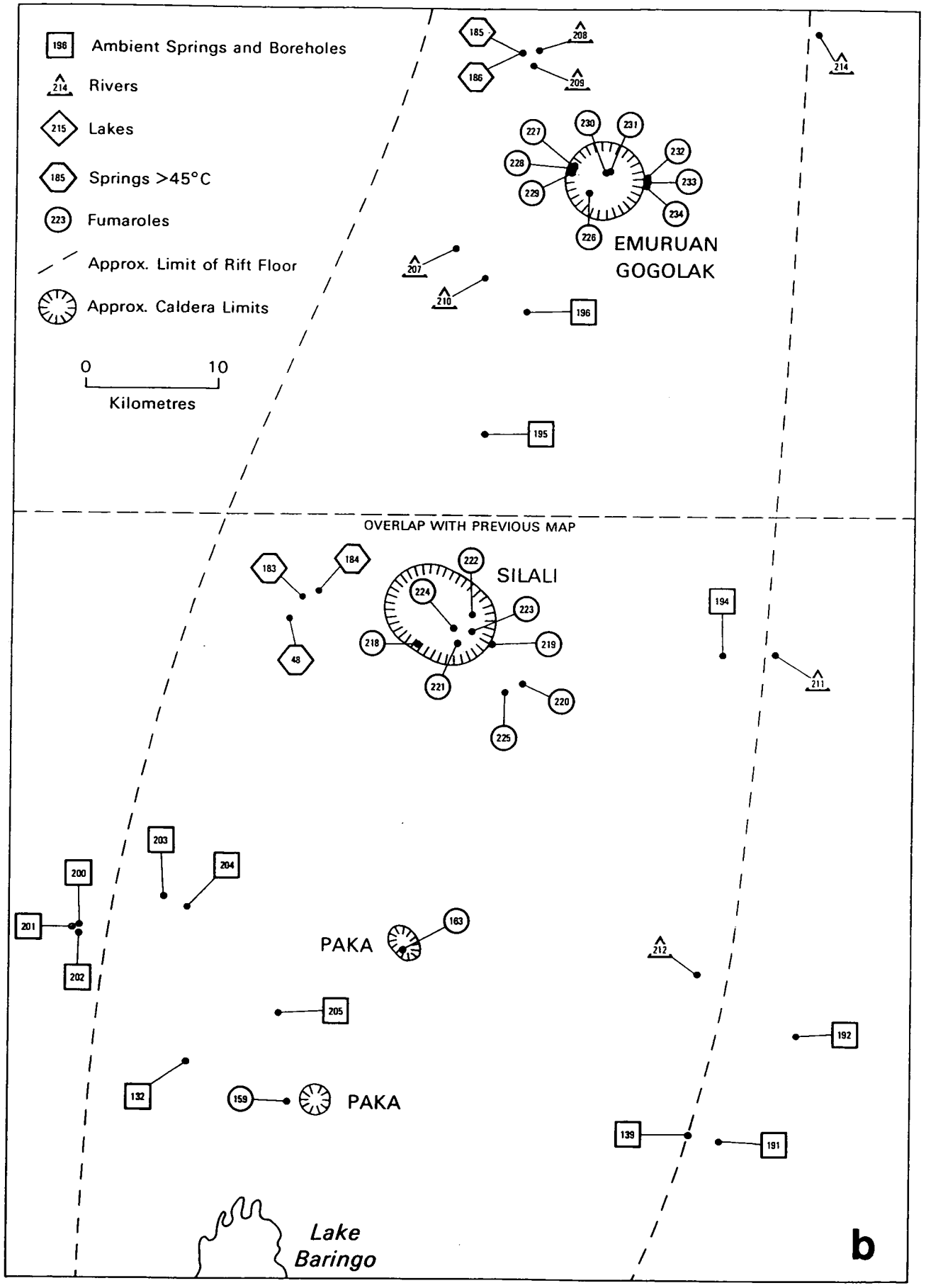

7.1(a)-(c) Map showing location of samples and sample type.

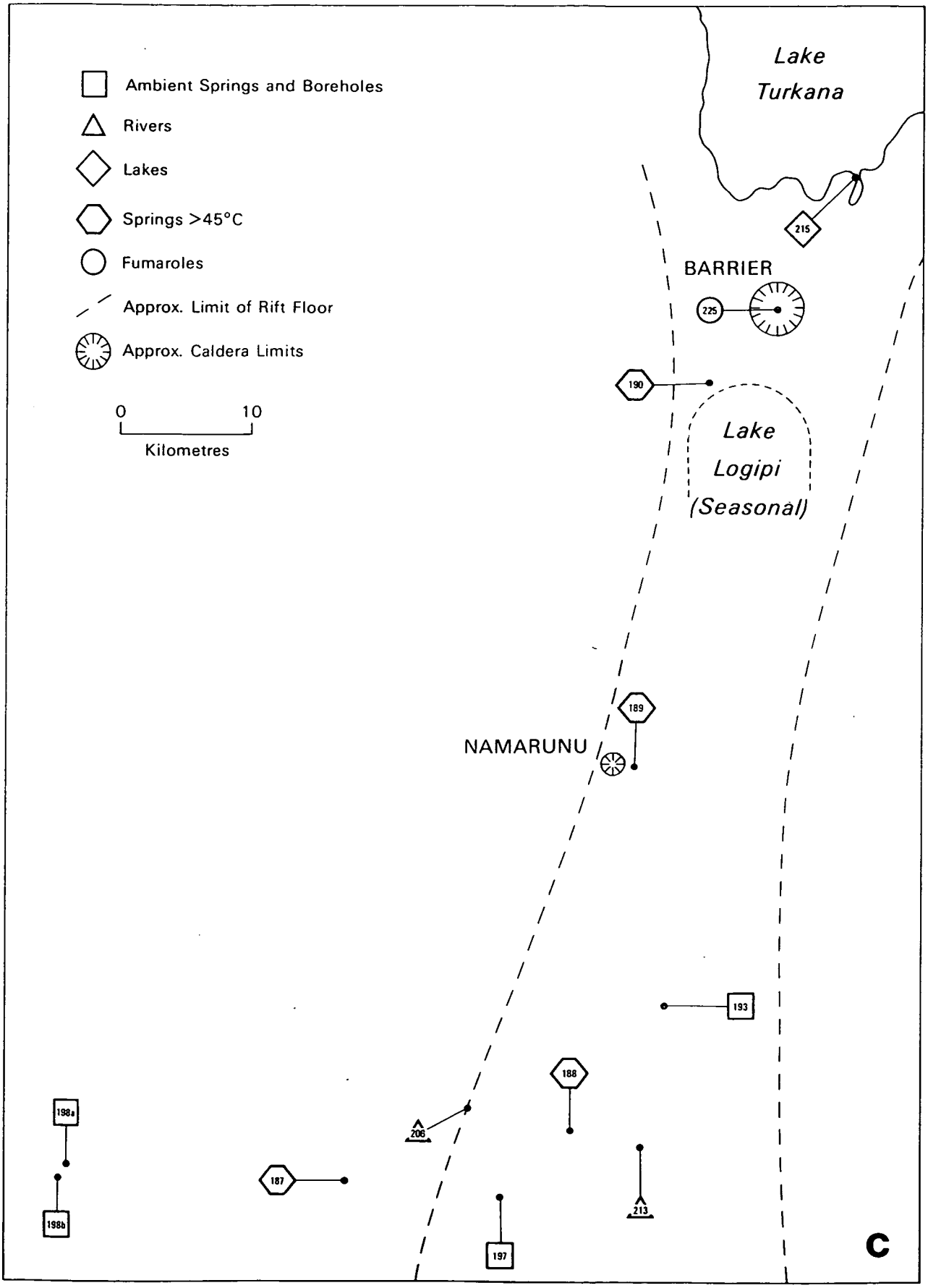

7.1(a)-(c) Map showing location of samples and sample type.

Table 7.1 Chemistry of waters in mg l^{-1}

No.	Locality	Temp °C	pH	Na	K	Ca	Mg	HCO_3	Cl	SO_4	Si	Li	B	F
HOT SPRINGS														
45	Lorusio[a]	81.0	7.65	2150	57.0	3.0	0.2	4710	295	197	35.7	0.96	0.96	
45	Lorusio[b]	82.2	7.45	2120	55.8	3.0	0.2	5000	300	200	33.2	0.96	0.92	48
48a	Kapedo[a]	50.0	8.25	988	22.0	1.6	0.6	2000	215	80.0	35.6	0.06	0.87	
48a	Kapedo[b]	50.8	8.25	1020	22.7	1.6	0.5	2140	210	83.0	33.0	0.05	0.92	28
48a	Kapedo[c]	50.0	8.35	994	23.3	1.7	0.6	2110	240	83.4	36.1	0.05	0.88	27
71a	Ol Kokwe Island[b]	95.8	6.90	22.1	4.5	1.5	0.5	121	1.4	76.1	38.3	0.02	<0.06	0.42
71b	Ol Kokwe Island[a]	94.0	9.10	832	36.0	0.5	<0.7	1960	260	40.0	87.0	0.56	1.04	
71b	Ol Kokwe Island[b]	96.0	9.05	922	39.3	1.0	<0.1	1980	260	30.5	126	0.61	1.19	19
71c	Ol Kokwe Island[b]	96.0	6.40	38.7	7.6	23.3	9.2	<1	6.2	1510	116	0.04	<0.06	5.4
183	Kapedo Spr SL26/2[c]			963	22.9	2.2	0.3	1900	250	84.9	41.0	0.07	0.94	28
184	Kapedo Spr SL27/5[c]	44.6	8.25	913	20.1	2.3	<0.1	1720	220	82.4	48.7	0.15	0.86	29
185	Suguta Spr SV3a[c]	68.4	8.25	1160	12.2	1.0	<0.1	2290	250	140	54.0	0.26	0.78	53
186	Suguta Spr SV3b[c]	64.0	8.30	1146	13.2	1.1	<0.1	2220	265	138	53.9	0.24	0.72	46
187	Kamuge Spr[c]	50.4	7.75	925	6.9	4.2	1.3	1930	160	100	38.4	0.22	0.47	37
188	Kageinya Spr[c]	67.8	9.50	5420	85.5	3.0	0.3	3350	2280	3700	81.5	0.23	13.6	190
189	Namarunu Spr[c]	66.2	8.80	5500	113	0.5	0.2	5860	3200	814	26.0	<0.01	6.53	140
190	Logipi Sprs[c]	61.4	8.30	4170	79.4	0.5	0.1	5160	3420	590	18.5	0.05	5.11	110
COOL SPRINGS														
138	Nginyang-Kapedo[b]	36.0	8.30	991	21.3	2.8	2.1	2140	200	80.7	32.7	0.05	0.82	26
139	Churo[b]	28.0	7.20	131	4.5	1.7	0.3	326	13.9	4.8	24.9	<0.01	<0.06	1.2
139	Churo[c]		8.15	133	4.7	1.6	0.3	313	17.5	5.0	24.3	<0.01	<0.06	1.1
140	Ebirisat[b]	37.5	9.00	178	1.9	0.4	<0.1	435	23.0	7.1	19.3	<0.01	<0.06	0.14
191	Nangarwa Spr[c]		8.85	153	2.4	0.5	<0.1	340	30.0	8.5	18.4	<0.01	<0.06	2.1
192	Amaya Spr[c]		8.35	142	3.0	0.8	0.1	328	20.0	7.7	15.6	<0.01	<0.06	1.9
193	N. Samburu Gates Spr[c]		8.85	638	4.7	4.9	1.2	1260	141	140	26.0	<0.01	0.53	19
194	Kachurkolh Spr[c]	31.0	9.15	1450	10.6	3.8	1.4	3370	191	126	10.0	0.61	0.06	18

Table 7.1 (Cont'd)

No.	Locality	Temp C	pH	Na	K	Ca	Mg	HCO_3	Cl	SO_4	Si	Li	B	F
195	Kalnangi Spr[c]	31.7	9.15	1040	18.0	0.5	<0.1	2880	260	102	36.0	0.16	1.04	35
196	Amakat Spr[c]		9.80	353	10.7	4.8	0.8	577	125	88	9.1	<0.01	1.09	16
197	S. Nangarabat Sprs[c]	31.1	9.15	1680	24.9	0.6	0.2	3440	370	213	25.3	0.02	1.80	60
198a	Napeiton Sprs[c]	32.5	7.80	351	6.2	5.1	2.6	731	65.0	47.7	29.9	0.06	0.06	14
198b	Napeiton Well[c]	37.2	7.60	468	8.0	7.1	4.3	855	155	77.5	28.3	0.06	0.08	14
198b	Napeiton Well[d]	36.8	7.80	471	7.8	7.1	4.2	899	156	79.7	27.2	0.061	0.08	
199	Nasaken Spr[c]	31.0	7.50	104	6.6	15.6	1.6	260	15.0	16.6	28.0	0.06	0.04	7.7
WELLS														
131	Kampi Ya Samaki[b]		7.70	263	21.0	18.8	16.7	727	55	22.7	31.1	0.05	0.13	43.0
131	Kampi Ya Samaki[d]		8.15	227	18.5	16.0	13.9	637	46.8	11.4	29.2	0.04	0.12	
132	Chesirimion B/h[b]		7.20	94.8	7.4	2.2	1.1	199	14.4	9.6	43.1	0.03	0.06	3.60
132	Chesirimion B/h[c]	34.0	7.10	107	7.5	2.4	1.2	235	21.0	9.5	50.4	0.04	0.07	3.5
133	Tangulbei B/h[b]	30.2	7.70	164	5.4	27.0	21.3	556	26.5	11.7	23.7	<0.01	<0.06	0.90
134	Kokwo Toto B/h[b]	28.0	7.05	76.0	11.3	69.4	11.7	399	10.7	3.3	31.2	<0.01	<0.06	1.28
135	Orus Solar B/h[b]	28.0	7.00	139	10.5	37.6	12.3	483	31.7		27.8	<0.01	<0.06	1.40
136	Orus Hand B/h[b]	28.0	6.45	49.2	5.0	8.8	3.4	121	18.8	6.6	23.3	<0.01	<0.06	0.76
137	Katangora B/h[b]	36.0	8.30	122	10.9	7.2	3.3	266	48.2	12.7	13.7	<0.01	<0.06	3.76
200	Kositei Project Well[b]		7.35	104	6.1	28.9	6.9	360	17.5	7.5	40.7	0.01	<0.06	3.1
201	Kositei Mission Well[b]		7.25	168	6.2	26.9	7.6	478	12.5	33.9	33.0	0.04	<0.06	2.2
202	Kositei B/h[b]	35.8	8.95	224	1.8	0.8	<0.1	482	15.5	15.8	23.5	0.08	0.06	11
203	Nginyang School B/h[c]			893	4.7	1.4	1.1	1950	100	85	18.5	0.06	0.21	20
204	Nginyang Poly. B/h[c]	35.5	8.40	1500	10.4	2.4	1.1	3490	218	165	18.7	0.09	0.23	44
204	Nginyang Poly. B/h[d]	34.0	8.45	1500	8.1	2.03	0.9	3460	195	145	17.6	0.08	0.21	
205	Chemolingot B/h[c]	37.7	8.35	269	3.1	2.9	0.5	614	20.5	27.1	24.1	0.04	0.06	5.4

Table 7.1 (Cont'd)

No.	Locality	Temp C	pH	Na	K	Ca	Mg	HCO_3	Cl	SO_4	Si	Li	B	F
RIVERS														
141	Ndau[b]		8.85	24.3	5.2	21.9	4.4	133	5.5	3.2	16.4	<0.01	<0.06	0.45
142	Tigeri[b]		7.65	10.7	4.9	7.2	1.4	483	3.7	1.9	14.3	<0.01	<0.06	0.40
144	Arabel[b]		8.55	47.1	7.4	8.0	2.7	101	37.0	1.8	13.2	<0.01	<0.06	0.52
145	Itwa[b]		8.60	91.2	8.2	5.5	2.3	500	25.3	2.5	18.8	<0.01	<0.06	0.86
146	Kabarmel[b]		8.05	45.4	10.0	16.8	3.9	135	26.4	8.6	18.8	<0.01	<0.06	0.35
147	Mukutan[b]		8.15	79.1	9.4	15.9	3.2	222	21.3	4.1	11.0	<0.01	<0.06	1.20
149	Cheptopokwo[b]		7.95	21.4	6.7	14.9	2.8	102	5.3	4.1	15.5	<0.01	<0.06	0.76
206	Suguta 1[c]			1150	21.6	3.1	1.9	2460	288	124	31.0	-	-	44
207	Suguta 2[c]			1030	24.0	3.9	1.9	2200	246	98.5	33.5	-	-	36
208	Suguta 3[c]			1104	20.3	3.4	1.7	2340	267	115	34.6	-	-	90
209	Suguta 4[c]			1093	22.4	3.8	2.1	2380	273	104	30.3	-	-	42
210	Suguta Trib.[c]			1340	20.1	1.6	0.3	2930	350	142	30.2	-	-	47
211	River Gerau[c]		8.70	54	9.0	12.5	3.6	128	28.5	5.0	12.3	-	-	0.83
212	River Amaya[c]			158	8.7	7.6	2.1	389	26.0	7.2	20.7	-	-	2.1
213	River Namarangule[c]		8.30	-	-	-	-	-	-	-	-	-	-	-
214	River Naliyo[c]		8.50	65	10.4	16.5	3.0	152	16.3	15.8	9.7	-	-	0.78
LAKES														
70	Baringo[a]		8.95	241	18.8	11.2	5.2	546	65	23	14.5	<0.01	0.15	-
150	Baringo[b]		9.05	192	15.4	9.2	2.5	384	48.5	19.7	15.2	0.01	0.14	6.40
150	Baringo[d]		9.00	231	18.0	12.3	4.3	495	54.8	20.1	14.9	<0.01	0.14	
215	Lake Turkana[c]			985	20.5	3.8	2.5	1580	515	43.3	12.0	<0.01	0.72	21
216	Lake Baringo north[c]		8.85	192	14.3	11.0	3.5	399	46	17.0	12.9	<0.01	0.11	7.1
217	Lake Baringo south[c]		8.75	170	14.9	11.3	3.5	375	44	15.3	13.8	<0.01	0.10	6.3

Year of Sampling: [a] - 1986, [b] - 1988, [c] - 1989, [d] - 1991

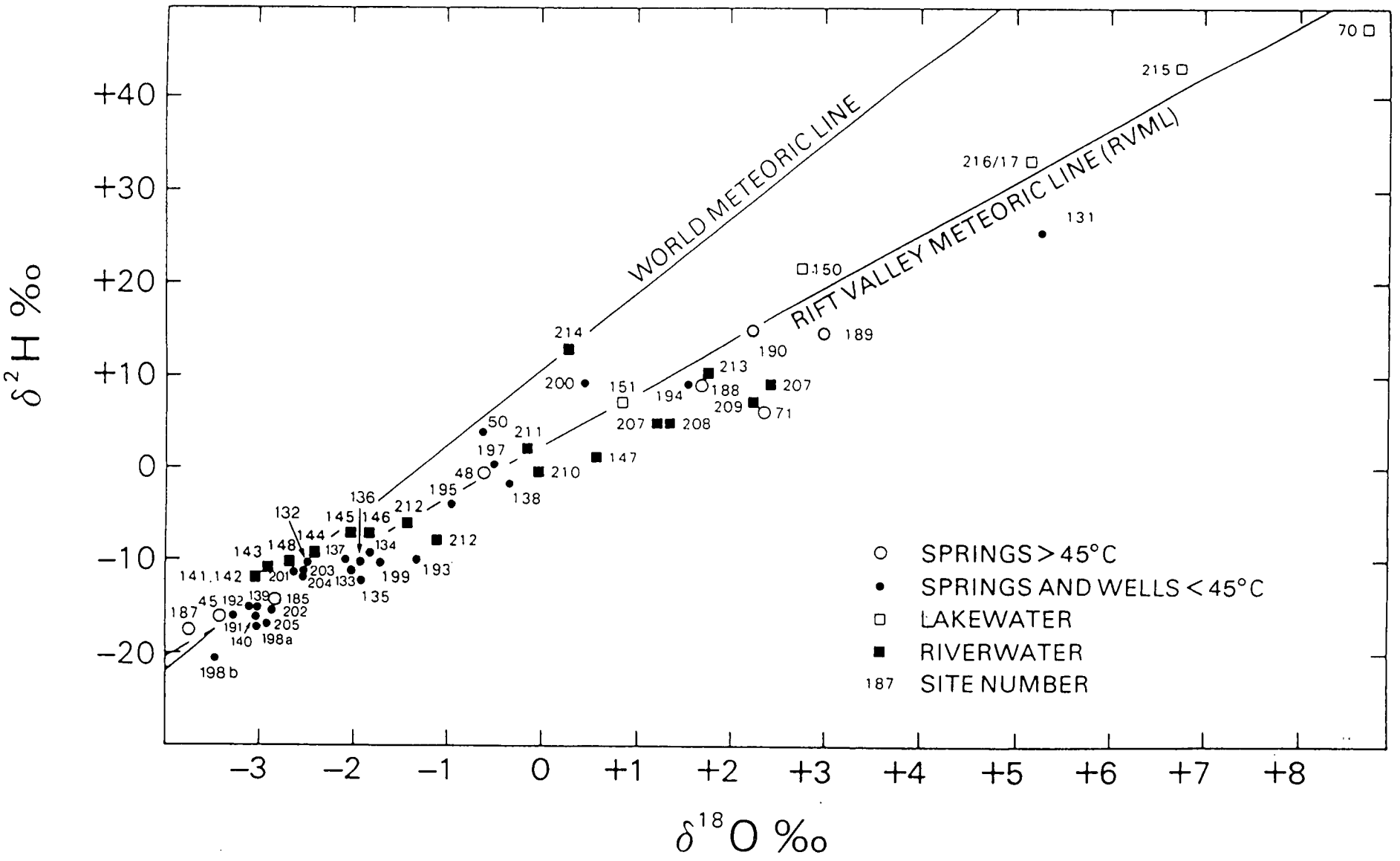

7.2 Plot of δ^2H vs $\delta^{18}O$ for all waters (values in permil with respect to SMOW).

northern part of the project area raises the potential for evaporation, and this is demonstrated by the isotopic composition of the rivers draining the eastern rift flanks (Table 7.2), particularly the Namarangule and the Naliyo (213, 214). Though rivers are not shown, the plot of $\delta^{18}O$ vs Cl^- (Figure 7.3) shows that isotopic enrichment at low chloride levels is an evaporitic trend.

The Suguta River flows perennially through the area because it is fed to a great extent by the Kapedo hot springs. By the time it reaches the area southwest of Emuruangogolak (207), total dissolved solids (TDS) have risen to somewhat in excess of the Kapedo value. The small tributary (210) joining near this point has a TDS significantly higher, but insufficient volume to affect the main river greatly. It probably consists largely of alkaline spring outflow. The main Suguta River flows past some hot springs northwest of Emuruangogolak just downstream of rapids formed by the edge of a lava flow. The springs (185, 186) have a similar chemistry to the river, but a depleted isotope composition. Their contribution to the river between sites 209 (upstream) and 208 (downstream of the springs) is enough to affect its isotopic composition slightly.

As would be expected from the high potential for evaporation, the river reaches a higher TDS and heavy isotope composition further to the north (206) before it disappears into the floor of the Suguta Valley or, when the seasonal Lake Logipi is large enough, reaches the lake through various distributaries.

Lake Turkana (215) is the next permanent water body to the north, and is situated well outside the project area. It is fed chiefly by the Turkwel and Omo rivers, the chemical and isotopic composition of which are not well known. From isotopic evidence (Figure 7.2), it is clear that the lake contains evaporated water.

Lake Logipi is separated from Lake Turkana by the Barrier volcano and is a shallow, seasonal lake fed at least partly by hot springs on the southern flanks of the Barrier (190). No data were obtained for lake chemistry because it was considered that such a shallow body of water would have suffered excessive modification by evaporation in such a hot part of the Rift.

7.2.3 Surface Waters - Summary

Lake Baringo is a freshwater lake whose chemistry is primarily the product of the rift flank rivers feeding it, with only very minor volcanic influences. Its isotopic and chemical compositions fluctuate seasonally because of the relatively small amount of water in the lake; the fluctuations are predictable, i.e. a higher TDS and heavy isotope content after evaporation in the dry season, followed by renewed dilution in the following wet season.

In the northern part of the project area, seasonal rivers draining the eastern rift flanks suffer evaporation progressively to the north, and terminate on the rift floor. Western seasonal rivers (Cheptopokwo, Nginyang) join the outflow from Kapedo to form the permanent Suguta River with a high TDS, which is further raised by outflows from ambient and thermal springs.

7.3 Groundwater, Ambient and Near-Ambient

This section deals with groundwater within the range of 28-38°C, i.e. from ambient to slightly thermal sources. In terms of temperature distribution there is a clear cut-off between 38°C and 45°C, which is taken as the minimum temperature to define a hot spring.

7.3.1 Springs

A group of springs from the eastern rift flanks (139, 140, 191, 192) defines with excellent precision the isotope values for rift flank groundwaters in the southeastern part of the project area (-16‰ δ^2H, -3.1‰ $\delta^{18}O$; Table 7.2). Such

Table 7.2 Hydrogen, oxygen and carbon stable isotope values for surface and groundwaters. In permil with respect to SMOW or PDB as appropriate.

No.	Locality	Temp °C	δ^2H	$\delta^{18}O$	$\delta^{13}C_{DIC}$
HOT SPRINGS					
45	Lorusio[a]	81.0	-23	- 3.1	
45	Lorusio[b]	82.2	-16	- 3.4	- 2.6
45	Lorusio[d]	81.0	-15	- 3.6	
48a	Kapedo[a]	50.0	- 7	- 3.5	
48a	Kapedo[b]	50.8	+ 2	- 0.5	- 4.1
48a	Kapedo[c]	50.0	- 2	- 0.9	- 3.3
48b	Kapedo[b]	50.0	- 3	- 0.6	
48c	Kapedo[b]	50.0	- 1	- 0.5	
71a	Ol Kokwe Island[b]	95.8	+15	+ 5.9	
71b	Ol Kokwe Island[a]	94.0	+ 7	+ 1.3	
71b	Ol Kokwe Island[b]	96.0	+ 4	+ 3.5	
71c	Ol Kokwe Island[b]	96.0	+11	+ 3.7	
183	SL26/2[c]	45.0	- 3	- 0.7	
184	SL27/5[c]	45.0	- 2	- 0.9	
185	Suguta SV3a[c]	68.4	-13	- 2.7	- 4.2
186	Suguta SV3b[c]	64.0	-14	- 2.8	
187	Kamuge[c]	50.4	-19	- 3.7	- 4.7
188	Kageinya[c]	67.8	+ 9	+ 1.7	- 4.0
189	Namarunu[c]	66.2	+14	+ 3.0	- 0.9
190	Logipi[c]	61.4	+15	+ 2.2	- 1.2
COOL SPRINGS					
50	Kapedo[b]	27.0	+ 4	- 0.7	
138	Nginyang-Kapedo[b]	36.0	- 2	- 0.3	
139	Churo[b]	28.0	-15	- 3.0	-11.6
139	Churo[c]		-15	- 3.1	-12.5
140	Ebirisat[b]	37.5	-16	- 3.1	-14.9
191	Nangarwa[c]		-16	- 3.3	-11.7
192	Amaya[c]		-15	- 3.2	-10.6
193	N. Samburu Gates[c]		-10	- 1.3	- 6.6
194	Kachurkolh[c]	31.0	+ 9	+ 1.6	- 0.5
195	Kalnangi[c]	31.7	- 4	- 0.9	- 2.7
196	Amakat[c]		+54	+12.0	- 9.3
197	S. Nangarabat[c]	31.1	0	- 0.5	- 2.8
198a	Napeiton[c]	32.5	-17	- 3.0	
199	Nasaken[c]	31.0	-10	- 1.7	- 8.7
WELLS					
131	Kampi Ya Samaki[b]		+27	+ 5.5	
131	Kampi Ya Samaki[d]		+25	+ 4.9	- 6.2
132	Chesirimion B/h[b]		-11	- 2.6	-14.9
132	Chesirimion B/h[c]	34.0	-10	- 2.3	-13.8
133	Tangulbei B/h[b]	30.2	-11	- 2.0	-13.7

Table 7.2 (Cont'd)

No.	Locality	Temp C	δ^2H	$\delta^{18}O$	$\delta^{13}C_{DIC}$
134	Kokwo Toto B/h[b]	28.0	- 9	- 1.8	-14.6
135	Orus solar B/h[b]	28.0	-12	- 1.9	-15.8
136	Orus hand B/h[b]	28.0	-10	- 1.9	-15.4
137	Katangora B/h[b]	36.0	-10	- 2.1	- 9.6
198b	Napeiton h/p[c]		-18	- 3.3	- 8.2
198b	Napeiton h/p[d]	36.8	-23	- 3.7	
200	Kositei Project[c]		+ 9	+ 0.5	
201	Kositei Mission[c]		-12	- 2.7	
202	Kositei B/h[c]	35.8	-15	- 2.9	-11.6
203	Nginyang Sch. B/h[c]		-11	- 2.5	- 9.9
204	Nginyang Poly B/h[c]	35.5	-11	- 2.3	-10.0
204	Nginyang Poly B/h[d]	34.0	-12	- 2.8	-10.6
205	Chemolingot B/h[c]	37.7	-17	- 2.9	-11.7
RIVERS					
141	Ndau[b]		-12	- 3.0	
142	Tigeri[b]		-12	- 3.0	
143	Molo[b]		-11	- 2.9	
144	Arabel[b]		-10	- 2.4	
145	Itwa[b]		- 7	- 2.0	
146	Kabarmel[b]		- 7	- 1.8	
147	Mukutan[b]		+ 1	+ 0.6	
148	Nginyang[b]		-11	- 2.7	
189	Cheptopokwo[b]		- 6	- 1.4	
206	Suguta 1[c]		+ 9	+ 2.5	
207	Suguta 2[c]		+ 5	+ 1.3	
208	Suguta 3[c]		+ 5	+ 1.4	
209	Suguta 4[c]		+ 7	+ 2.3	
210	Suguta Tributary[c]		- 1	0.0	
211	Gerau[c]		+ 2	- 0.1	
212	Amaya[c]		- 8	- 1.1	
213	Namarangule[c]		+10	+ 1.8	
214	Naliyo[c]		+13	+ 0.3	
LAKES					
70	Baringo[a]		+47	+ 8.8	
150	Baringo[b]		+21	+ 2.8	
150	Baringo[d]		+40	+ 7.6	
151	Tilam[b]		+ 7	+ 0.9	
215	Turkana[c]		+43	+ 6.8	
216	Baringo N.[c]		+32	+ 5.3	
217	Baringo S.[c]		+34	+ 5.0	

Year of Sampling: [a] - 1986, [b] - 1988, [c] - 1989, [d] - 1991

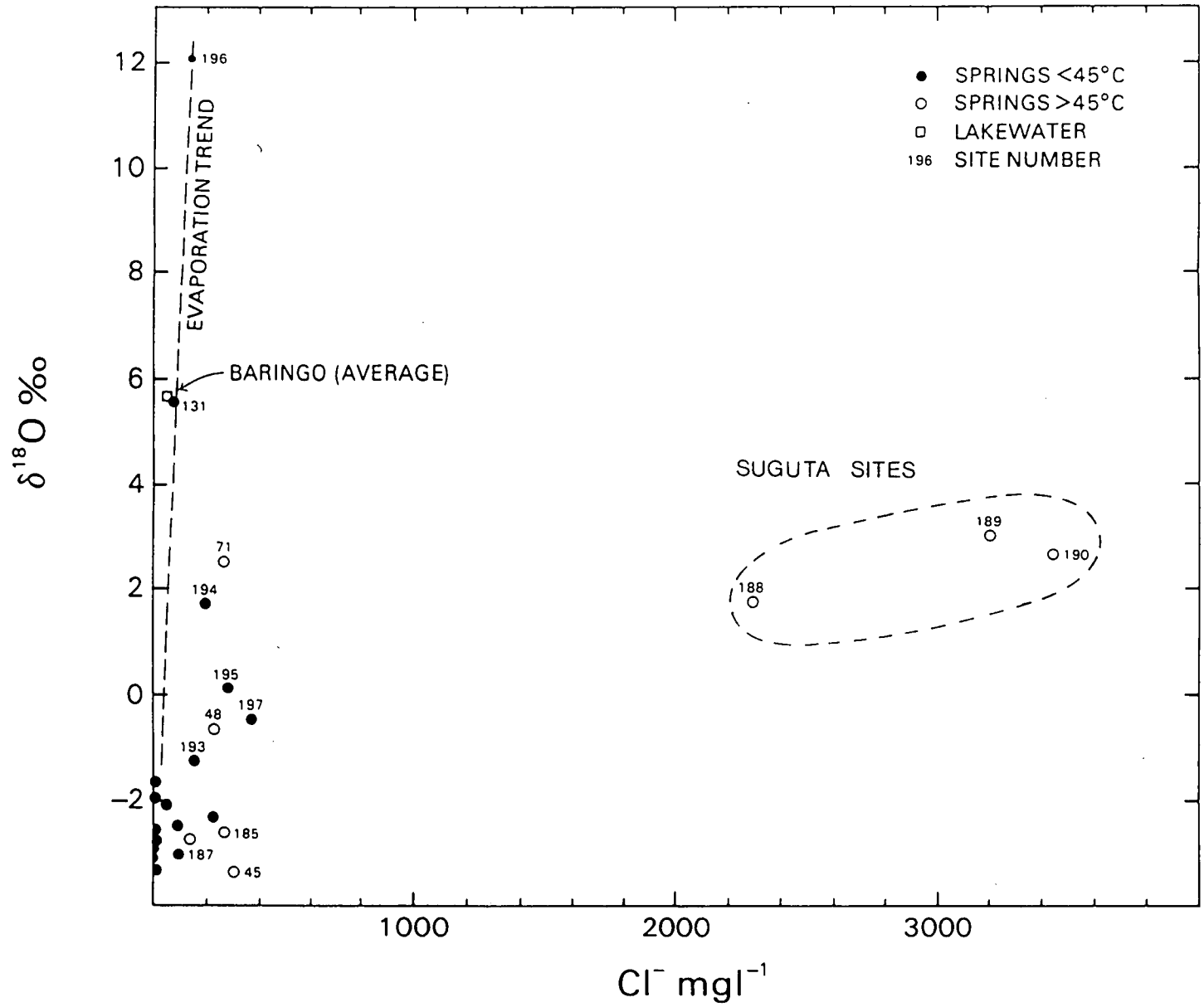

7.3 Plot of $\delta^{18}O$ vs Cl^- for groundwaters (values in permil SMOW and mg l^{-1}).

values are compatible with the meteoric line calculated for the whole of the rift (Allen et al., 1989) and, if fed into the altitude/isotope correlation developed in that report, give a plausible average recharge altitude of some 1800 m.

Some springs on both flanks were little more than seepages (N. Samburu Gates, Napeiton, Nasaken; 193, 198, 199) and may have been affected by evaporation. This could account for slightly enriched values at N. Samburu Gates and Nasaken, although Napeiton has very similar isotope values to the southeastern springs despite its situation in the northwest of the area. This implies there is relatively little difference in meteoric water isotope values between any parts of the rift flanks within the project area. Chemically, however, there is a difference: the TDS at Napeiton is about twice the level in the southeastern springs and contains detectable Li, B and F (Table 7.1). Values of δ^{13}C-DIC in the southeastern springs are low (Table 7.2), averaging -12.3‰ and therefore typical of fairly unmodified meteoric water. No δ^{13}C-DIC sample was collected at the Napeiton seepage, but one from a nearby well (with a slightly more depleted ^{2}H and ^{18}O isotopic composition) gave a value of -8.2‰. This, combined with the chemical differences, indicates that the northwestern water may have circulated to greater depths down rift boundary faults before cooling and reaching the surface again.

The other springs are situated on the rift floor, except for Kachurkolh (194) where the sample was drawn from the side of a pool and may have been mixed with evaporated water.

Of the samples from the rift floor, Amakat pool (196) has suffered excessive evaporation (Figure 7.3) but its TDS remains relatively low and it probably consists largely of rainwater. The spring at the Nginyang-Kapedo confluence (138) despite a temperature of 36°C has much in common with the Kapedo hot springs and will be treated with those in Section 7.4. This leaves the Kalnangi and S. Nangarabat springs for consideration (195, 197). Each source is associated with water flowing out from beneath lava flows north of Silali and Emuruangogolak respectively. Each has a comparable TDS, chemistry and stable isotopic composition (Tables 7.1, 7.2) and from their locations could be assumed to represent cooled outflow waters from the Silali and Emuruangogolak hydrothermal systems, though such an interpretation is not supported by detailed examination of the chemistry. Figure 7.3 shows that the waters have been modified by an evaporative process. On a plot of δ^{13}C-DIC vs HCO_3^- (Figure 7.4), both springs fall on the dissolution trend among the hot springs. The implications of this will be further considered in 7.4 below.

7.3.2 Wells

All of the wells sampled were situated on the rift floor in the southern part of the area, except for Napeiton (198b) on the northwestern rift flanks. Most were boreholes with motorised pumps, though two boreholes were hand-pumped (Napeiton and Orus, 136). Two dug wells at Kositei (200 and 201) were included in the survey. The wells can conveniently be divided into two main groups, one to the east of the volcanic centres, the other to the west. Napeiton and Kampi Ya Samaki (131) are not included in these groups and are considered separately.

The eastern group of wells presents a coherent body of data in both chemical and isotopic terms (Tables 7.1, 7.2). The isotope values indicate that, unless the water has suffered mixing, recharge has taken place at a lower average altitude than the rift-flank springs considered earlier. This would be consistent with recharge taking place on the lower flanks (and possibly the volcanic centres) or the rift floor. The chemical analyses reveal a good-quality drinking water low in F^- and this, together with low δ^{13}C-DIC values (Table 7.2) indicates that the eastern wells in this area contain relatively unmodified meteoric water. Even Katangora (137), relatively close to Paka and

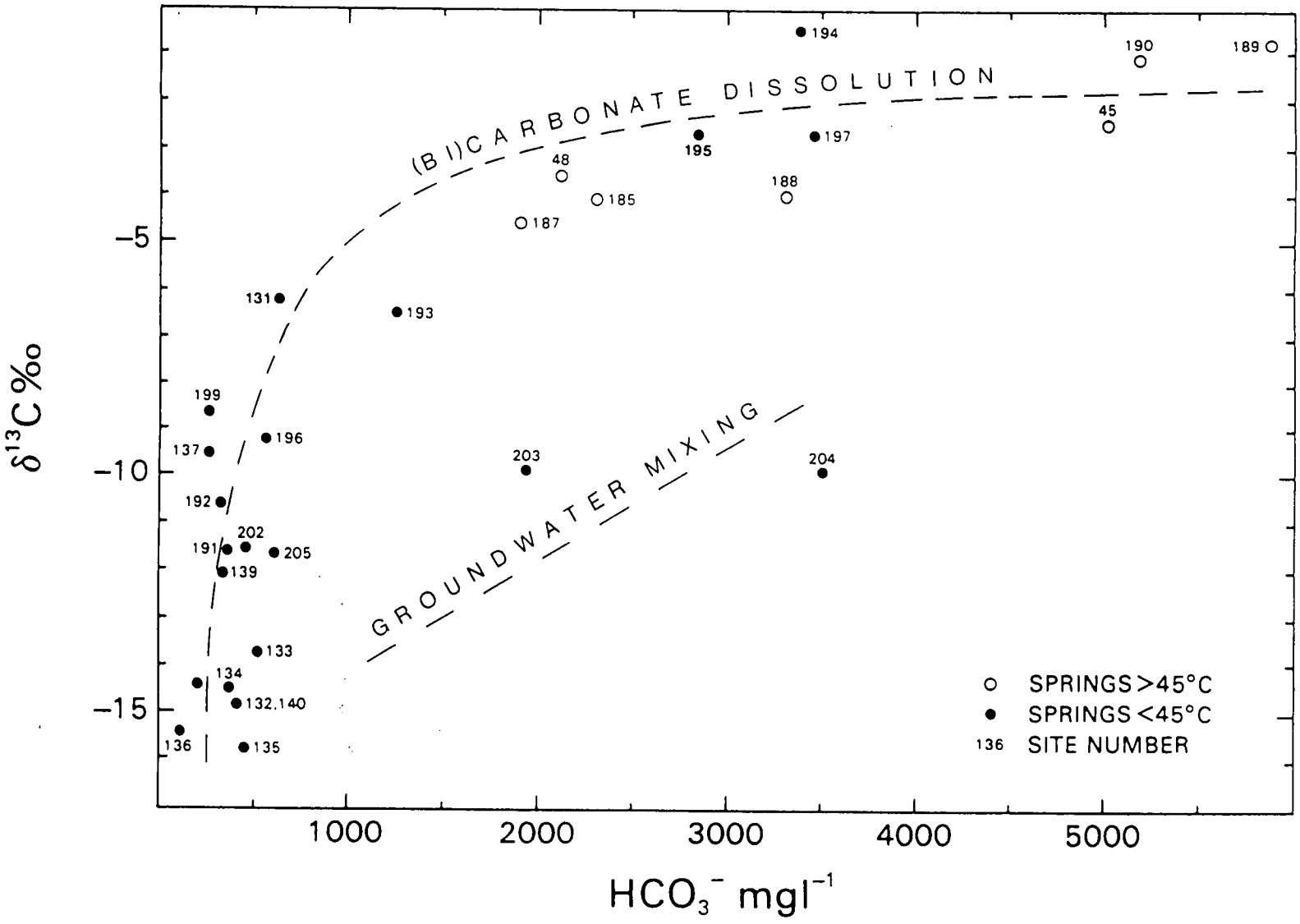

7.4 Plot of $\delta^{13}C$ vs HCO_3^- for groundwaters (values in permil PDB and mg l^{-1}).

with a slightly elevated temperature of 36°C shows no influences beyond higher than average F^- and δ^{13}C-DIC values.

Western wells are more variable. Kositei and Chemolingot (202, 205) are similar in terms of chemistry and H, O and C isotopes (Tables 7.1, 7.2), but not in location (Figure 7.1). Their isotope values suggest an origin for the water on the higher western rift flanks. This is plausible for Kositei but less easy to explain for Chemolingot. Chesirimion and the Nginyang wells (132, 203, 204) have H and O stable isotope values consistent with a greater rift-floor contribution from rainfall, but resemblances end there. While Chesirimion water is similar to the eastern wells, the two Nginyang wells are extremely high in HCO_3^- (Table 7.1). The reasons for this are not immediately obvious; carbon isotope values are not especially elevated and the Nginyang well waters are the only samples which do not follow the dissolution relationship noted for δ^{13}C-DIC and HCO_3^- (Figure 7.4). However, this is treated in more detail in Section 7.4 below.

The Napeiton hand-pumped well (198b) is interpreted in a similar way to the spring considered earlier, i.e. a rift flank groundwater which has undergone deep circulation and evolution. Kampi Ya Samaki (131) is a borehole situated adjacent to Lake Baringo. The possibility that the isotope composition of this water might represent a time-averaged composition for lakewater seems to be confirmed by Figure 7.3 where the Kampi Ya Samaki sample and Baringo average of samples collected in 1986, 1988 and 1989 overlap on a plot of δ^{18}O vs Cl^-.

7.3.3 Ambient Groundwater - Summary

Rift flank spring data are mostly consistent with a relatively local and unmodified meteoric origin. Kachurkolh and Napeiton on the eastern and western flanks respectively have indications of deeper circulation than the other springs. The Rift floor springs of Kalnangi and S. Nangarabat are not notably thermal although they share some chemical characteristics with hot springs, probably owing to dissolution of evaporites.

Wells to the east of the volcanic centres are consistent in their geochemistry and appear to be recharged locally by meteoric water. Wells to the west are more variable. The two Nginyang boreholes fail to obey the usual relationship between δ^{13}C-DIC and HCO_3^-. Kampi Ya Samaki draws its water mainly from Lake Baringo.

Hydrogeological indications based on water levels and topography are that axial flow of groundwater from south to north tends to take place to the west of the volcanic centres (see Section 6.2.2). The differences between the eastern and western well chemistries are no doubt related to this situation. However, although there are many indications (hydrogeological and geochemical) that subsurface outflow to the north is taking place from Lake Baringo, there is no evidence from stable isotopes that any well penetrates the lakewater plume or mixing zone.

7.4 Thermal Groundwater

Waters of 45°C and over are not necessarily found in close association with volcanic centres (Figure 6.2). On the basis of their chemistry, they can be divided into all hot springs within the project area, and the few hot springs outside to the north, i.e. Kageinya, Namarunu and Logipi.

7.4.1 Hot Springs within the Project Area

This category will include some of the cooler waters which have a similar chemistry to the hot springs.

Plots of bicarbonate and sulphate vs Cl^- prove to be a useful way of differentiating the various waters (Figure 7.5). This shows that thermal waters are quite distinct from most ambient waters, and that there is no trend between the groups, except for one case (Napeiton, 198b). Cool waters that plot in the hot spring field include the Nginyang wells (203, 204), Kalnangi and Nangarabat springs (195, 197), and Kachurkolh spring (194). Each has an enriched δ^{13}C-DIC that fits the observed trend (Figure 7.4) except for the Nginyang wells, as has been mentioned above. The exact relationship of the various waters and their links (if any) with volcanically-driven hydrothermal activity will now be considered.

The disposition of thermal springs on a stable isotope crossplot is best seen in Figure 7.8. The waters cover a range from rift wall-like composition (Lorusio, 45 and Kamuge, 187) to enriched values (Ol Kokwe, 71 and Kageinya, 188) which must have a proportion of evaporated water. Of all the springs within the Project area, Ol Kokwe has the most enriched composition doubtless due to mixing with water from Lake Baringo either before or after heating (this is discussed in more detail in 7.7 below). The other thermal springs, and non-thermal springs of similar chemistry such as Kalnangi and S. Nangarabat (195, 197), are assumed to represent different amounts of mixing between underflow from Lake Baringo and meteoric water from the rift flanks or the volcanic centres. The percentage markings on Figure 7.8 refer to the proportion of lakewater in the springs; it can be seen that Kapedo (48) has some 30% lakewater as do the cool springs of Kalnangi and S. Nangarabat (195, 197). On the other hand springs like SV3 and Lorusio (185, 45) are nearer to the Rift wall and have little or no lakewater in their output.

This apparent mixing of water types is not reflected in chemical composition. All the thermal springs have TDS values in excess of 3000 mgl^{-1} which are dominated by Na^+ and HCO_3^- (the terms 'HCO_3^-' or 'bicarbonate' used here also denote any contribution to alkalinity by carbonate, the existence of which is pH-dependent). Although concentrations can be higher in the project area, for example ~7500 mgl^{-1} at Lorusio (45), and substantially higher in the Suguta Valley to the north (>13000 mgl^{-1}) there is no evidence of chemical mixing between different bodies of groundwater. For example, a plot of δ^2H versus Cl^- (Figure 7.6) shows no particular trend; what is does show is that while all waters are within the range of a rift wall-lakewater mixing series they can have a variable chemistry that is not the result of straightforward mixing.

However, all the thermal springs plot close to the theoretical sodium (bi)carbonate dissolution trend of Figure 7.4. It is assumed here for the purposes of modelling such dissolution that water with a typical unevolved, initially post-recharge composition of 250 mgl^{-1} HCO_3^- and -16‰ $\delta^{13}C_{DIC}$ (produced by a combination of soil zone CO_2 with alkaline earth carbonates) progressively acquires from evaporitic or other sources bicarbonate with a typical value of -1‰, resulting in the plotted curve. There is no *a priori* connection with geothermal activity other than that the hotter waters are likely to be more effective at redissolving bicarbonates, which in most cases will result in a significantly higher TDS and a somewhat higher $\delta^{13}C_{DIC}$ value. While there is no certain way of distinguishing whether near-ambient high TDS springs like Kalnangi and S. Nangarabat are cooled thermal waters, or merely waters which have resided long enough to acquire a greater than usual concentration of bicarbonate, a plot of HCO_3^- versus sampling temperature (not shown) reveals a generally linear trend except for sites like Kalnangi and S. Nangarabat, which on this empirical basis could have had maximum temperatures up to 65°C.

Since Na^+ and HCO_3^-/CO_3^{2-} are the dominant ions in virtually all Rift waters it is reasonable to suppose that sodium bicarbonate will dominate evaporitic deposits, as it does for example at Magadi in the southern Rift. Doubtless the ultimate source of the bicarbonate has been the ubiquitous volcanic activity in the Rift but, as stated above, it does not necessarily indicate a close association with present high-temperature geothermal activity. None

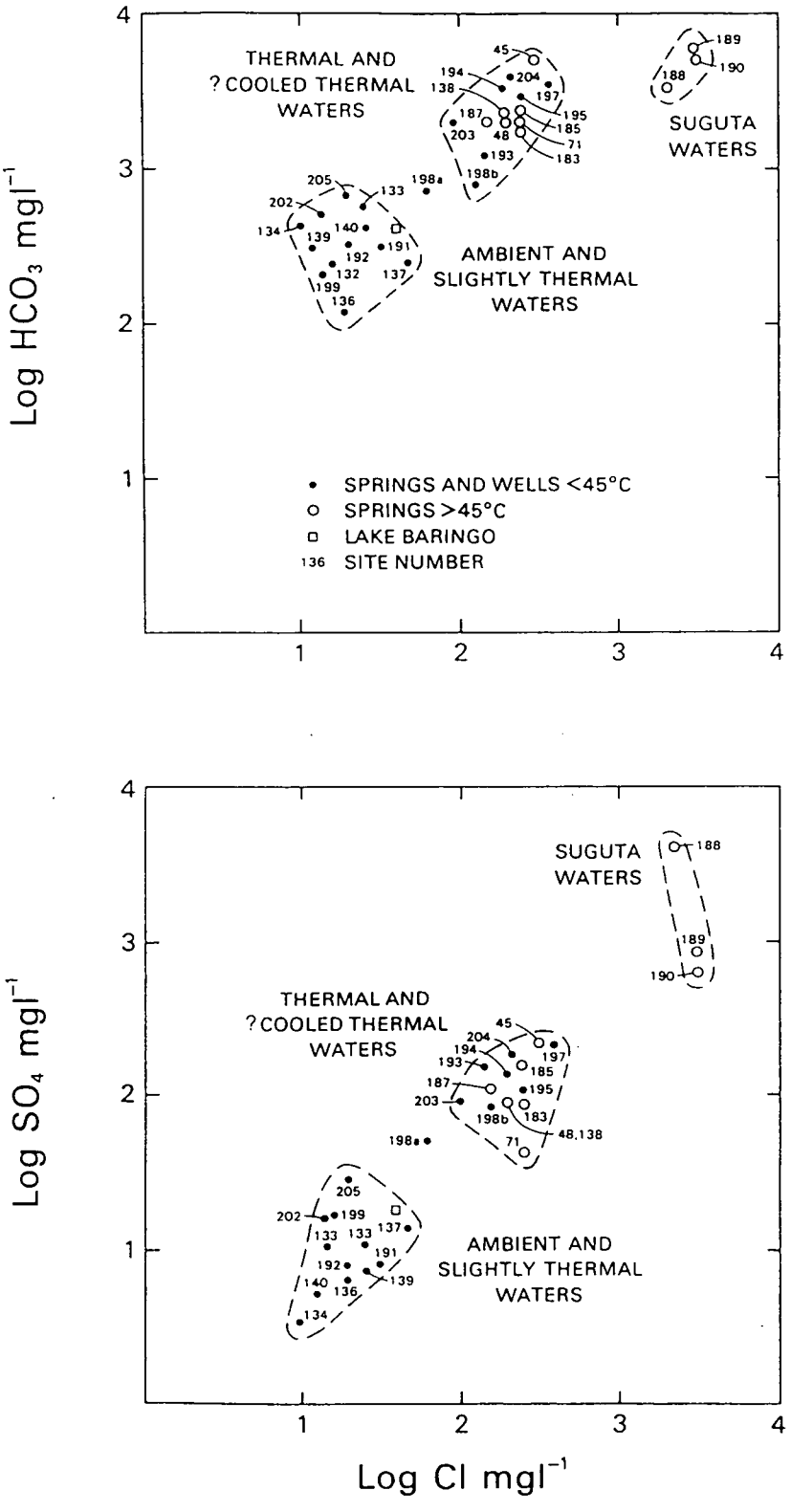

7.5 Plots of log HCO_3^- and SO_4^{2-} vs log Cl^- for groundwaters (values in mg l^{-1}).

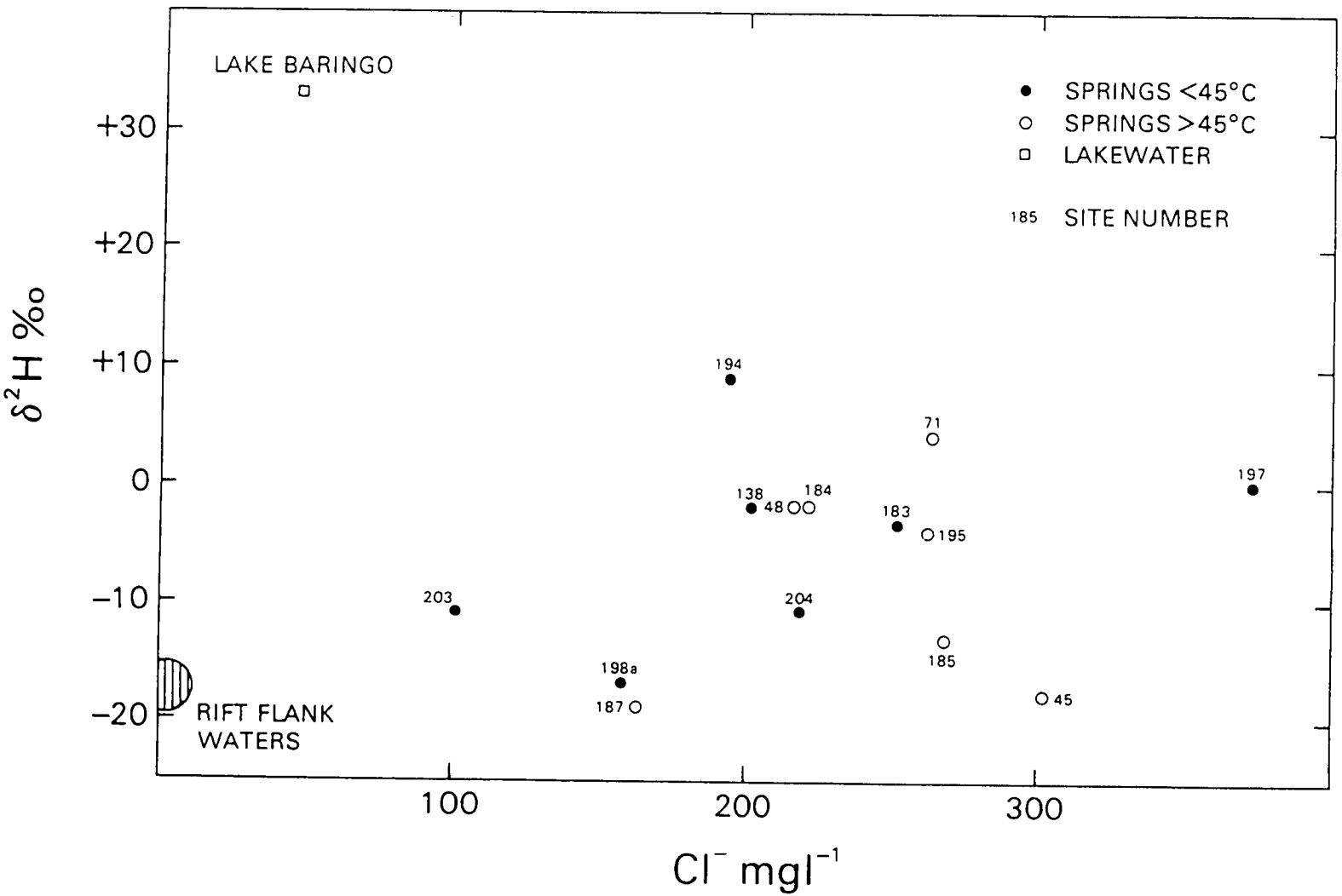

7.6 Plot of δ^2H vs Cl^- for hot spring and associated waters (values in permil SMOW and mg l^{-1}).

of the thermal springs shows evidence of being an outflow from a high-temperature (>150°C) system except for Ol Kokwe. The other thermal springs are likely to be simply the result of deep circulation, although there may be local zones of higher heat flow which have some magmatic characteristics such as at Lorusio with its abundant CO_2 gas and relatively high $^3He/^4He$ value.

As stated earlier, there is no reason why cool springs should not have a high bicarbonate content from evaporitic sources, and some do (Kalnangi, S. Nangarabat). The rather anomalous position of the two Nginyang wells (203, 204) in Figure 7.4 requires a different explanation. Both sites lie on mixing trends between background bicarbonate and evaporitic type waters. The simplest explanation is that water from the nearby R. Nginyang is infiltrating and mixing progressively with a high HCO_3^-/low $\delta^{13}C$ groundwater.

The source of the (bi)carbonate involved in the dissolution process is presumed to have been an enlarged Lake Baringo for most of the sites, although north of Emuruangogolak Lake Suguta would have been the source. Desiccation episodes during these higher lakestands would have caused the deposition of evaporites. It must however be noted that there is a possibility of high bicarbonate waters arising *in situ* from a combination of silicate breakdown caused by CO_2 flux and low rates of flushing by groundwater. This would not necessarily be easy to distinguish from the effects of evaporite dissolution. Lorusio (45) may be a case in point; it has the highest HCO_3^- concentration and CO_2 flux of all the springs in the project area.

7.4.2 Thermal Waters North of the Project Area

The springs at Kageinya, Namarunu and Logipi (188-190) have much higher TDS values (~15000 mgl^{-1}) than those in the project area. This whole zone of the northern Suguta Valley is the present terminal drainage area for the northern Rift and as such would have the greatest amount of salts available for recycling in thermal waters. It would be anticipated that during passage to this sump area (which in many respects resembles the Magadi basin of the southern Rift), waters forced by evaporation to precipitate some of their dissolved load would tend to precipitate bicarbonate before chloride. This may account for the fact that chloride increases relative to bicarbonate in the north, as is demonstrated in Figure 7.5.

These northern springs are found in association with the volcanic centres of Emuruangogolak, Namarunu and the Barrier (though not a very close association in the first case). They do not have any convincing indications of being high-temperature outflows though Namarunu and Logipi have high $^3He/^4He$ ratios. These areas will be considered in greater detail in the report of RVGP Phase III investigations.

7.4.3 Thermal Waters - Summary

Thermal and cooler waters with rather similar characteristics are found to the west and north of the Silali and Emuruangogolak volcanic centres. In terms of water content they appear to be the product of mixing between lake and meteoric waters, but their chemistry appears to be primarily the result of varying amounts of dissolution of evaporites presumably remaining from desiccation episodes when Lake Baringo was considerably higher than at present. There is no overt evidence of high-temperature geothermal activity in these springs except at Ol Kokwe; the main heating agent is probably deep circulation, though Lorusio with its 'magmatic' gas contents may represent a situation of locally higher heat flow.

The three sites to the north of the project area have higher TDS contents with proportionally higher Cl which indicates an evolution in the evaporite sequence towards the increasingly desiccated northern end of the Suguta Valley. None of these sites has strong evidence of high-temperature thermal activity.

7.5 Fumarole Condensates

Steam condensates were collected usually from the stronger fumaroles on each of the volcanic centres. The condensates received chemical and isotopic analysis, and the results are now treated separately.

7.5.1 Steam Condensates - Chemistry

Table 7.3 gives the results of fumarole steam condensate analysis for chemical and isotopic species. Several ions (K^+, Mg^{2+} and Li^+) were at or below detection limit in all fumarole samples and are not reported here. Generally speaking, the lower the pH and solute content of steam condensate, the less interference by shallow groundwaters has taken place. This is largely dependent on the strength of steam flows; weaker fumaroles are obviously more prone to dilution and condensation. In terms of crude ionic mgl^{-1} averages for each site, the order is Paka < Emuruangogolak < Silali < Korosi. Korosi fumaroles are therefore the weakest, and Paka fumaroles the strongest. This accords reasonably well with the field evidence.

Ammonia tends to partition into steam in inverse proportion to temperature. If crude averages are again taken, the temperature order is (from the highest) Paka > Emuruangogolak > Silali > Korosi. Since NH_3 makes up a fair proportion of the ionic content of most fumarole condensates, it is not surprising that the order is as before.

The use of ion ratios, particularly Na/K to provide some temperature information, would be desirable in theory. However, the analytical precision to attempt this cannot yet be routinely attained, and it must also be borne in mind that fumarolic steam may contain droplets of condensation which may have undergone re-equilibration with wall rock at a significantly lower temperature than the reservoir.

7.5.2 Steam Condensates - Isotopic Composition

Oxygen and hydrogen stable isotope data for all fumaroles are plotted in Figure 7.7. Also shown in the diagram are ambient groundwaters and lakewaters. The extreme range of water isotope values in the region are therefore demonstrated: from about +40 to -100‰ δ^2H, and about +8 to -18‰ $\delta^{18}O$. The results from the fumaroles cover more than two-thirds of each range.

It is clear that there is insufficient variation in local groundwaters to account for all the steam condensates by a simple process of primary steam separation from these waters. Firstly, there are fumarole samples more enriched in heavy isotopes than local ambient groundwater, the PK1 series (163-165), and secondly there are condensates so depleted that only waters from very high altitudes could explain them.

Figure 7.8 shows an expanded portion of Figure 7.7 to include the main group of fumaroles and the hot springs. Primary steam condensate curves are shown on the diagram based on 10% steps in a Rift flank-lakewater mixing series (a value based on the 1989 samples has been chosen to represent Lake Baringo). The method used is similar to the one employed by Darling et al. (1990). It is apparent that most of the fumaroles in the main group can be accommodated within this scheme, though not the PK1 series of Paka or the EM7 and EM9 series of Emuruangogolak. The EM9 series are not particularly strong fumaroles and may be explicable in terms of secondary steam origin (steam heated groundwater), but the Paka fumaroles are strong and high in CO_2 (Table 7.4) so a secondary origin can probably be ruled out. Only a water that had already lost steam could reach anywhere near a suitable isotopic composition to provide steam of the required values, but on the other hand the nearby fumaroles of the PK4 series just outside the main crater give 'normal' values, as do the PK7 series in the explosion crater to the southeast of the main crater.

Table 7.3 Fumarole condensate chemistry, ions in mg l^{-1}, stable isotopes in permil vs SMOW.

No.	Locality	Temp °C	pH	Na	Ca	Cl	SO_4	Si	B	F	NH_4-N	δ^2H	$\delta^{18}O$
FUMAROLE CONDENSATES													
152	Ol Kokwe OK 1	95.8	5.90	0.89	0.21	1.60	1.1	0.5	1.03	<0.05	38.2	-18	- 3.6
153	Korosi KR 10	85.5	5.60									-70	-10.6
154	Korosi KR 12	95.7	5.05	12.2	0.17	1.60	1.5	4.2	0.04	0.24	4.0	-38	- 7.1
155	Korosi KR 16	94.0	5.30	0.20	0.08	<0.20	0.8	<0.1	<0.03	<0.05	4.3	-48	- 8.8
156	Korosi KR 18	96.4		6.3	0.23	1.10	<0.8	3.1	<0.03	0.34	5.2	-55	- 9.5
157	Korosi KR 19	95.9	4.90	1.03	0.13	0.20	<0.8	0.2	0.20	<0.05	9.0	-50	- 9.0
158	Korosi KR 21	90.1	6.00	1.97	0.43	<0.20	<0.8	3.0	<0.03	0.18	6.8	-51	- 8.6
159	Korosi KR 23	95.4	3.60	1.58	0.10	0.40	<0.8	0.3	1.65	<0.05	8.5	-33	- 6.5
159	Korosi KR 23*	96.0	5.70	0.56	0.08	0.55	<0.5	1.1	0.39	0.08	10.6	-42	- 7.6
160	Korosi KR 24	82.5	6.45									-48	- 8.4
172	Korosi KR 27			<0.05	0.07	0.20	<0.8	<0.1	<0.03		10.2	-60	-13.2
161	Korosi KR 32	91.5	6.05									-53	- 9.6
162	Korosi KR 34	91.0	5.30	0.26	0.18	0.30	0.9	1.8	0.03	0.06	31.5	-112	-18.2
162	Korosi KR 34**	94.5										-99	-15.9
163	Paka PK 1a	96.2		0.57	0.09	0.30	<0.8	1.3	0.49	0.05	0.08	+ 7	- 2.3
163	Paka PK 1a*	95.0	4.10	0.24	0.13	<0.20	<0.5	0.4	<0.03	<0.05	0.09	+ 2	- 2.4
164	Paka PK 1b	91.2										+10	- 1.2
165	Paka PK 1c	91.0										+ 2	- 2.8
173	Paka PK 3			0.15	0.08	0.40	<0.8	<0.1	0.12		2.5	-15	- 2.4
166	Paka PK 4a	95.3	4.55	1.05	0.23	0.40	1.0	0.6	0.11	<0.05	1.3	-14	- 4.3
167	Paka PK 4b	95.5	4.50	0.21	0.09	0.20	3.8	0.6	<0.03	<0.05	<0.05	-18	- 4.0
174	Paka PK 6e			0.17	<0.05	<0.20	<0.8	<0.1	<0.03		0.34	- 5	- 2.8
168	Paka PK 7a	94.0	3.90	3.10	0.05	0.60	4.7	0.4	1.59	0.06	<0.05	-13	- 3.5
169	Paka PK 7b	91.0	5.00									-22	- 5.2
170	Paka PK 7c	91.0	5.25									-21	- 4.8
171	Paka PK 7d	92.0	4.90	0.26	0.06	0.20	<0.8	<0.1		<0.05	0.15	-26	- 5.7
175	Paka PK 7e			0.30	0.29	<0.20	<0.8	0.1	<0.03		0.30	-36	- 7.1

Table 7.3 (Cont'd)

No.	Locality	Temp °C	pH	Na	Ca	Cl	SO_4	Si	B	F	NH_4-N	δ^2H	$\delta^{18}O$
176	Paka PK 20a			<0.05	<0.05	<0.20	<0.8	<0.1	<0.03		3.6	-17	- 4.3
177	Paka PK 20b			0.08	<0.05	<0.20	<0.8	<0.1	<0.03		2.0	-17	- 4.5
178	Paka PK 23			0.15	<0.05	<0.20	<0.8	<0.1	<0.03		1.1	-18	- 4.9
179	Paka PK 31			0.79	0.06	0.20	<0.8	0.2	0.69		1.7	-21	- 5.0
180	Paka PK 39			0.48	0.06	<0.20	<0.8	0.2	0.32		0.90	-69	-11.9
181	Paka PK 42			<0.05	<0.05	<0.20	<0.8	<0.1	<0.03		1.5	-52	- 9.3
182	Paka PK 49			0.11	0.20	0.6	<0.8	0.3	<0.03		0.05	-76	-13.4
218	Silali SL4	96.5	6.25	0.18	0.06	<0.20	<0.8	0.7	0.21	<0.05	34.8	-28	- 5.5
219	Silali SL7	95.3	3.90	<0.05	0.05	0.20	3.4	0.5	0.03	<0.05	0.03	- 6	- 2.6
220	Silali SL11	94.4	5.05	0.06	<0.05	<0.20	<0.8	0.3	0.05	<0.05	10.3	-52	- 8.0
221	Silali SL14	95.8	4.15	<0.05	0.09	0.25	1.4	0.4	0.03	<0.05	1.42	-22	- 5.8
222	Silali SL15	96.6	4.20	0.15	<0.05	0.30	0.9	0.4	0.13	<0.05	2.22	-18	- 4.6
223	Silali SL16	96.1	4.55	0.14	0.07	<0.20	<0.8	0.5	0.11	<0.05	0.07	-27	- 4.7
224	Silali SL19	95.7	4.70	0.06	<0.05	<0.20	<0.8	0.7	<0.03	<0.05	6.54	-50	- 7.1
225	Silali SL22	92.3	4.05	0.33	0.12	0.65	0.5	0.7	0.35	<0.05	0.37	-86	-11.0
226	Emuruangogolak EM7	90.6	4.53	<0.05	0.11	<0.20	<0.8	0.9	<0.03	<0.05	0.53	-13	- 6.1
227	Emuruangogolak EM9/23	92.6	4.30	0.21	<0.05	<0.20	<0.8	0.6	<0.03	<0.05	0.48	-10	- 5.2
228	Emuruangogolak EM9/27	94.7	4.75	<0.05	0.35	<0.20	<0.8	0.7	<0.03	<0.05	0.70	-13	- 5.4
229	Emuruangogolak EM9/40	90.6	5.85	0.49	0.10	0.20	<0.8	0.7	0.36	<0.05	0.47	- 2	- 3.3
230	Emuruangogolak EM16/2a	90.0	5.60	0.09	<0.05	<0.20	<0.8	0.6	<0.03	<0.05	1.35	-19	- 4.4
231	Emuruangogolak EM16/2b	90.4	5.00	<0.05	0.06	<0.20	<0.8	0.4	<0.03	<0.05	0.66	-22	- 5.0
232	Emuruangogolak EM20a	96.0	4.60	1.39	0.07	<0.20	<0.8	0.2	1.21	<0.05	1.98	-27	- 6.0
233	Emuruangogolak EM20b	95.6	4.85	0.84	0.06	0.20	0.8	0.8	0.79	<0.05	1.89	-25	- 5.8
234	Emuruangogolak EM20c	92.4	5.12	0.12	0.09	0.25	<0.8	1.0	<0.03	<0.05	2.32	-54	- 9.2
235	Barrier BR1	96.0		0.66	0.16	<0.20	<0.8	1.2	0.04	<0.05	3.04	- 5	- 3.1

NB: OK, KR and PK sites sampled in 1988 except * in 1989 and ** in 1991. SL, EM and BR sites sampled in 1989.

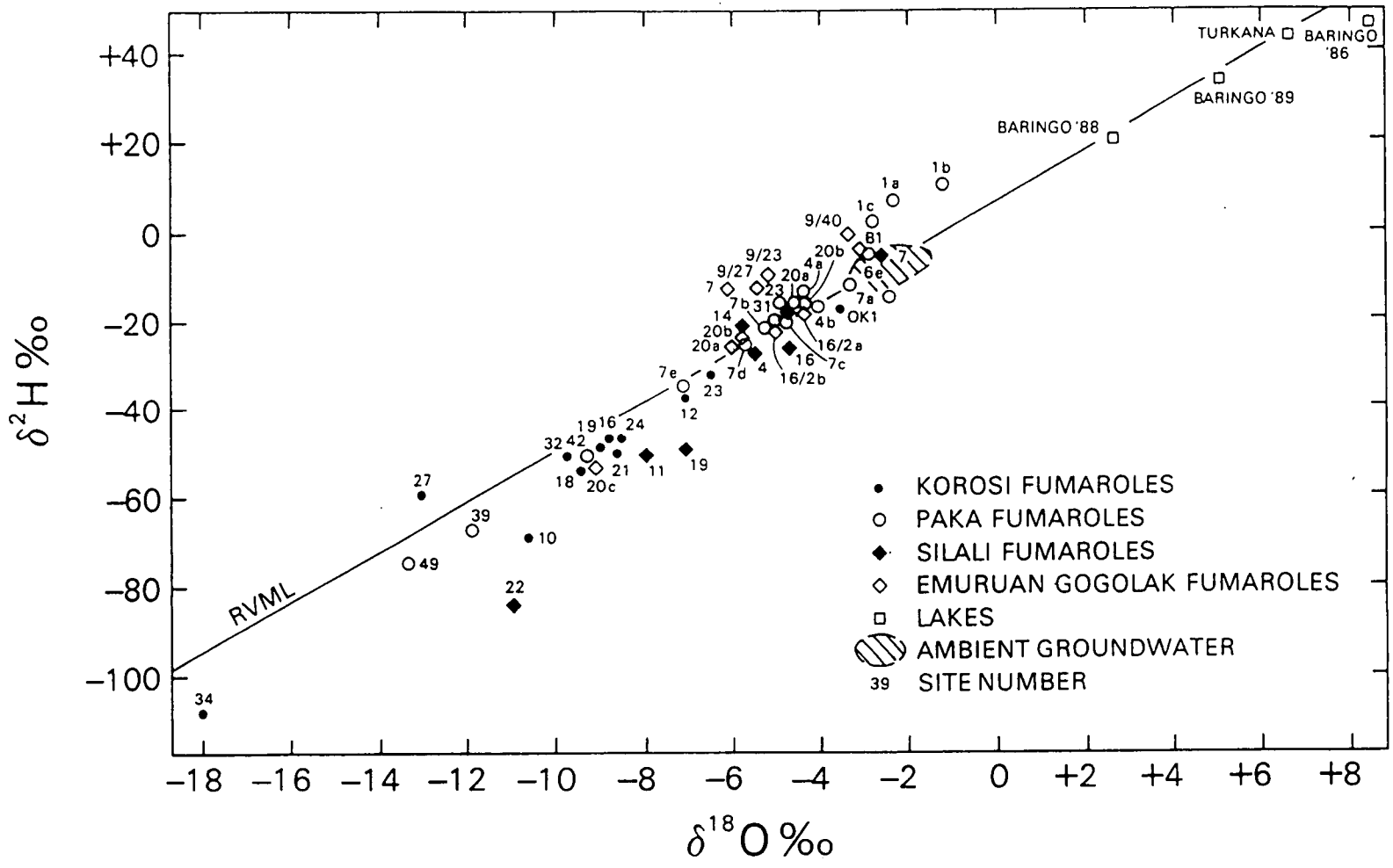

7.7 Plot of δ^2H vs $\delta^{18}O$ for all fumarole steam condensates (values in permil SMOW and mg l^{-1}).

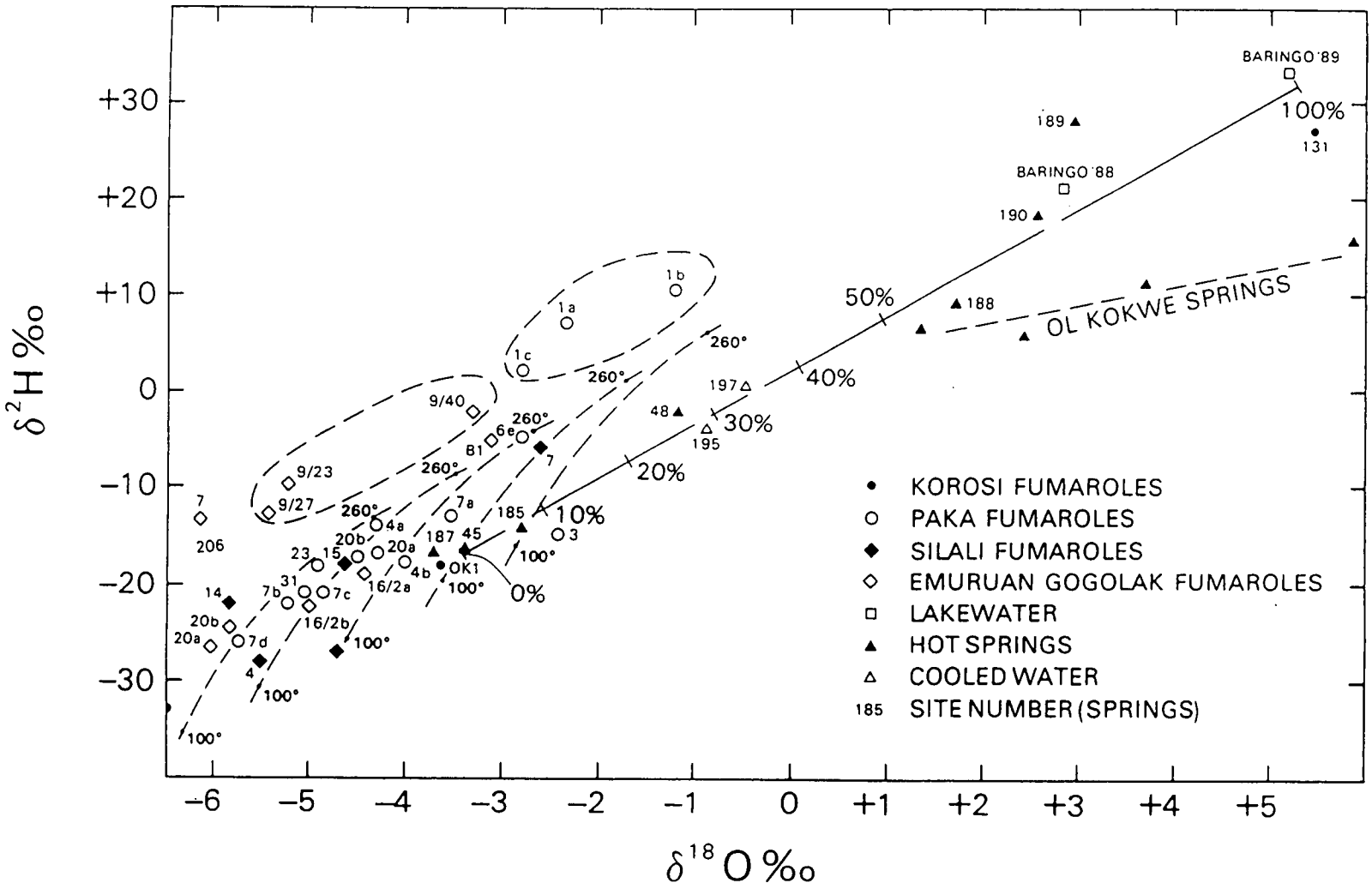

7.8 Plot of δ^2H vs $\delta^{18}O$ for selected fumarole steam condensates (values in permil SMOW).

No Korosi fumaroles with the exception of OK1 and possibly KR23 can be directly related to the proposed groundwater-local water mixing series. Some Paka, Silali and Emuruangogolak fumaroles also lie in the isotopically depleted area in Figure 7.7. The reason for this appears to be subsurface steam condensation; this could have the effect of lowering the heavy isotopic content of steam quite considerably in some cases. The Rayleigh process of condensation examined in Darling and Armannsson (1989) could account for quite large isotopic fractionations, particularly for 'last gasp' fumaroles at a large distance from their upflow. The prime example of this is the fumarole at Loruk, KR34 (162). However the fumarole data indicate that the process operates on a significant scale even at a local level: for example the Paka 1 and 7 series, and the Emuruangogolak 9 and 20 series. There is even evidence that condensation is affecting carbon isotope ratios in fumarole CH_4 (section 7.6).

Given the problems of significant condensation even on a local scale, the safest option is to consider that the most enriched isotopic composition in any one area is the most representative of the steam origin. There is of course always the possibility that even the most enriched fumarole is suffering from condensation. This could be the case with Korosi. It is apparent from Figure 7.8 that Paka, Silali and Emuruangogolak contain fumaroles which indicate up to about 45%, 25% and 10% of lakewater respectively, i.e. consistent with progressive dilution towards the north. It is unlikely that Korosi is bypassed by the lakewater, but the gas results (section 7.6) indicate that Korosi fumaroles are generally weaker than the others. The sole Barrier volcano fumarole sampled, BR1 (235), appears to be the product of steam separation from a Rift flank water unmixed with any Turkana lakewater, but the fumarole was fairly weak and could conceivably have been affected by condensation.

Although simple condensation processes and derivation of fumarole steam from a lakewater-meteoric water mixing series is the simplest way of explaining the steam stable isotope composition measured in many fumaroles, the possibility of other mechanisms must be briefly considered. For example, some very depleted isotopic compositions might be merely the product of an individual, rather depleted storm event infiltrating into a volume of hot rock and being largely or completely vaporised. However, three dissimilar fumaroles within the area were measured in separate years when weather conditions were very different. The sites include KR34, with the most depleted steam composition yet found in the Rift, and PK1, a vigorous 'heavy' fumarole. Table 7.3 shows that while there are variations in year-to-year compositions, these are relatively minor and therefore the basic interpretations can still be made with reasonable safety.

This observation also suggests that a second putative mechanism, reflux condensation, is not a significant cause of isotopic variation. Such a process would work if steam condensate, which would be significantly heavier isotopically than the remaining vapour, could be re-vaporised independently. Under steady-state conditions, which have been generally assumed to apply to fumaroles and which the duplicate results of Table 7.3 support, this could not happen because of the re-equilibration between the condensed water and further steam. Only if condensate could drain to some different volume of hot, dry rock could vaporisation of condensate take place without subsequent modification of the resulting enriched steam. It might be possible for this to occur locally, but would suggest that highly depleted fumaroles should occur relatively near to fumaroles with heavy steam. On the whole this does not occur; the most vigorous fumaroles (those least prone to modification) are usually situated within crater or caldera areas, while those further away from these presumed upflow zones show in a fairly predictable way signs of depletion due to condensation and dilution of any lakewater contribution by lighter water from meteoric sources. While this may suggest a quite local meteoric input it is assumed that, as is the case further south in the Rift (and indeed in most of the rest of the world), this recharge has a time-

averaged composition little different from rift-flank water and therefore effectively indistinguishable from it.

Additionally, if the isotopically heavy steam fumaroles were the result of separation via a condensation process, a very low gas content would be anticipated. Instead the 'heavy' fumaroles usually have relatively strong gas flows uncontaminated by air and enriched in ^3He, the magmatic tracer isotope.

None of the foregoing arguments is to say that all isotope ratio-modifying processes act in a completely predictable manner, and it is possible that the notably anomalous compositions such as the PK1 and EM9 groups owe something to the alternative mechanisms proposed above. However, the bulk of measured isotopic ratios fit the simplest model and this is therefore retained for the purposes of interpretation.

7.5.3 Steam Condensates - Summary

Both condensate TDS and NH_3 values point to fumaroles increasing in strength in the order Korosi-Silali-Emuruangogolak-Paka, with Korosi being very much the weakest centre. This ties in with the isotope evidence; there is every indication that lakewater is incorporated into the hydrothermal systems beneath the three more northerly volcanic centres, but condensation processes appear to be obliterating any evidence from Korosi. Condensation does however affect all centres to some extent, and care needs to be taken when interpreting steam isotope data.

7.6 Fumarole and Hot Spring Gases

Representative fumaroles on each of the four volcanic centres in the project area were sampled for gases. In appropriate cases $NaOH/CdCl_2$ condensates were also collected. All samples were collected in glass containers with the exception of samples for $^3He/^4He$, which were collected in copper tubes. The results are considered separately in terms of gas chemistry and isotopes. Hot spring gases are also included.

7.6.1 Gas Chemistry

Results of gas analysis are presented in terms of mole percent in Table 7.4. Of the hot springs, only Lorusio and Kageinya (45, 188) had large amounts of gas present. The major gas at Lorusio was CO_2, but at Kageinya nitrogen dominated, perhaps because alkaline buffering prevented the existence of free CO_2. On the basis of their high gas contents these two springs are the most 'geothermal', and this ties in with their chemistry (though see 7.7.1 below). Table 7.6 gives details of isotopic measurements: He R_A values which have already been mentioned in section 7.4 show that Lorusio is the most ^3He-enriched water within the project area but that Namarunu and Logipi have higher values. Kageinya was not sampled for He but did provide a sample for the analysis of $\delta^{13}C$-CH4. The result obtained was comparable to the fumarole values. Measurements of $\delta^{13}C$-CO2 do not mean a great deal in isolation from the $\delta^{13}C$-DIC values, since most of the carbon is in the dissolved phase in these waters. In the case of Lorusio and Namarunu they are more or less in equilibrium for the sampling temperature, but at SV3 and Logipi the measurement of $\delta^{13}C$-CO2 values might have been affected by the very low amount of gas in solution.

Table 7.4 shows that fumarole CO_2 values cover the range from 14-99%, depending on the amount of air contamination. This is a problem with nearly all the weaker fumaroles, and also some of the stronger fumaroles where they issue from large orifices. However it is unlikely that all contamination occurs at or near the point of sampling; air can penetrate the ground, particularly where the fumaroles occur on steep slopes, e.g. KR23 (159), or can be dissolved in the local perched aquifers which affect the chemistry of steam in weaker fumaroles.

Table 7.4 Gas compositions for springs and fumaroles in mole percent (except C_2-C_4 in ppmv).

Site	H_2	O_2+Ar	N_2	CO_2	CH_4	C_2H_6	C_3H_8	C_4H_{10}
HOT SPRINGS								
Lorusio (45)	0.79	2.3	13.3	83.6	0.11	1	nd	nd
Kapedo (48)	0.31	19.6	79.7	0.44	0.0008	nd	nd	nd
SV 3a (185)	nd	11.2	69.5	18.9	0.39	0.2	nd	nd
Kageinya (188)	0.003	1.08	97.5	nd	1.41	280	120	33
Namarunu (189)	nd	16.3	71.3	12.4	0.013	1	nd	nd
Logipi (190)	0.026	17.8	80.4	1.6	0.14	28	nd	nd
FUMAROLES								
OK 1 (152)	0.79	0.1	9.8	88.9	0.32	20	4	nd
KR 12 (154)	nd	10.3	46.8	42.7	0.21	8	3	nd
KR 18 (156)	nd	0.3	1.9	96.3	1.5	340	130	43
KR 19 (157)	nd	0.05	1.0	97.6	1.3	290	130	21
KR 23 (159)	0.40	18.2	65.1	16.1	0.015	9	0.5	nd
KR 23 (159)*	0.0003	18.8	66.9	14.3	0.024	2.5	1.3	0.1
KR 34 (162)	nd	11.4	45.9	42.3	0.35	44	17	6
PK 1a (163)	nd	3.4	11.3	83.8	1.5	1	nd	nd
PK 1a (163)*	nd	14.2	55.4	30.0	0.45	1	nd	nd
PK 4a (166)	4.1	0.61	2.1	91.8	1.3	1	nd	nd
PK 7a (168)	0.92	0.61	30.2	67.0	0.85	39	14	6
SL 7 (219)	0.87	0.09	0.34	98.4	0.25	0.7	nd	nd
SL 11 (220)	nd	10.4	37.1	52.0	0.48	18	4	nd
SL 14 (221)	0.65	0.05	0.29	98.7	0.25	0.6	0.1	nd
SL 15 (222)	0.93	0.06	0.22	98.6	0.24	1	0.1	nd
SL 16/16 (223)	0.044	15.7	58.2	26.0	0.026	0.3	0.2	nd
SL 19 (224)	0.0002	4.4	16.8	77.8	1.1	0.5	nd	nd
SL 22 (225)	0.0009	5.9	24.4	69.5	0.17	0.6	0.1	nd
EM 7 (226)	nd	16.0	61.3	22.2	0.51	nd	nd	nd
EM 9/27 (228)	0.001	13.4	57.1	28.8	0.64	2	nd	nd
EM 20a (232)	0.002	7.9	32.5	59.1	0.51	0.1	nd	nd
EM 20b (233)	nd	7.5	30.6	61.3	0.56	nd	nd	nd
BR 1 (235)	0.008	18.0	64.8	17.1	0.044	0.1	nd	nd

* repeat sampling 1 year later

nd - below detection limit

Table 7.5 Amounts of fumarole gases in steam in m mole kg^{-1}

Site	H_2	O_2 + Ar	N_2	CO_2	CH_4	H_2S	NH_3
OK 1 (152)	11.1	1.4	138	1254	4.5	3.2	2.6
KR 12 (154)	-	182	825	753	3.7	2.8	0.27
KR 18 (156)	-	3.7	23	1178	18	0.37	0.35
KR 19 (157)	-	0.77	15	1494	20	0.79	0.60
KR 23 (159)	0.030	1867	6643	1420	2.4	0.15	0.56
KR 34 (162)	-	426	1715	1580	13.0	0.81	2.0
PK 1 (163)	-	18	61	450	8.1	4.0	0.0056
PK 1 (163)*	-	423	1649	893	13	7.8	0.0059
PK 4 (166)	9.6	1.4	4.9	215	3.0	0.44	0.091
PK 7 (168)	9.4	6.2	308	684	8.7	3.9	0.0035
SL 7 (219)	3.0	0.31	1.2	336	0.85	2.4	0.0021
SL 11 (220)	-	67	240	336	3.1	57	0.72
SL 14 (221)	2.5	0.19	1.1	377	0.95	2.3	0.099
SL 15 (222)	1.3	0.086	0.32	142	0.35	0.84	0.16
SL 16 (223)	1.0	369	1368	611	0.61	12	0.0046
SL 19 (224)	0.014	298	1139	5273	75	16	0.36
SL 22 (225)	0.072	475	1963	5591	14	6.5	0.020
EM 9/27 (228)	0.079	1057	4505	2272	51	12	0.040
EM 20a (232)	0.052	207	850	1545	13	29	0.13
BR 1 (235)	0.097	219	788	208	0.54	0.23	0.21

Hydrogen and methane are often taken to be indicators of proximity to, or strength of, hydrothermal upflows. As with other contra-indications of potential, Korosi fumaroles have least hydrogen, normally below detection. Emuruangogolak fumaroles are also poorly endowed in H_2, as is PK1a (163). The latter was unexpected, because in most other respects it appears to be a highly favourable locality. However, the site was resampled one year later and H_2 was still below detection limit. It will be noted from Table 7.4 that more air was present on the second occasion, but that the ratio of CO_2/CH_4 remains approximately the same: it is for this reason that geothermometers relying on gas ratios are more dependable for relatively weak fumaroles of the Rift (see section 7.8). The resampling of KR23 one year later gave a more consistent set of results, except for H_2 which was considerably lower.

Methane was present in all samples, but no particular pattern emerged. The ratio of methane to higher alkanes is however of interest and will be considered in 7.6.2 below. Hydrogen sulphide was analysed in the gas phase for some samples to show if other forms of sulphur (e.g. COS) were present. However, compounds other than H_2S were below detection (1 ppmv).

While gas analyses in mole percent are useful for a qualitative comparison of gas types, they offer no information about the relative amount of water vapour present. Table 7.5 gives gas data in the form of m mole kg^{-1}, and includes NH_3 and gravimetric or titrated H_2S results. It will be seen that in general the stronger fumaroles (e.g. PK1, 4, 7 and SL14, 15) have the lowest amount of gas relative to water vapour. This is entirely consistent, because the strongest fumaroles will probably be hot enough to prevent excessive condensation of water, whereas distant fumaroles such as KR34 will have relative large gas contents because water has dropped out. The highest relative gas contents of all are seen on Silali, where the fumaroles concerned, SL19 and 22, also have a stable isotope composition indicative of condensation, and on Emuruangogolak, where EM9/27 has a unique though not particularly condensed isotopic composition (see previous section). The difference between the two centres is that EM9/27 has a high air content compared to high CO_2 at Silali.

7.6.2 Gas Isotopic Compositions

A sizeable number of samples was subjected to isotope analysis for δ^{13}C-CO2, δ^{13}C-CH4 and ^{3}He/^{4}He. The results are reported in Table 7.6. In the first place they can be a test of analytical precision; PK1a and KR23 were sampled two consecutive years and their δ^{13}C-CO2 values are only just outside the normally quoted CO_2 measurement precision of ±0.1‰. Considering the sometimes difficult conditions for fumarole sampling, this is a satisfactory result. The δ^{13}C-CH4 for PK1 was also fairly repeatable, though the oxidation step necessary before analysis means that precision is never likely to be as good as for CO_2. In the light of these results, a reasonable assumption is that CO_2 results are good to ±0.2‰ and CH_4 results to ±0.5‰. Unfortunately, owing to the low concentrations of CH_4 it did not prove possible to obtain reliable δ^2H-CH4 measurements.

The results of ^{3}He/^{4}He isotope analysis are shown in Table 7.6 in the form of R_A, i.e. the ratio of ^{3}He/^{4}He in the sample to that of the atmosphere (1.4×10^{-6}). Sample ^{3}He/^{4}He ratios were corrected for any air contamination using ratios of He to Ne. All samples have values in excess of 1, indicating an enrichment in mantle He to varying extents. Values rise to a maximum of 8.0; individual fumaroles in all areas can give much lower values, but geological and geochemical evidence indicates that such fumaroles are at some distance from the main hydrothermal upflows, and therefore more prone to alteration by near-surface processes. It is unlikely that these lower R_A values are due to dilution by crustally produced ^{4}He, since research in the southern half of the Rift indicates that flowpaths are generally short and provide little opportunity for scavenging radiogenic ^{4}He from rock (Allen et al., 1989). The maximum measured R_A value of 8.0 is within typical MORB

Table 7.6 Isotope analyses of gas phase components from hot springs and fumaroles ($\delta^{13}C$ in permil vs PDB, He ratio in R_A).

No.	Locality	$\delta^{13}C_{CO_2}$	$\delta^{13}C_{CH_4}$	$^3He/^4He$*
HOT SPRINGS				
45	Lorusio	- 6.0		5.00
48a	Kapedo			3.92
185	SV 3a	-12.4		4.61
188	Kageinya		-31.8	
189	Namarunu	- 8.9		7.10
190	Logipi	-14.6		6.50
FUMAROLES				
152	OK 1	- 3.5	-18.3	4.90
154	KR 12	- 4.3		3.90
156	KR 18	- 3.9	-24.5	2.50
157	KR 19	- 3.9	-23.4	
159	KR 23	- 6.3		
159	KR 23*	- 6.1	-19.7	1.63
162	KR 34	- 4.3	-27.6	3.17
163	PK 1a	- 2.9	-24.9	7.90
163	PK 1a*	- 3.2	-24.0	
166	PK 4a	- 3.4	-27.8	6.17
168	PK 7a	- 2.7	-22.2	3.63
219	SL 7	- 3.8	-23.0	7.52
220	SL 11		-24.3	
221	SL 14	- 3.7	-24.3	8.00
222	SL 15	- 3.9	-25.0	
223	SL 16/16	- 4.7	-23.5	
224	SL 19	- 4.6		
225	SL 22	- 3.6	-21.7	7.86
226	EM 7	- 3.9	-26.9	
228	EM 9/27	- 4.7	-20.7	4.16
232	EM 20a	- 4.0	-22.5	6.02
235	BR 1	- 3.3	-26.3	3.31

* Analyst Ms E Griesshaber at Cambridge University

values. The value of $^3He/^4He$ measurements lies in the indication they provide of proximity to upflow. This may be more useful in the case of fumaroles than hot springs, where evidence exists that high R_A values can be found at some distance from any possible contributory upflow (e.g. site 124 in the southern Rift, Logipi springs to the north of the present area).

There is no correlation between $\delta^{13}C$ values of CO_2 and CH_4 (Figure 7.9) and nor is there any clear relationship of either with He isotope value. However, the bulk of the CO_2 is likely to come from crustal sources owing to its consistently heavy ^{13}C content. Although the KR23 fumarole is depleted in ^{13}C, this is likely to be due to CO_2 from soil organic sources rather than the mantle.

A plot of C_1/C_{2+} alkanes versus $\delta^{13}C\text{-}CH_4$ is shown in Figure 7.10. Care may be needed when interpreting gas isotope data; the arrows on the diagram indicate increasing amounts of subsurface steam condensation for particular sample suites as indicated by O and H isotope data. In most cases there is a negative shift in $\delta^{13}C$ with increasing condensation, suggesting that isotopic fractionation is taking place during this process. However, there are sufficient 'uncondensed' data points tending to show a negative correlation between $\delta^{13}C$ and log C_1/C_{2+}, and therefore ultimately between $\delta^{13}C$ and He R_A (see next paragraph). From its $\delta^{13}C$ values, approximately -20 to -30‰, the methane cannot be biogenic in origin, but neither is it likely to be synthesised at high temperatures because of the absence of the alkene gases which are thought to be produced by this process. In the Rift, systems of apparently widely differing temperatures produce methanes with similar $\delta^{13}C$ values, and this points to a relatively low-temperature thermogenic origin, perhaps around 100°C. Much of the water flowing into the hydrothermal systems appears to come from lake sources, which would be richer in organics than rainwater (there is comparatively little sediment in the Rift to provide a source of *in situ* organic material, but on the other hand the amounts of CH_4 involved are not particularly large).

Although there is at first sight no correlation between $\delta^{13}C\text{-}CH_4$ and He isotope ratio, Figure 7.11 shows a good correlation between the ratio of CH_4 to higher hydrocarbons and He when plotted as log C_1/C_{2+} alkanes versus He R_A value. The correlation is best at lower values of C_1/C_{2+}, probably because at higher values the C_{2+} hydrocarbons are approaching limits of detectability. Only the two northernmost fumarole localities of Emuruangogolak and the Barrier do not fit the relationship, for reasons which remain unclear. If methanes from two different sources are mixing, for example poor in C_{2+} from the mantle and richer in C_{2+} from a crustal source, then not only might a non-logarithmic C_1/C_{2+} versus ^3He relationship be expected, but also a significant $\delta^{13}C$ correlation with ^3He. The observed relationship is probably related to temperature. All other things being equal, the higher the He R_A value the closer the sampling point to the centre of the hydrothermal plume of the upflow. Methane relatively rich in C_{2+} is drawn into the hotter parts of these plumes, where the C_{2+} hydrocarbons suffer a rapidly increasing rate of breakdown to CH_4 as the temperature rises (see 7.7.2 below).

7.6.3 Spring and Fumarole Gases - Summary

Of the hot springs, Lorusio had the most indications of thermal activity (high CO_2). The $\delta^{13}C\text{-}CH4$ measured on Kageinya was similar to fumarole values. Helium isotope ratios were reasonably high at Lorusio, Kapedo and SV3, but significantly higher at the Namarunu and Logipi sites to the north of the project area.

Fumarole gases showed no particular pattern of distribution, although H_2, usually considered to be a good geothermal indicator, was least abundant in Korosi and Emuruangogolak. In terms of ratio of gases to water vapour, Paka and Silali fumaroles showed the least signs of steam condensation below surface.

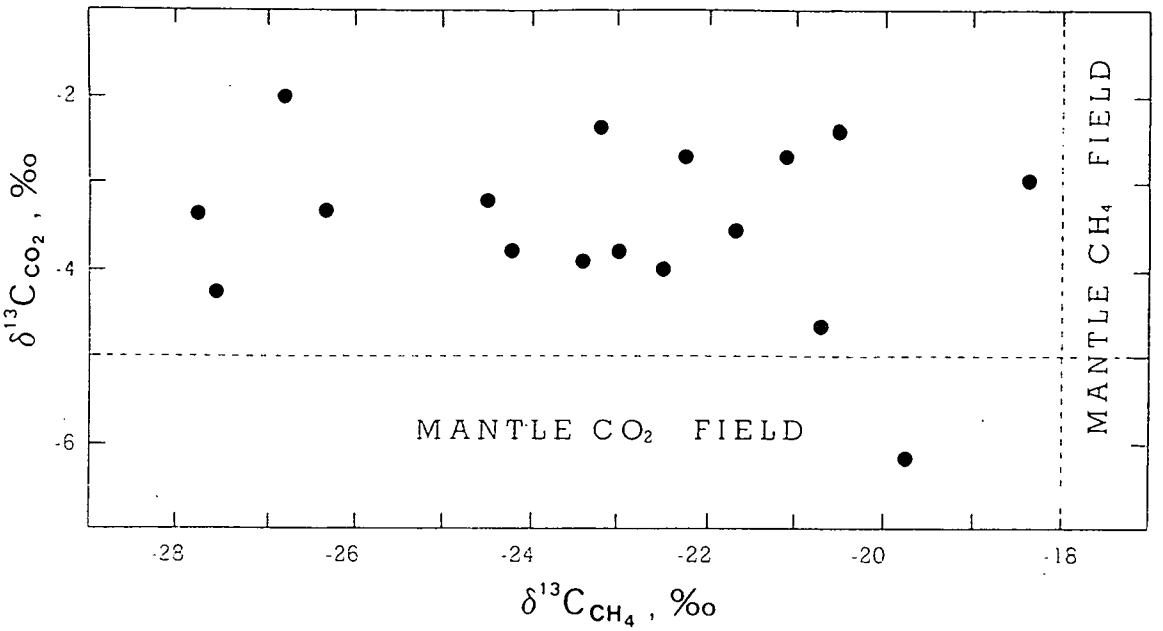

7.9 Plot of $\delta^{13}C_{CO2}$ vs $\delta^{13}C_{CH4}$ for fumarole gases (values in permil PDB).

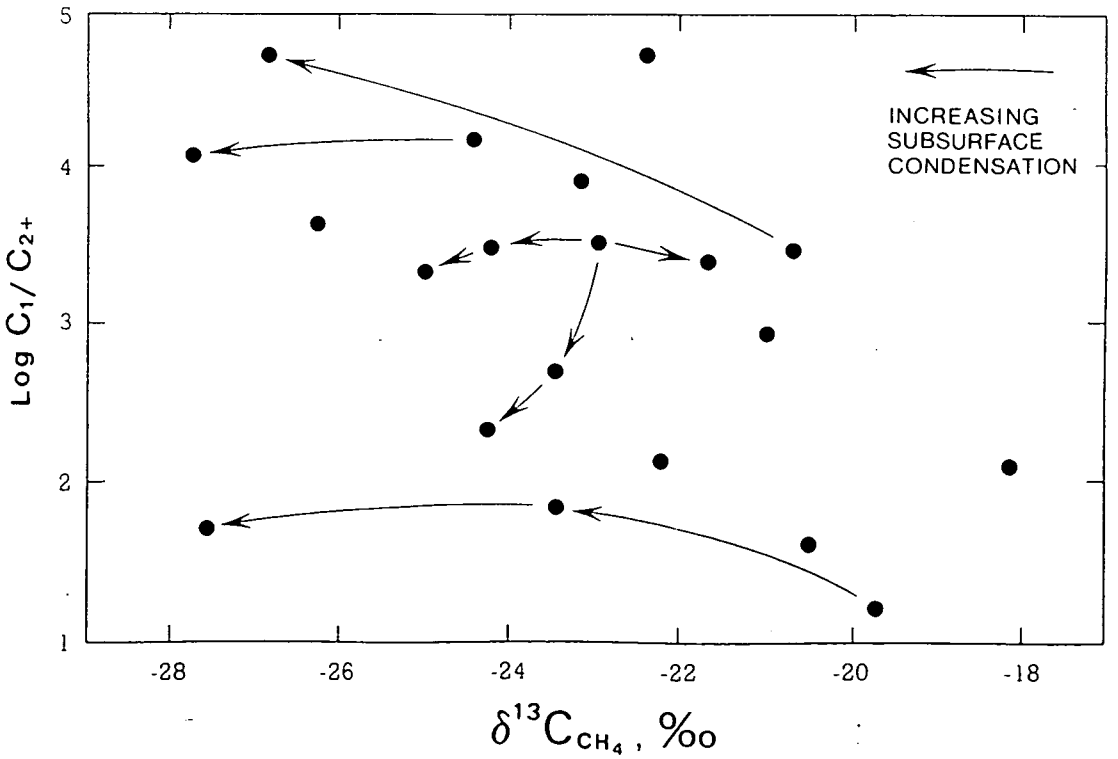

7.10 Plot of log C_1/C_{2+} alkanes vs $\delta^{13}C_{CH4}$ (values in permil PDB).

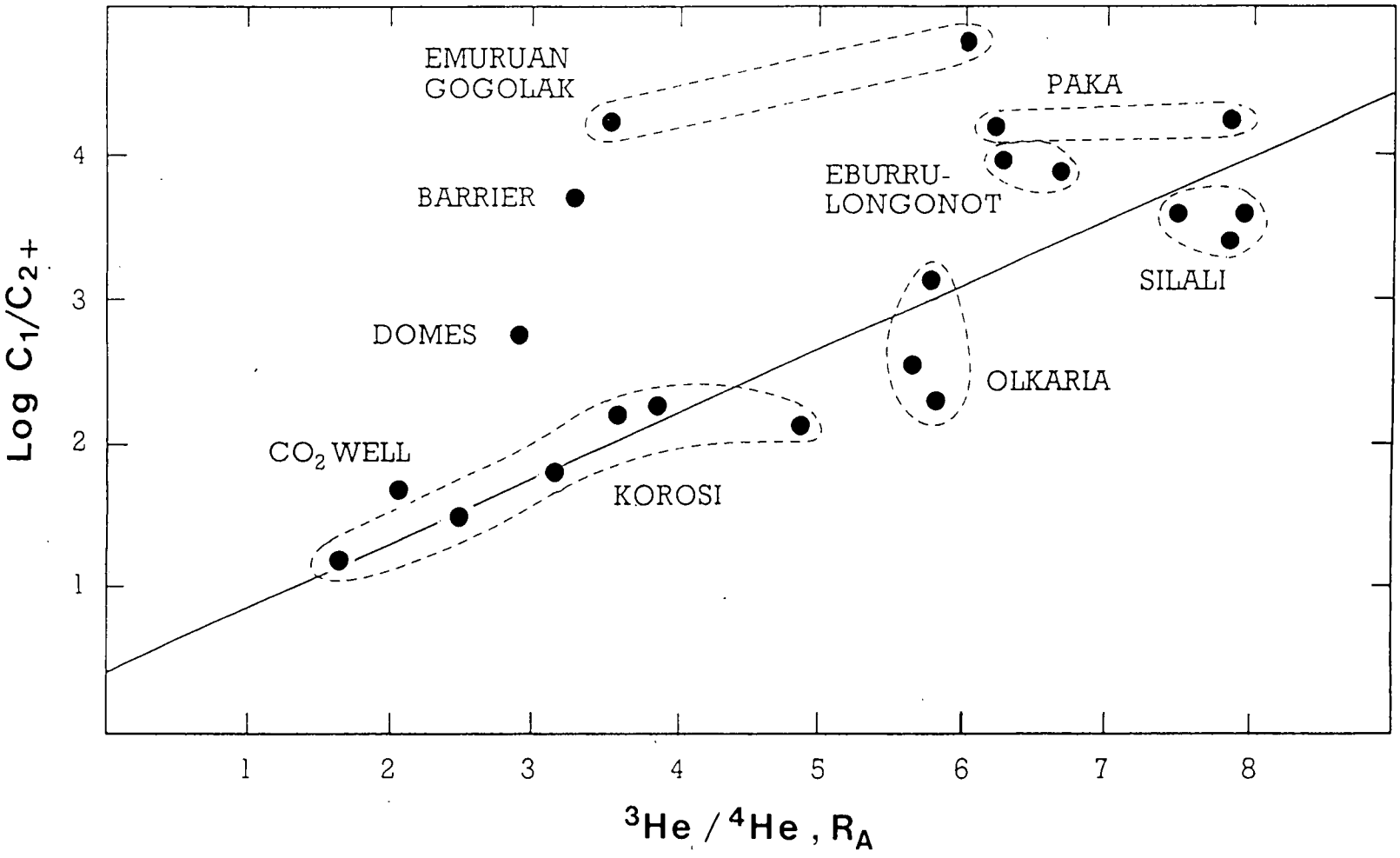

7.11 Plot of log C_1/C_{2+} alkanes vs $^3He/^4He$ (values in R_A). Figure includes data from Southern Rift sites.

In terms of helium isotope values, Paka and Silali were the most favourable sites. Over the whole project area both δ^{13}C-CO2 and δ^{13}C-CH4 results fell in restricted ranges and showed no particular pattern. However, a good correlation between $^3He/^4He$ and C_1/C_{2+} alkanes was found (except for Emuruangogolak and the single sample from the Barrier volcano to the north). This particular relationship is likely to be a function of system temperature.

7.7 Geothermometry

Geothermometry is an important facet of the geochemistry of thermal areas. It relies on the fact (or at least the belief) that certain, highly temperature-dependent reactions are solely responsible for the concentration of a particular element or gas. The results from the Phase 2 area are now reviewed.

7.7.1 Aqueous Geothermometers

The use of cation and silica-based geothermometers is based on the assumption that chemical equilibrium is obtained between water and rock at elevated temperatures. Application of these geothermometers to the thermal springs of the project area is constrained by the fact that most of the dissolved solids load in these waters appears to have been acquired by evaporite dissolution rather than by interaction between water and rock in its more limited sense. Evidence that such water-rock equilibrium is not being obtained is provided by Mg concentrations, which are often below the expected values for the observed Na/K ratios if those ratios were the product of equilibration with feldspar at a particular temperature.

The calculated temperatures in Table 7.7 must therefore usually be treated with reservation; the Na/K geothermometer may be overestimating temperatures by as much as 20°C. Similarly the highly alkaline nature of these waters may mean that silica concentrations are higher than they would be for the pH 7 water-rock equilibrium assumed for the purposes of SiO_2 geothermometry (Fournier, 1981). The effect of this would be to overestimate temperatures at typical thermal spring sites like Kapedo or SV3 (48, 185) by up to 15°C, and significantly more at highly alkaline sites like Kageinya (188).

These processes probably operate at most sites to a greater or lesser extent. It does however depend on how the observed surface concentrations and pH have arisen. For example, a high-temperature thermal water could have become 'diluted' by mixing with high bicarbonate water on its way to the surface. Similarly, loss of CO_2 at the surface could lower the pH significantly without causing a rise in silica concentration beyond that resulting from water-rock equilibration. Ol Kokwe (71) is the most likely site to have been affected in this way, and its temperature values for the adiabatic quartz geothermometer may be substantially correct.

For the other lower temperature springs the chalcedony geothermometer is probably the most appropriate, while bearing in mind the limitations outlined above. The chalcedony temperatures in Table 7.7 reveal that few of the thermal spring waters can have reached much more than 100°C. It does however show that the Kalnangi and S. Nangarabat springs (195, 197) could be cooled thermal waters which accords with the empirical evidence provided by the HCO_3 content (7.4.1 above).

Of the other geothermometers applied to the springs based on gases, only H_2 gives particularly plausible results.

7.7.2 Fumarole Gas Geothermometers

Table 7.8 gives the temperatures calculated from various geothermometry equations: those of Arnorsson and Gunnlaugsson (1985), the empirical geothermometer of D'Amore and Panichi (1980) and the carbon isotope

Table 7.7 Geothermometry temperatures (°C) for hot springs.

No.	Locality	Temp. °C	Na/K	Qz	Qz-A	Ch	CO_2	H_2	CO_2/H_2	D/P	$\Delta^{13}C$
45	Lorusio	81	125	123	120	94	277	181	493	-	-
48	Kapedo	50	116	122	121	96	-	139	-	-	-
71	Ol Kokwe	94	155	175	176	170	-	-	-	-	-
183	SL 26/2	45	120	129	130	106	-	-	-	-	-
184	SL 27/5	45	114	140	135	114	-	-	-	-	-
185	SV 3a	68	79	145	139	119	-	-	-	64	-
186	SV 3b	64	83	145	139	119	-	-	-	-	-
187	Kamuge	50	64	126	124	100	-	-	-	-	-
188	Kageinya	68	98	171	161	148	-	205	-	426	260
189	Namarunu	66	112	106	108	78	-	-	-	85	-
190	Logipi	61	107	72	94	61	-	101	286	217	-
194	Kachurkolh	31	67	64	71	34	-	-	-	-	-
195	Kalnangi	32	103	125	121	96	-	-	-	-	-
197	S.Nangarabat	31	95	104	106	76	-	-	-	-	-

Na/K and Qz (quartz), Qz-A (quartz, adiabatic) and Ch (chalcedony) based on Fournier (1981). CO_2, H_2 and CO_2/H_2 gas geothermometers from Arnorsson and Gunnlaugsson (1985). D/P from D'Amore and Panichi (1980). $\Delta^{13}C$ from Panichi et al (1975).

Table 7.8 Geothermometry temperatures (°C) for fumaroles.

Fumarole	CO_2	H_2S	H_2	CO_2/H_2	H_2S/H_2	H_2S	H_2	CO_2/H_2	D-P	$\Delta^{13}C$	C_1/C_2
	—— Cl > 500 mgl^{-1} ——					– Cl < 500 mgl^{-1} –					
OK1[c]	335	269	299	283	325	206	253	175	210	498	
KR12[c]	321	267				202			64		261
KR18[c]	333	227				145			103	368	202
KR19[c]	340	242				167			108	389	203
KR23	339	210	245	208	276	120	153	0	47	533	197
KR34[c]	342	243				167			51	323	224
PK1[c](ave.)	317	281				222			100	354	323
PK4[c]	286	231	298	303	357	150	250	222	238	307	329
PK7[c]	318	273	298	288	319	212	250	187	160	389	256
SL7[c]	299	264	287	283	308	198	230	175	226	395	312
SL11[c]	299	325				287			83		261
SL14[c]	302	263	285	279	305	197	227	166	217	368	314
SL15[c]	274	243	280	284	312	168	217	177	226	359	306
SL16[c]	315	295	278	263	262	243	213	127	148	403	288
SL19[c]	384	301	238	182	183	252	140	-61	100		335
SL22[c]	386	283	253	202	227	226	168	-14	53	417	309
EM9[c]	353	295	254	214	218	243	170	14	65	466	310
EM20[c]	341	312	250	214	196	268	163	13	76	409	343
BR1[c]	286	218	256	247	289	132	173	90	98	328	315

OK - Ol Kokwe Island; KR - Korosi; PK - Paka; SL - Silali; EM - Emuruangogolak; BR - Barrier

D-P - D'Amore and Panichi empirical geothermometer; $\Delta^{13}C$ - carbon isotope geothermometer

C_1/C_2 - methane/ethane geothermometer

geothermometer described by Panichi et al, (1975). Of the five single gas or gas ratio geothermometers, two depend on H_2S and three on H_2, both of which are often near or even below detection limit. As for CO_2, its concentration in fumarole gas has been shown to be highly dependent on the amount of condensation undergone during passage to the surface (Darling and Talbot, 1991). Some of the geothermometers have different versions which effectively depend on whether reservoir Cl is above or below 500 mgl^{-1}. There is no evidence to suggest that Cl exceeds 500 mgl^{-1} in the project area, but both temperatures are given in Table 7.8. The fumarole temperature data must be interpreted with these limitations in mind.

The CO_2 geothermometer, depending as it does on a correlation between concentration in steam and temperature, is clearly likely to give high temperatures where condensation has raised the apparent concentration. Therefore fumaroles like KR34 and SL22 probably wrongly indicate very high temperatures. Only the strongest fumaroles are likely to give anything like genuine CO_2 temperatures, for example PK1, 4 and 7 (286-317°C), or SL14 and 15 (302, 274°C).

The H_2S temperatures (albeit in the 'wrong' Cl range) are more plausible in terms of likely geothermal system temperatures but do not differentiate particularly effectively between systems, except in as much as temperatures are lower on average in the Korosi fumaroles, as would be expected from the other indicators. Much the same remarks apply to the H_2 geothermometer, when it can be applied.

In principle, ratio geothermometers such as CO_2/H_2 should give the best results because ratios are less subject to alteration than concentrations. In the probably 'wrong' version (>500 mgl^{-1} Cl) the CO_2/H_2 geothermometer gives a credible set of temperatures, but in the 'correct' version temperatures are likely to be much too low for most sites. H_2S/H_2 performs inconsistently, giving some temperatures (e.g. at Ol Kokwe) that are likely to be much too high. This geothermometer only applies in the >500 mgl^{-1} Cl version and therefore probably should not be applied within the project area.

The empirical gas geothermometer of D'Amore and Panichi (1980) involves the four geothermal gases CO_2, CH_4, H_2 and H_2S. When any of these gases are below detection, D'Amore and Panichi suggest that a detection limit concentration or a value of 0.001% be inserted, whichever is the lower. This procedure was adopted for these calculations when H_2 was below detection. The performance of this geothermometer is however generally inconsistent in this part of the Rift.

The carbon isotope geothermometer always tends to give higher temperatures than are likely to be encountered even at some depth. It is possible that the temperatures may be representative of conditions at a greater depth than some of the other geothermometers can register, since the CH_4-CO_2 isotopic equilibrium will take a very long time to become established at temperatures below 500°C, and fluids moving towards the surface may not have had time to re-equilibrate. However, all this assumes that CH_4 is produced at depth by high-temperature inorganic synthesis. As the gas chemistry shows, this is highly unlikely, if only on the grounds that alkanes rather than the predicted alkenes are commonly detected in addition to methane.

The relationship shown in Figure 7.11, between log C_1/C_{2+} and $^3He/^4He$ and therefore presumably system temperature, has been formalised into a C_1/C_2 geothermometer by calibration against geothermal wells in the East African Rift System (Darling and Talbot, 1991). Temperatures given by this geothermometer are included in Table 7.8, which shows results that are in reasonable agreement with the field evidence and some of the other geochemical indicators. These temperatures confirm Korosi as the least good prospect and Paka and Silali as the best, but the position of Emuruangogolak (also with high temperatures) is more in accord with the field evidence of recent

volcanic activity than with the supporting geochemical evidence. The Emuruangogolak and Barrier $^3He/^4He$ and log C_1/C_2 values notably fail to emulate the correlation between He R_A and log C_1/C_2 seen for volcanic centres from Silali southwards (Figure 7.11), and the reasons for this (although unknown as yet) may be connected with the apparent ambiguity in the ranking of Emuruangogolak.

7.7.3 Geothermometers - Summary

The alkali and quartz geothermometers give results for the hot springs which must be interpreted with caution because of the effects of evaporite dissolution and high pH values on water chemistry. Only one site, Ol Kokwe (71), has a corrected temperature much above 100°C. Sites like Kalnangi and S. Nangarabat (195, 197) may be cooled thermal waters of the Kapedo type. Ol Kokwe is likely to be the sole representative of outflow specifically linked to a >150°C geothermal system.

The gas geothermometers appear to be constrained by the general weakness of the Rift Valley fumaroles. Firstly, gases like H_2 and H_2S are only present in low concentrations, and secondly subsurface steam condensation can affect the balance between gases and water. This affects geothermometers based on single gases and ratios alike. Some of the conventional geothermometers do differentiate between the four volcanic centres, but only in relative terms. The new methane/ethane geothermometer appears to surmount certain of the difficulties encountered with other gas geothermometers. This places Paka, Silali and Emuruangogolak as roughly equal in terms of reservoir temperatures, while Korosi appears to be a markedly poorer prospect.

7.8 Fluid Geochemistry of the Project Area compared to that of the Southern Rift

Indications that high-temperature geothermal resources exist in the project area are relatively few. There are no significant boiling springs, and fumarolic discharges are on the whole relatively feeble. These lines of evidence could be taken to imply that there is little water at depth, and that what is there can only be at moderate temperatures.

However, consideration of the situation in the Olkaria area shows that there is much similarity between the northern and southern parts of the Kenya Rift. There are no major boiling springs in the vicinity of Olkaria - the only possibly related discharges of any size are at Little Magadi some 100 km to the south. Yet it is known from hydrogeological evidence that Lake Naivasha has a sizeable outflow to the south, and there is confirmation of this from the deep fluids in the Olkaria wellfield and from fumarolic isotope composition from the various volcanic centres (Darling et al, 1990). The situation is therefore comparable to the northern Rift, where Lake Baringo is known to have a discharge to the north, which presumably terminates at Lake Logipi, perhaps mainly by way of the extensive Elboitong spring complex opposite Namarunu. The evidence from Olkaria (and Eburru) is that it is not necessary to have large-scale hot spring activity as a precondition of high temperatures at depth or to prove the existence of deep reservoirs.

It is true that the Olkaria area has rather extensive fumarolic activity compared to any other volcanic complex in the Kenya Rift, but individually the fumaroles there are of the same type as are found elsewhere, ranging from feeble to moderate. Merely because a fumarole is feeble does not however mean that it must be providing information of inferior quality; a good example of this would be fumarole OK-W at Olkaria which has a $^3He/^4He$ R_A value almost identical with those measured in three separate geothermal wells. Fumarolic strength is therefore not in itself a contra-indication of geothermal potential, in terms of temperature at least. Eburru is however perhaps a centre more similar to those of the northern Rift in terms of amount of alteration. The geochemical characteristics of the stronger Eburru fumaroles,

including such parameters as $^{3}He/^{4}He$, are very similar to those at Paka and Silali indicating that there may well be similarly high temperatures at depth. The implications from the southern Rift fumaroles are therefore that fumarolic strength is not an infallible indicator of geothermal potential.

On a wider scale it may be noted that the Langano geothermal field of the Main Ethiopian Rift is developed on a volcanic centre (Aluto) with many similarities to the volcanoes of northern Kenya, including fairly limited surface activity.

In summary it can be said that while geochemical indications of high-temperature reservoirs in the northern Rift may be few, there are analogues in southern Kenya and Ethiopia which suggest that such reservoirs do exist. However it must also be stated that there is little evidence that water moves rapidly through these reservoirs, with the implication that permeabilities are likely to be low. In this respect any geothermal reservoirs in the northern Kenya Rift would be similar to all the geothermal fields drilled so far in the East African Rift System from Olkaria to Djibouti.

8. CONCLUSIONS

(i) *Reservoir Properties*

Borehole data in the project area are limited, with information available for a total of only 70 boreholes. Most of these (90%) have some productivity data, but only 45% have enough information for specific capacity values to be calculated and transmissivity estimates can only be obtained from 25% of the total. None of the boreholes were drilled to depths much greater than 200 m and therefore there is no direct information on the physical properties of the underlying geothermal reservoirs.

The available data from drillers' logs suggest that aquifer types are fractured volcanics, weathered contacts between different lithological units and sediments. Such aquifers may be discrete on a small scale but on a regional scale hydraulic connection between aquifers is likely. It is quite likely that these types of aquifers constitute geothermal reservoirs at depth.

The hydraulic properties of the aquifers, estimated from the borehole data, are in general poor. It is estimated that the average value of transmissivity is only 17 m^2/day, with even lower values suggested by specific capacity data. However regional estimates of aquifer properties, derived from analysis of subsurface flows from Lake Baringo suggest higher values. It is almost certain that individual geothermal reservoirs will be substantially affected by local faulting.

(ii) *Groundwater Flow and Recharge*

Groundwater flows in the Project Area are a combination of northerly axial flows along the rift floor (generally directed to the west of the volcanic centres) and lateral flows from the sides of the rift. The volcanic centres in the rift may have local recharge mounds which would locally perturbate the regional flow systems. The interaction between lateral and axial flows is modified by faults which cause lateral flows to follow longer, deeper flowpaths and may tend to align flow paths within the rift along its axis. However structural effects do not appear to be as severe as those seen further south around Suswa volcano.

Recharge of groundwater occurs from several sources:

(a) Lateral groundwater flows are recharged in the rift flanks,

(b) Lake Baringo recharges groundwaters on the rift floor (Baringo waters may penetrate to the north of Silali),

(c) Local recharge on the rift floor is likely, and particularly on the volcanic centres themselves.

The availability of local recharge, the magnitude of subsurface flow from Lake Baringo and the availability of groundwater from the rift flanks all suggest that geothermal production on a scale similar to that at Olkaria would not greatly affect regional water resources.

(iii) *Thermal Waters*

Thermal waters with quite similar chemical characteristics are found to the west and north of Silali and Emuruangogolak together with near-ambient waters of similar composition. On isotopic evidence they appear to be the result of mixing between Baringo lakewater and waters from the rift flank or the volcanic centres, though original chemical compositions have been masked by dissolution of evaporite deposits remaining from earlier, higher lakestands.

Geochemical evidence suggests that high-temperature thermal waters do not play a significant part in the mixing process; instead the waters may be heated in zones of moderate rather than high heat flow and are probably effectively separated from the steam-generating zones beneath the volcanic centres. The existence of Lorusio (the hottest spring complex at ~80°C) near the west rift wall suggests that zones of moderate heat flow are not restricted to the immediate vicinity of the centres, although it is always possible that the observed temperature differences are merely due to different depths of water circulation rather than areal variations in heat flow. However, some evidence that a magmatic heat source is ultimately responsible for the heat observed at Lorusio is provided by the isotopic compositions of CO_2 and helium.

(iv) *Fumarole Activity*

Isotope ratios in condensed steam from fumaroles of the volcanic centres strongly suggest that their respective hydrothermal systems are being fed by various combinations of Baringo lakewater and meteoric waters from the rift flanks or the centres themselves. Condensate chemistry, although a fairly crude index, suggests that the strength of fumaroles decreases in the order Paka > Emuruangogolak > Silali > Korosi.

Gas results show that the highest percentages of the more mobile and magma-derived gases (H_2, ^3He) were found within the calderas of Paka and Silali. Subsurface steam condensation was most notable on Korosi.

(v) *Geothermometry*

Alkali and quartz geothermometry could not be applied to the thermal springs of the area with great accuracy because of the masking of any temperature-related water-rock equilibria by the dissolution of evaporites. Nevertheless it was sufficient to show that none of the springs has a major component of outflow from a high-temperature geothermal system, except for Ol Kokwe.

Gas geothermometers appear to be constrained by the general weakness of Rift Valley fumaroles, though the results broadly indicate (in a relative way) the ranking of Paka > Silali > Emuruangogolak > Korosi. The new methane/ethane geothermometer developed specifically for the Rift gives similar temperatures for the first three centres of ~300°C, but about 200°C for Korosi.

In summary, the main conclusions at this stage are:

(1) The geothermal prospects of the four volcanic centres appear to be ranked in the order: Paka > Silali > Emuruangogolak > Korosi, with Korosi very much the weakest.

(2) There is some evidence of a widespread thermal water with a heat source (or sources) not necessarily linked with an obvious volcanic centre.

(3) Aquifer properties at depth are not expected to be good, but faulting may significantly enhance permeability locally.

(4) Despite the location of the volcanic centres in an arid area, natural recharge is likely to be sufficient to support geothermal production.

REFERENCES

Adams, B 1977 A simple program for the calculation of Soil Moisture Deficits and actual evapotranspiration. Hydrogeological Report, Institute of Geological Sciences, No. WD/ST/77/5.

Allen, D J, Darling, W G and Burgess, W G 1989 Geothermics and hydrogeology of the southern part of the Kenya Rift Valley with emphasis on the Magadi-Nakuru area. British Geological Survey Research Report, SD/89/1.

Arnorsson, S and Gunlaugsson, E 1985 New gas geothermometers for geothermal exploration - calibration and application. Geochimica et Cosmochimica Acta, 49, 1307-1325.

Birmingham University 1978 South Humberbank Salinity Research Project. Final Report.

D'Amore, F and Panichi, C 1980 Evaluation of deep temperatures in hydrothermal systems by a new gas geothermometer. Geochimica et Cosmochimica Acta, 44, 549-556.

Darling, W G and Armannsson, H 1989 Stable isotopic aspects of fluid flow in the Krafla, Namafjall and Theistareykir geothermal systems of northeast Iceland. Chemical Geology 76, No. 3/4.

Darling, W G and Talbot, J C 1991 Evaluation and development of gas geothermometry for geothermal exploration in the East African Rift System. British Geological Survey Technical Report WD/91/72.

Darling, W G, Allen, D J and Armannsson, H 1990 Indirect detection of subsurface outflow from a Rift Valley Lake. Journal of Hydrology, 113, 297-305.

Dunkley, P N and Smith, M 1990 The geothermal activity and geology of the northern part of the Kenya Rift Valley between Lake Baringo and Emuruangogolak. British Geological Survey unpublished report.

Fournier, R O 1981 Application of water geochemistry to geothermal exploration and reservoir engineering, in Geothermal Systems: Principles and Case Histories, eds. L Rybach and L J P Muffler, Wiley, New York, 109-143.

Morgan, P 1973 Terrestrial heat flow studies in Cyprus and Kenya. PhD thesis, Imperial College, London, UK.

Panichi, C, Ferrara, G C and Gonfiantini, R 1975 Isotope geochemistry in the Lardarello geothermal field. Geothermics 5, 81-88.

Penman, H L 1949 The dependence of transpiration on weather and soil conditions. Journal of Soil Science, Oxford, 1, 74-89.

Thiem, G 1906 Hydrologische Methoden. Gebhardt, Leipzig, 56 pp.

Woodhead, T 1968 Studies of potential evaporation in Kenya. East African Agricultural Forestry Research Organisation, Nairobi, Kenya.

Water Resources Assessment Project (WRAP) 1987a Water Resources Assessment Study in Baringo District. Water Resources Assessment Division Report, Ministry of Water Development, Nairobi, Kenya.

Water Resources Assessment Project (WRAP) 1987b Water Resources Assessment Study in Laikipia District. Water Resources Assessment Division Report, Ministry of Water Development, Nairobi, Kenya.

Wright, E P and Gunston, H (Editors) 1988 The Chyulu Hills Water Resources Study, Kenya: 1984-1987. British Geological Survey Technical Report WD/88/5C.

Appendix 1 - Rainfall Data

Rainfall Database 'KENRAIN'

(i) Basic Data

Station Name	Alt. (m)	Period of Record
AMAYA	1620	Oct 1987 - Feb 1989
BARAGOI, D.O. ELBARTA	1350	1938 - 1985
BARSALOI SCHOOL	1143	1973 - 1977,1979,1988
BARTABWA	1600	1983 - 1986
BARTALINO	1983	1964, 66, 68-69, 71-86
BARWESA	1679	1958 - 1976, 1978 - 1983
CHEBLOCH PRIMARY SCHOOL	1220	1949 - 1972
CHURO SCHOOL	1740	1985 - 1987
KABARNET D.C.	1980	1915 - 1986
KABARTONJA MISSION	2257	1935 - 1978
KAPEDO MISSION	720	1966 - 1988
KAPKALEWA	1373	1975 - 1983
KATIACK FOREST	2288	1970 - 1983
KINYACH		
KITURO DEMONSTRATION PLOT	2135	1974 - 1986
KOLLOA		1967 - 1968
KOSITEI MISSION	1051	1979 - 1988
KOWOP BOREHOLE	1371	1975 - 1976
LESIRIKAN TRAINING CENTRE	1551	1977 - 1981
LOBOI DISPENSARY	1068	1975 - 1980, 1982
LODWAR MET STATION	506	1919 - 1987
LOIEYANGALANI POLICE POST	387	1973 - 1982
LOKORI MET	600	1975 - 1985
LORUK SCHOOL	1007	1975 - 1982
LAKE BARINGO FISHERIES	961	1950
MARALAL D.C.	1951	1935 - 1987
MARIGAT PEKERRA MET	1060	1954 - 1987
MARUN MISSION		1976 - 1986
MERTI MARALAL	1372	1961 - 1966
MUKATAN	1080	1982 - 1987
MUTUTAN		
NGINYANG	915	1949 - 1987
POI DISPENSARY	1678	1948 - 1986
POROR FOREST STATION	2408	1954 - 1985
RADAD SCHOOL	1159	1965 - 1987
SACHO DISPENSARY	2135	1983 - 1987
SNAKE FARM (KAMPI YA SAMAKI)	1000	1965 - 1986
SOUTH HORR CATHOLIC MISSION	1006	1959 - 1984
SUGUTA MAMAR	1896	1976 - 1986
TALAI AGRICULTURAL STATION	2135	1960 - 1987
TANGULBEI	1525	1939 - 1984
TENGES FOREST	1891	1969 - 1987
TIMBOIWA SCHOOL	2288	1965 - 1985
TIRIONININ CHURON	2135	1976 - 1977, 1979 - 1983
TUUM SCHOOL	1676	1974 - 1978, 1980 - 1988

Rainfall Database 'KENRAIN'

(ii) Location

Station Name	Station Number	Lat	Long	Easting	Northing
AMAYA		0 52 N	36 28 E	2197	0954
BARAGOI, D.O. ELBARTA	88.36.01	1 47 N	36 48 E	2532	1975
BARSALOI SCHOOL	88.36.07	1 20 N	36 52 E	2613	1490
BARTABWA	89.35.195	0 51 N	35 49 E	1446	0938
BARTALINO	89.35.153	0 41 N	35 49 E	1439	0760
BARWESA	89.35.146	0 42 N	35 44 E	1345	0824
CHEBLOCH PRIMARY SCHOOL	89.35.93	0 27 N	35 40 E	1288	0504
CHURO SCHOOL	89.36.81	0 47 N	36 34 E	2109	0865
KABARNET D.C.	89.35.20	0 30 N	35 45 E	1386	0555
KABARTONJA MISSION	89.35.51	0 39 N	35 48 E	1413	0706
KAPEDO MISSION	88.36.10	1 10 N	36 05 E	1773	1304
KAPKALEWA	89.35.197	0 23 N	35 43 E	1324	0413
KATIACK FOREST	89.35.177	0 40 N	35 50 E	1456	0738
KINYACH				1325	1045
KITURO DEMONSTRATION PLOT	89.35.135	0 30 N	35 50 E	1428	0538
KOLLOA	89.35.40	1 15 N	35 45 E	1385	1388
KOSITEI MISSION				1594	1026
KOWOP BOREHOLE	88.36.05	1 59 N	36 46 E	2524	2188
LESIRIKAN TRAINING CENTRE	88.36.13	1 47 N	36 57 E	2713	1973
LOBOI DISPENSARY	89.36.80	0 21 N	36 04 E	1733	0391
LODWAR MET STATION				1200	3471
LOIEYANGALANI POLICE POST				2455	3056
LOKORI MET				1694	2152
LORUK SCHOOL	89.36.82	0 43 N	36 02 E	1696	0789
LAKE BARINGO FISHERIES	89.36.41	0 35 N	36 02 E	1699	0648
MARALAL D.C.	88.36.00	1 05 N	36 42 E	2433	1117
MARIGAT PEKERRA MET	89.35.35	0 26 N	35 56 E	1583	0480
MARUN MISSION	88.35.145	1 12 N	35 55 E	1558	1320
MERTI MARALAL	88.36.06	1 29 N	36 43 E	2458	1643
MUKATAN	89.36.88			1959	0697
MUTUTAN	89.36.088				
NGINYANG	89.36.20	0 57 N	36 01 E	1679	1074
POI DISPENSARY	89.35.92	0 43 N	35 42 E	1323	0795
POROR FOREST STATION	88.36.03	1 14 N	36 36 E	2340	1376
RADAD SCHOOL	89.35.144	0 21 N	35 57 E	1567	0338
SACHO DISPENSARY	89.35.191	0 23 N	35 47 E	1420	0429
SNAKE FARM (KAMPI YA SAMAKI)	89.35.67	0 38 N	36 03 E	1694	0699
SOUTH HORR CATHOLIC MISSION	87.36.00	2 06 N	36 54 E	2672	2330
SUGUTA MAMAR	89.36.74	0 50 N	36 41 E	2416	0914
TALAI AGRICULTURAL STATION	89.35.149	0 35 N	35 50 E	1451	0664
TANGULBEI	89.36.19	0 48 N	36 18 E	1968	0908
TENGES FOREST	89.35.91	0 26 N	35 52 E	1439	0352
TIMBOIWA SCHOOL	84.35.94	0 26 N	35 47 E	1428	0470
TIRIONININ CHURON	89.35.196	0 39 N	35 49 E	1437	0725
TUUM SCHOOL	87.36.01	2 09 N	36 47 E	2530	2385

Rainfall Database

(iii) Mean Monthly Rainfall (mm)

Station Name	JANUARY	FEBRUARY	MARCH	APRIL	MAY	JUNE	JULY
AMAYA	5.9	10.0	46.5	235.9	72.7	11.2	162.8
BARAGOI, D.O. ELBARTA	21.9	33.3	63.9	104.3	55.2	16.2	22.2
BARTABWA	8.2	11.7	33.6	259.0	134.5	50.7	191.7
CHURO SCHOOL	12.4	9.1	23.0	178.2	155.2	232.7	79.9
KABARNET D.C.	30.6	48.5	75.6	193.7	168.7	130.5	201.5
KAPEDO MISSION	9.9	13.3	23.6	68.3	56.8	42.7	57.4
KINYACH							
KITURO DEMONSTRATION PLOT	52.6	31.3	99.1	177.1	136.4	100.4	127.2
KOSITEI MISSION							
KOWOP BOREHOLE	2.9	0.9	6.6	39.0	38.1	6.4	25.9
LODWAR MET STATION	8.5	7.6	20.6	49.0	24.3	6.9	16.2
LOIEYANGALANI POLICE POST	0.0	3.6	45.8	15.7	42.7	0.0	0.0
LOKORI MET	10.4	21.4	30.8	42.9	45.1	25.9	38.5
MARALAL D.C.	13.9	20.2	37.6	82.8	64.1	54.8	88.6
MARIGAT PEKERRA MET	28.1	25.2	49.1	88.9	74.9	57.4	87.7
MARUN MISSION	9.2	11.7	35.3	117.3	128.3	67.8	116.5
MERTI MARALAL	11.4	4.8	13.2	61.0	11 4	24 2	32.1
MUKATAN	4.5	23.2	29.1	190.4	143.1	32.1	81.9
NGINYANG	16.2	18.5	36.1	86.0	90.9	63.6	89.5
POI DISPENSARY	13.2	20.5	62.6	164.6	154.9	93.9	133.0
POROR FOREST STATION	11.3	17.8	29.2	71.1	56.4	63.1	89.8
RADAD SCHOOL	34.6	37.6	57.1	112.1	113.8	52.4	110.3
SACHO DISPENSARY	19.9	10.5	61.2	160.8	125.1	172.9	203.0
SNAKE FARM (KAMPI YA SAMAKI)	22.8	33.4	44.2	94.0	77.5	67.2	95.9
SOUTH HORR CATHOLIC MISSION	27.5	22.0	44.9	87.8	52.3	7.0	19.6
SUGUTA MAMAR	18.1	21.2	31.9	65.4	55.0	67.0	149.6
TALAI AGRICULTURAL STATION	49.1	39.9	97.4	184.8	176.5	115.7	139.0
TANGULBEI	16.8	20.1	45.9	85.3	120.7	60.9	100.7
TENGES FOREST	28.6	59.9	81.4	173.5	179.0	141.4	167.5
TIMBOIWA SCHOOL	44.7	67.5	108.0	184.9	186.4	137.6	193.1
TUUM SCHOOL	11.6	15.1	47.9	136.9	71.1	29.6	42.5

Rainfall Database 'KENRAIN'

(iv) Mean Monthly Rainfall (mm) continued

Station Name	AUGUST	SEPTEMBER	OCTOBER	NOVEMBER	DECEMBER	TOTAL
AMAYA	107.2	170.2	15.9	42.3	8.0	888.6
BARAGOI, D.O. ELBARTA	20.6	10.1	53.9	80.9	35.2	517.7
BARTABWA	107.4	19.4	28.6	156.7	1.7	1003.2
CHURO SCHOOL	57.0	45.8	14.2	29.5	21.0	858.0
KABARNET D.C.	219.7	83.5	60.2	91.6	52.9	1357.0
KAPEDO MISSION	66.9	28.0	36.6	33.0	8.2	444.7
KINYACH						875.0
KITURO DEMONSTRATION PLOT	137.8	40.0	52.6	83.6	77.7	1115.8
KOSITEI MISSION						701.0
KOWOP BOREHOLE	1.7	11.6	0.0	9.8	1.7	144.6
LODWAR MET STATION	8.5	3.2	7.9	17.6	11.5	181.8
LOIEYANGALANI POLICE POST	0.8	0.0	7.8	50.1	0.0	166.5
LOKORI MET	9.9	30.2	15.7	17.2	6.9	294.9
MARALAL D.C.	87.7	32.2	38.1	52.3	20.7	593.0
MARIGAT PEKERRA MET	81.7	33.6	33.7	48.6	27.9	636.8
MARUN MISSION	131.4	43.4	65.6	76.2	17.4	820.1
MERTI MARALAL	16.3	17.2	21 7	30 3	29.2	272.8
MUKATAN	106.3	46.0	51.8	106.7	33.3	848.9
NGINYANG	79.1	35.5	28.1	36.7	14.3	594.5
POI DISPENSARY	129.5	57.6	45.7	99.7	46.5	1021.7
PORTOR FOREST STATION	73.4	41.8	37.2	61.3	18.6	571.0
RADAD SCHOOL	101.3	45.9	48.8	69.8	41.7	825.9
SACHO DISPENSARY	99.2	11.3	61.3	128.0	22.0	1075.2
SNAKE FARM (KAMPI YA SAMAKI)	90.5	33.4	29.6	58.3	26.7	674.4
SOUTH HORR CATHOLIC MISSION	2.6	0.0	20.2	106.6	37.0	428.2
SUGUTA MAMAR	31.7	34.5	36.0	66.0	37.1	613.5
TALAI AGRICULTURAL STATION	175.7	62.9	68.7	131.9	60.0	1298.6
TANGULBEI	101.9	49.8	33.1	53.7	76.2	765.1
TENGES FOREST	175.6	65.2	62.4	91.6	51.7	1277.8
TIMBOIWA SCHOOL	253.0	97.1	59.5	119.6	88.1	1539.5
TUUM SCHOOL	19.3	34.5	34.2	97.1	19.4	559.2

Appendix 2 - Temperature Data

Temperature Database 'KENTEMP'

(i) Basic Data

Name	Met. Station Number	Alt. (m)	Period of Record
Lodwar met station		506	1946 - 1980
Lokori (met)		600	1976 - 1980
Marrigat Pekerra irrigation scheme (met)	89.35.35	1060	1957 - 1980

(ii) Location

Station Name	Easting	Northing
Lodwar met station	1200	3471
Lokori (met)	1694	2152
Marrigat Pekerra irrigation scheme (met)	1583	0480

Temperature Database 'KENTEMP'

(iii) Long Term Monthly Mean - Maximum Temperatures

	Jan	Feb	Mar	Apr	May	Jun	jul	Aug	Sep	Oct	Nov	Dec	Year
** Lodwar met station	35.5	36.1	36.3	35.2	34.7	34.1	33.0	33.5	34.9	35.3	34.5	34.9	34.8
** Lokori (met)	36.2	37.0	37.8	36.2	35.7	35.3	34.3	35.6	36.7	37.1	35.0	37.8	36.2
** Marrigat Pekerra irrigation scheme (met)	33.2	34.0	34.0	33.1	32.5	32.2	30.4	31.1	33.0	33.2	31.7	32.1	32.5

(iv) Long Term Monthly Mean - Minimum Temperatures

	Jan	Feb	Mar	Apr	may	Jun	Jul	Aug	Sep	Oct	Nov	Dec
** Lodwar met station	22.2	23.3	24.2	24.5	24.6	24.2	23.7	23.8	24.2	24.8	23.8	22.5
** Lokori (met)	21.4	21.5	22.1	21.3	19.9	18.5	17.8	19.6	21.3	22.7	22.1	22.3
** Marrigat Pekerra irrigation scheme (met)	16.3	17.0	17.6	17.8	17.0	16.4	16.7	15.9	15.6	16.4	17.1	16.4

Temperature Database 'KENTEMP'

(v) Extreme Temperatures - High

	Jan	Feb	Mar	Apr	May	Jun	Jul	Aug	Sep	Oct	Nov	Dec
** Lodwar met station	38.7	39.8	39.7	39.8	38.7	37.6	36.7	37.7	38.8	39.2	37.6	38.0
** Lokori (met)	38.5	40.0	40.5	40.5	38.0	37.0	37.5	37.0	39.5	39.5	39.0	38.5
** Marrigat Pekerra irrigation scheme (met)	36.7	38.0	37.7	37.2	36.7	35.8	34.6	35.1	37.3	36.7	39.0	36.1

(vi) Extreme Temperatures - Low

	Jan	Feb	Mar	Apr	May	Jun	Jul	Aug	Sep	Oct	Nov	Dec
** Lodwar met station	14.6	15.0	18.2	18.2	18.3	19.5	17.7	18.2	18.0	19.2	18.6	16.1
** Lokori (met)	16.0	14.0	13.5	11.0	8.0	8.0	4.5	13.0	12.0	12.0	14.5	17.5
** Marrigat Pekerra irrigation scheme (met)	10.5	10.6	10.5	13.1	13.0	10.2	11.0	11.0	10.2	11.9	11.8	10.2

Appendix 3 - Evaporation Data

Potential Evaporation Database 'KENEVAP'

(i) Basic Data

Station Name	Met Station Number	Alt. (m)	Period of Record
Amaya MOWD		1620	Oct 1987 - Feb 1989
Kabarnet MOWD	89.35.20	1980	1959 - 1984
Kapedo mission MOWD	88.36.10	720	1985 - 1988
Kinyach dispensary MOWD		1070	1982 - 1987
Lodwar MOWD		500	1950 - 1981
Lodwar met		506	1961 - 1980
Lokori MET		600	1976 - 1980
Lokori MOWD			1973 - 1983
Marigat Pekerra MOWD	89.35.35	1060	1959 - 1987
Marigat Pekerra irrigation scheme (met)	89.35.35	1060	1964 - 1980
Marun AIC Mission MOWD	88.35.145		1982 - 1985

(ii) Location

Station Name	Easting	Northing
Amaya MOWD	2197	0954
Kabarnet MOWD	1386	0555
Kapedo mission MOWD	1773	1304
Kinyach dispensary MOWD	1325	1045
Lodwar MOWD	1200	3471
Lodwar met	1200	3471
Lokori MET	1694	2152
Lokori MOWD	1694	2152
Marigat Pekerra MOWD	1583	0480
Marigat Pekerra irrigation scheme (met)	1583	0480
Marun AIC Mission MOWD	1558	1320

Potential Evaporation Database 'KENEVAP'

(iii) Mean Monthly Potential Evaporation (mm)

Station Name	Jan	Feb	Mar	Apr	May	Jun	Jul	Aug	Sep
Amaya MOWD	252.2	259.5	284.5	258.9	193.2	292.7	162.3	144.2	177.2
Kabarnet MOWD	208.0	194.0	223.0	169.0	140.0	122.0	110.0	119.0	148.0
Kapedo mission MOWD	325.4	322.8	318.6	272.6	241.9	232.5	237.6	256.2	293.4
Kinyach dispensary MOWD	237.7	232.4	236.0	182.6	211.1	190.2	190.0	184.2	231.9
Lodwar MOWD	310.4	300.2	343.7	278.1	281.7	276.3	278.1	299.2	331.7
Lodwar met	298.0	284.0	325.0	269.0	271.0	268.0	273.0	284.0	314.0
Lokori MET	341.0	325.0	394.0	317.0	288.0	297.0	293.0	336.0	361.0
Lokori MOWD	364.7	347.5	382.3	314.4	305.3	302.3	278.1	324.6	341.1
Marigat Pekerra MOWD	268.7	236.5	260.9	204.5	204.0	195.6	181.6	193.0	212.9
Marigat Pekerra irrigation scheme (met)	238.0	233.0	259.0	202.0	199.0	193.0	180.0	188.0	216.0
Marun AIC Mission MOWD	260.9	241.3	260.2	250.2	201.7	239.0	211.5	208.0	265.2

(iv) Mean Monthly Potential Evaporation (mm) - continued

Station Name	Oct	Nov	Dec	Total	Notes
Amaya MOWD	216.9	222.3	234.4	2698.3	LOCALITY ASSUMED SAME AS AMAYA
Kabarnet MOWD	173.0	150.0	178.0	1934.0	ALT. APPROX.: LOCALITY ASSUMED SAME AS KABARNET D.C.
Kapedo mission MOWD	319.4	252.9	299.3	3372.6	
Kinyach dispensary MOWD	230.4	185.4	221.7	2533.6	alt. approx.
Lodwar MOWD	356.6	302.5	298.5	3657.0	ALT. APPROX.: LOCALITY ASSUMED SAME AS LODWAR MET
Lodwar met	342.0	280.0	280.0	3488.0	
Lokori MET	391.0	302.0	300.0	3945.0	alt. approx.
Lokori MOWD	374.6	324.8	338.8	3998.5	LOCALITY ASSUMED SAME AS LOKORI MET
Marigat Pekerra MOWD	229.4	200.7	219.5	2607.3	LOCALITY ASSUMED SAME AS MARIGAT PEKERRA IRRIGATION SCHEME (MET)
Marigat Pekerra irrigation scheme (met)	227.0	196.0	228.0	2559.0	APPROX. LOCALITY (6 fig. G.R. only)
Marun AIC Mission MOWD	212.1	153.9	219.7	2823.7	

Appendix 4 - River Gauging Stations

River Gauging Station Database 'KENRIVER'

Gauge No.	River	Map No.	East	North	Type	Period
2D1	Suguta	77/3	779	310	staff	
2D2	Amaya	91/2	2178	958	staff/weir	Oct 1987-present
2EG3	Molo	105/1	674	498	staff	
2EH3	Endao	90/4	190	573	staff	
2EE6	Perkerra	105/1	685	510	staff	1958 - 1960
2EE2	Perkerra	104/2			staff	1934
2EE3	Perkerra	104/2	299	507	staff	1955 - 1960
2EE7	Perkerra	104/2	299	507	staff	1962 - present
2EE10	Perkerra	104/2	308	512	staff	1968 - 1969

River gauging Station Database 'KENRIVER' - continued

Gauge No.	Rated ?	Notes
2D1	not rated	
2D2	Not rated	
2EG3	not rated	
2EH3	not rated	
2EE6	not rated	
2EE2	rated	
2EE3	rated	
2EE7	rated	2EE7 reoccupied the exact site of 2EE3.
2EE10	not rated	

Appendix 5 - Spring Data

Spring Number	Location	EASTING	NORTHING	Map Number	Temp. Deg. C
W1	Napuon	1369	0553	104/1	21.0
W2	Ngusurai	1377	0559	104/1	24.5
W3	Kimwemoi	1400	0515	104/1	21.0
W4	Batolimo School	1460	0756	90/4	25.0
W5	Birein (talai)	1445	0652	90/4	18.5
W6	Chebariyaya (talai)	1429	0640	90/4	22.0
W7	L. Bogoria N.	1740	0380	105/1	32.0
W8	L. Bogoria E.	1758	0273	105/3	83.0
W9	Maji Moto	1710	0295	105/1	36.0
W10	Emsos	1774	0179	105/3	34.0
W11	Kamar	1683	0302	105/1	24.5
W12A	Njora Nyoka	1513	0319	104/2	27.0
W12B	Njora Nyoka	1513	0319	104/2	33.0
W13	Loboi	1716	0398	105/1	34.0
W14	Sandai	1760	0437	105/1	31.0
W15	Kapedo (before Centre)	1667	1293	77/3	30.5
W16	Kapedo hot springs	1776	1295	77/3	42.0
W17	Kaplunai	1814	0233	105/3	18.5
W18	Chebinying	1822	0478	105/1	26.5
W19	Mukutan (cold)	1930	0680	91/3	22.0
W20	Mukutan (warm)	1930	0680	91/3	48.0
W21	Churo	2113	0857	91/2	25.0
W22	Nakapuron	1768	0894	91/2	62.0
Ok1	Ol Kokwe Island	1752	0695	77/3	97.2
SL1	Lorusio	1789	1381	77/1	82.2
PK3	Paka	1865	1038	91/1	97.8
Pk22	Paka	1890	1025	91/1	93.9
Pk36	Paka	1908	1053	91/1	35.5
Pk41	Paka	1872	1048	91/1	80.2
Pk52	Paka	1887	1047	91/1	94.7
SL18	silali caldera	1973	1272	77/3	78.3
SL26	Silali west/Kapedo	1784	1312	77/3	53.0
SL27	Silali west/Kapedo	1795	1318	77/3	42.2
SL28	Silali north	1950	1460	77/2	38.2
EM21	Emruangogolak N flanks	2140	1897	64/4	69.2
EM22	Emruangogolak N flanks	2155	1923	64/4	51.3
EM25	Emruangogolak summit	2043	1697	64/4	73.3
SV1	Suguta Valley south	1955	1862	64/4	50.0
SV2	Suguta Valley south	2087	1868	64/4	38.1
SV3	Suguta Valley south	1974	1776	64/4	69.7
S187	Kamuge	1955	1862		50.4
S188	Kageinya cone	2140	1897		67.8
S189	Namarunu	2197	2194		66.2
S190	Logipi	2265	2503		61.4
S191	Nangarwa	2061	0894		ambient
S192	Amaya	2198	0894		ambient
S193	N. Samburu Gates	2213	2000		ambient
S194	Kachurkolh	2140	1897		ambient
S195	Kalnangi	1932	1445		31.7
S196	Amakat	1965	1545		ambient
S197	N. Emruangogolok	2083	1846		31.1
S198	Napeiton	1712	1862		32.5
S199	Nasaken	1757	1807		31.0

Key

W = WRAP spring data (WRAP, 1987a)
Ok,SL,Pk,EM,SV = BGS geological localities
S = BGS hydrogeochemical localities (see Appendix 7)

Spring Number	Flow Rate l/s	Elect. Conduct. µS/cm	GEOLOGY
W1	0.5	500	Trachyte
W2	0.5	80	Trachyte
W3	1.0	190	Trachyte
W4		400	Trachyte
W5	2.0	100	Trachyte
W6	0.5	65	Trachyte
W7	0.5	420	Sediment
W8		4800	Trachyphonolites
W9	25.0	520	Sediments/phonolites
W10	60.0	420	Trachyphonolite
W11		65	Trachyphonolite
W12A	3.5	220	Trachyphonolite
W12B	4.0	360	Trachyphonolite
W13	125.0	480	Trachyphonolite
W14	2.0	280	Trachyphonolite
W15		1000	Pyroclastics
W16	800.0	4000	Pyroclastics
W17		150	Phonolites
W18	0.9		
W19	1.8	1200	Basalts
W20	1.2	1500	Basalts
W21	3.6	485	Phonolites
W22		40	Trachytes
Ok1	low		basalt
SL1	vigorous		alluvium/pyroclastic
PK3	seepages		pyroclastics
Pk22	seepages		pyroclastics
Pk36	seepages		basalt scoria
Pk41	seepages		trachyte/pyroclasic
Pk52	seepages		pyroclastics
SL18	seepages		scree/trachyte
SL26	small springs		trachyte pumice
SL27	small springs		pyroclastics
SL28	low flow		basalt/alluvium
EM21	low		basalt tuff ring
EM22			basalt tuff ring
EM25	seepages		trachyte
SV1	low		basalt
SV2	low		basalt
SV3	good		lake sediments
S187			
S188			
S189			
S190			
S191			
S192			
S193			
S194			
S195			
S196			
S197			
S198			
S199	seepages		

Spring Number	Notes
W1	
W2	
W3	
W4	flowrate not given
W5	
W6	
W7	
W8	flowrate not given
W9	
W10	
W11	no flowrate; pool
W12A	
W12B	
W13	
W14	
W15	flowrate not given
W16	
W17	flowrate given as 0.00
W18	
W19	
W20	
W21	
W22	
Ok1	Fumaroles up to 96.5, hot spring up to 97.2. Sulphur crystals and sinter developed along western fault.
SL1	
PK3	
Pk22	
Pk36	
Pk41	
Pk52	
SL18	
SL26	
SL27	
SL28	
EM21	
EM22	
EM25	
SV1	
SV2	
SV3	
S187	Spring on western Rift flanks
S188	Spring on edge of lake in recent volcanic cone
S189	Springs at base of recent volcanic pile
S190	Many seepages at base of Barrier volcano
S191	Spring feeding pool on E. Rift flanks
S192	Springs in valley of Amaya River
S193	Seepages near foot of E. Rift wall
S194	Spring feeding pool on E. Rift flanks
S195	Springs at base of large lava flow, feeding lake
S196	Spring in large hole in basalt lava
S197	Spring on edge of lavas N. of Emruangogolok
S198	Seeps on W. Rift flanks
S199	

Appendix 6 - Borehole Data

BOREHOLE	LOCALITY	EASTING	NORTHING	MAPNO	COMPDATE
C0342		2297	494	106/1	/04/45
C0444	Maralal	2433	1215	78/3	31/07/46
C0479	Maralal	2413	1178	78/3	31/10/46
C0611	Mamar Ranch	2416	837	92/1	07/11/47
C0913		2071	547	105/2	/04/51
C1018	Ol Morani House-Turi	2182	623	91/4	28/11/49
C1237	Luoniec	2236	784	92/3	06/12/50
C1397	Luoniec	2235	785	92/3	14/12/51
C1473	Luoniec	2261	831	92/1	24/07/51
C1505	Maralal	2439	1219	78/3	09/08/51
C1553	Samburu	2455	1765		10/10/51
C1613	Nkichita	2524	2188	65	24/11/51
C1639	Nkurei	2457	2188	78/1	11/01/52
C1723	DC's office Maralal	2433	1210	78/3	23/02/52
C1785	Luoniec	2265	795	92/3	16/06/52
C1833	Luoniec	2168	847	91/2	18/09/52
C1845		2428	574	92/3	/52
C1882	Lariak	2228	670	92/3	25/11/52
C1895		2112	515	105/2	/01/53
C1896	Mamar Ranch	2457	845	92/1	20/01/53
C1921		2301	401	106/1	/03/53
C2144		1964	451	105/2	/01/54
C2318	Banyi Bun - Laikipia	2146	574	91/4	08/11/55
C2345	Naromaro	2210	710	92/3	19/02/55
C2434	Lonkewan	2264	955	92/1	23/06/55
C2727		2228	374	106/1	/11/57
C2844	Larlak Farm	2210	705	91/4	02/12/58
C2847	Sukuta Marmar	2275	1013	92/1	31/11/58
C2972	Samburu Ranch	2334	949	92/1	15/11/59
C3055	Mugie Ranch	2321	862	92/1	06/08/60
C3119	Loip (manager's house), Lanak Est.	2196	600	91/4	29/04/61
C3437	Tangulbei	1953	899	91/2	29/05/67
C3456	Baragoi Settlement	2536	1972	65	28/08/67
C3461	Losikiriumoi	1861	1213	77/3	05/10/67
C3466	Nyaunyau	1761	997	91/1	09/11/67
C3470	Chemolingot	1644	1080	90/2	10/07/67
C3506	Kabarnet	1365	549	104/1	27/07/68
C3526	Kabartonto	1426	704	90/4	16/10/68
C3609	Mission - Maralal	2451	1212	78/3	26/08/69
C3651	Lesirikan	2725	1974	65	15/12/69
C3692	Maralal Township	2442	1184	78/3	08/07/70
C3833	Sirata Oirobi	2393	1168	78/3	03/06/72
C3855	Baragoi	2560	1988	65	28/07/72
C3868	Nginyang	1669	1051	91/1	11/10/72
C3869	Baragoi (Catholic Mission)	2551	1967	65	28/09/72
C4417	Baragoi Settlement	2532	1956	65	07/11/77
C4449	Kawop	2556	2190	65	03/01/78
C4722	Kabarnet	1364	551	104/1	18/03/80
C4780	Kabarnet Town	1385	555	104/2	14/05/81
C4838	Kamnorok	1279	642	90/3	09/01/81
C5069		1990	451	105/2	30/04/82
C5072	Chemeron (College)	1560	540	104/2	
C5170	Kiboino	1308	514	104/1	21/09/82
C5333	Kolowa	1389	1354	76/4	04/08/83
C5349	Tot Bridge	1325	1343	76/3	27/07/83
C5370	Mkorwa	1343	345	104/1	30/08/83
C5487	Kinyach	1299	1035	90/1	23/11/83
C6362	Salabani	1713	611	91/3	18/07/85

BOREHOLE	LOCALITY	EASTING	NORTHING	MAPNO	COMPDATE
C6363	Kositei	1598	1026	90/2	22/07/85
C6364	Chesirimion	1687	924	91/1	27/07/85
C6365	Ngambo	1725	560	105/1	20/07/85
C6970	Kapsoo	1401	515	104/2	07/10/86
C7122	Tangulbei	1978	886	91/2	18/11/86
D1	Katangora	1934	975	91/1	
D2	Katangora	1934	974	91/1	
D3	Chemsic	1965	1023	91/2	
D4a	Orus Mission (handpump)	2004	1058	91/2	
D4b	Orus Mission (solar)	2005	1060	91/2	
D5	Naitai (N of Orus)				
D7	Kokwototo	1994	990	09900	

BOREHOLE	ALTITUDE (m)	DEPTH (m)	DIAMETER (m)	PLAINCASE (m)	LITHOLOGY
C0342	1839.0	111.00	0.000	0.00	
C0444	2060.0	121.92	0.152	39.32	Basement
C0479	1950.0	90.20	0.152	5.18	Basement
C0611	1800.0	71.62	0.152		Volcanics (lava)
C0913	1990.0	244.00	0.000	0.00	
C1018	1990.0	251.00	0.203	10.67	weathered lava
C1237	1960.0	138.68	0.152	6.71	weathered phonolite
C1397	1970.0	259.08	0.152	1.52	hard + weathered phonolite
C1473	1950.0	134.10	0.203	17.37	phonolite
C1505	1945.0	105.46	0.152	30.48	pebbly sediments
C1553	1370.0	135.63	0.152	70.10	weathered lava
C1613	1320.0	120.40	0.152	6.71	weathered basement
C1639	1600.0	102.10	0.152	13.46	basement?
C1723	1935.0	121.92	0.152	45.72	weathered schist
C1785	1950.0	178.91	0.154	12.34	weathered lava
C1833	1850.0	182.90	0.152	22.56	lava/sediments
C1845	1859.0	177.00	0.000	0.00	
C1882	1600.0	263.65	0.152	23.90	Weathered lava
C1895	1992.0	239.00	0.000	0.00	
C1896	1800.0	103.63	0.154	18.59	weathered tuff
C1921	1836.0	220.00	0.000	0.00	
C2144	2140.0	244.00	0.000	0.00	
C2318	1870.0	152.40	0.152	17.22	weathered lava
C2345	0.0	114.30	0.203	0.00	Lava
C2434	2080.0	182.90	0.152	29.87	fractured lava
C2727	1889.0	179.00	0.000	0.00	
C2844	1940.0	285.60	0.152	17.37	hard lava
C2847	2040.0	179.83	0.152	32.92	tuff
C2972	2005.0	259.00	0.152	6.86	lava
C3055	1880.0	91.44	0.154	26.52	weathered lava
C3119	1970.0	234.70	0.152	19.81	weathered phonolite
C3437	1180.0	182.90	0.304	124.36	weathered lava
C3456	1240.0	152.40	0.152	12.50	Basement?
C3461	800.0	134.10	0.152	121.00	Volcanics
C3466	870.0	76.20	0.152	41.45	Volcanics
C3470	860.0	121.92	0.152	115.82	Weathered volcanics
C3506	2000.0	152.40	0.203	92.30	Weathered volcanics
C3526	2285.0	166.10	0.203	0.00	Weathered volcanics
C3609	1920.0	71.00	0.152	28.04	Weathed basement
C3651	1500.0	64.31	0.152	24.38	
C3692	1880.0	49.37	0.152	0.00	Basement
C3833	1959.0	122.50	0.203	0.00	Weathered phonolite
C3855	1260.0	182.88	0.152	0.00	
C3868	840.0	122.22	0.203	36.58	Volcanics
C3869	1268.0	91.44	0.203	42.00	
C4417	1260.0	120.00	0.150	30.75	Weathered volcanics?
C4449	1380.0	83.00	0.150	0.00	
C4722	2000.0	155.00	0.203	0.00	Volcanics
C4780	2090.0	150.00	0.250	75.00	Weathered rock
C4838	1110.0	143.00	0.252	0.00	
C5069	2032.0	154.00	0.000	0.00	
C5072	1220.0			0.00	
C5170	1420.0	120.00		0.00	
C5333	960.0	75.00		0.00	
C5349	940.0	23.00	0.203	15.50	Sand
C5370	1400.0	55.00		0.00	
C5487	1070.0	55.00		0.00	
C6362	980.0	60.00	0.220	48.00	Uncemented silt/clay/pebbles
C6363	1050.0	107.00	0.205	84.00	Fractured phonolite

BOREHOLE	ALTITUDE (m)	DEPTH (m)	DIAMETER (m)	PLAINCASE (m)	LITHOLOGY
C6364	905.0	120.00	0.203	102.00	Fractured basalt
C6365	980.0	60.00	0.203	42.00	Clay/sand/gravel
C6970	2010.0	138.00		0.00	
C7122	1210.0	91.00		0.00	
D1	1180.0	160.00			Weathered basalt
D2	1180.0	0.00			
D3	1250.0	22.90			
D4a	1340.0	57.60			
D4b	1325.0	68.58			
D5		111.25			
D7	1235.0			0.00	

BOREHOLE	NOTES	STATUS
C0342		
C0444		
C0479	Yield considered permanent	
C0611	Yield considered permanent. Good quality water.	
C0913		
C1018	Water yellow but quality good. Drilled by Karlsson and Finne Ltd.	
C1237	Intermediate water strike at 128.0 m. Water quality good.	
C1397	Water also struck at 216.4 m and 272.79 m. Yield considered permanent. Craelius Drilling Company. Water quality good.	
C1473	Yield considered permanent. Water quality good.	
C1505	Water quality good. Yield considered permanent. Main minerals from drilling log (down to 104.85 m) are highly weathered feldspars, biotite, quartz and hornblende.	
C1553	Yield considered permanent. Water quality good.	
C1613	Yield considered permanent. Water quality good. Main minerals quartz, feldspars, biotite, hornblende, chlorite.	
C1639	Yield considered permanent. Quartz and biotite at 102.1 m.	
C1723	Yield considered permanent. Water quality good. Schist with some biotite.	
C1785	Water taste normal. Chemistry data: F=2, Cl=21, TDS=80 (units not given). PH = 8.8.	
C1833	Water quality good. Yield considered permanent. Below 152.4 m problems caused by falling rocks. Craelius Drilling Company.	
C1845		
C1882	Drilled by Craelius E.A. Drilling Co. Ltd.	
C1895		
C1896	Water quality very good. Yield considered permanent. Lava caved at 98.45 m.	
C1921		
C2144		
C2318	Water clear. Yield considered permanent. Craelius Drilling Company. Lava caved at 137.16 m.	
C2345	Drilled by Mowlem Construction Co. Ltd.	
C2434	Water quality very good. Yield considered permanent. Hole caved - broken lava - 152.4 m to 176.8 m.	
C2727		
C2844	Yield considered permanent. Water clear below 900 m. Rocks hard, drilling difficult.	
C2847	Water quality good. Yield considered permanent. No chemistry analysis at MWD.	
C2972	Water quality good. Yield consideed permanent. Borehole caved at 182.8 m.	
C3055	Water quality good. Yield considered permanent. Craelius E.A. Drilling Co. Ltd.	
C3119	Water quality good. Craelius E.A. Drilling Ltd. Additional water strike at 152.4, RWL=60.96 m. Some caving up to 152.4 m.	
C3437	Water quality good. Yield considered permanent. No chemistry seen. Intermediate water strike at	In use

BOREHOLE NO	NOTES	STATUS
	147.82 m, RWL=97.53 m.	
C3456	Slightly salty water. Yield considered Permanent. Drilled by Craelius E.A. Drilling Co. Ltd.	
C3461	Yield considered permanent. No water analysis in records. Drilled by Craelius E.A. Drilling Co. Ltd.	
C3466	Water hot, and alkaline. Yield considered permanent. Drilled by Craelius E.A. Drilling Co. Ltd.	Serviceable
C3470	Water alkaline. Drilled by Craelius E.A. Drilling Co. Ltd. Caving between 94.5 m and 121.9 m.	In use
C3506	Soft, slightly acid water.	In use
C3526	Water from upper aquifers lost at 115.824 m in lava. Borehole plugged at 91.44 m, (and abandoned?). No water analysis in records.	Abandoned
C3609	Water quality good.	
C3651	Water quality satisfactory. Yield considered permanent. No drawdown during pumping test? Drilled by Diocese of Marsabit.	
C3692	Drilling abandoned at 49.37 m - slow penetration and caving after 45.72 m.	
C3833	Water quality good. Yield considered permanent. Drilled by Craelius E.A. Drilling Co. Ltd. Much caving during drilling.	
C3855	Moderately hard water. Drilled by Craelius E.A. Drilling Co. Ltd.	
C3868	Water brackish.	In use
C3869	Water quality good. Yield considered permanent. Drilled by Diocese of Marsabit.	
C4417	Salty water. Drilled by Atlas Copco Torratest Ltd.	
C4449	Drilling abandoned, dry hole.	Abandoned
C4722	Normal water taste. Recovery test. Drilled by kenya Drilling Company.	
C4780	Water tasteless. Recovery test. Drilled by Kenya Drilling Company.	No pump
C4838	Under construction. TNO data. Water also struck at 82 m and 84 m. RWL = 4 m.	Under construction
C5069		
C5072	TNO data. No MWD data.	In use
C5170	TNO data. No data at MWD.	Under construction
C5333	TNO data. No MWD data.	Capped
C5349	TNO data + MWD data.	Capped
C5370	TNO data. No MWD data.	Capped
C5487	TNO data. No MWD data.	Capped
C6362	Saline water. Recovery test.	Capped
C6363	Recovery test. Drilled by Instapump Ltd.	'Equipped'
C6364	Recovery test.	Capped
C6365	Saline water. Recovery test.	Capped
C6970	TNO data. No MWD data.	Capped
C7122	No data at MWD.	Capped
D1	Drilled by Art Davis.	Working?
D2	Dry hole. Drilled by A. Davis.	
D3	Dry hole. Drilled by A. Davis.	
D4a	Good water. Drilled by A Davis.	Working

BOREHOLE	NOTES	STATUS
D4b	Low yield (600 gph for 2 Hr - hole pumped dry). Drilled by A Davis.	Working
D5	Exact location unknown. Drilled by A Davis.	
D7	Drilled by A Davis.	

BOREHOLE	Initial Strike (m)	Final Strike (m)	Initial Rest Level (m)	Final Rest Level (m)	Rest Water Altitude (m)
C0342	49.00	110.00	0.00	37.00	1802.0
C0444	45.72		28.34	28.34	2031.7
C0479	55.47	69.18	10.97	10.97	1939.0
C0611	54.00	67.00	18.00	18.00	1782.0
C0913	92.00	239.00	0.00	46.00	1944.0
C1018	141.70	230.12	119.17	115.20	1874.0
C1237	103.93	138.68		97.53	1862.0
C1397	205.70	254.50	130.45	122.83	1847.2
C1473	121.92		45.72	45.72	1904.3
C1505	25.60		22.56	22.56	1922.4
C1553	70.10		59.43	59.43	1310.6
C1613	68.60		65.22	65.22	1254.8
C1639	69.20		60.30	60.30	1539.7
C1723	35.05		30.17	30.17	1904.8
C1785	21.33	161.50		68.58	1881.4
C1833	108.50	173.74	109.72	109.72	1740.3
C1845	59.00	174.00	0.00	50.00	1809.0
C1882	121.92	262.13	93.88	93.88	1506.0
C1895	-1.00	76.00	0.00	63.00	1929.0
C1896	26.82	98.45	24.38	24.38	1775.6
C1921	30.00	189.00	0.00	28.00	1808.0
C2144	31.00	233.00	0.00	44.00	2096.0
C2318	109.10	137.16	70.10	60.96	1808.1
C2345	76.20	0.00	73.15	73.15	0.0
C2434	168.80		146.30	146.30	1933.7
C2727	73.00	176.00	0.00	60.00	1829.0
C2844	152.40	275.23	142.95	140.18	1799.8
C2847	109.72		70.71	70.71	1969.3
C2972	45.70	173.70	49.40	49.40	1955.6
C3055	30.48	78.63	27.43	27.43	1852.6
C3119	76.20	220.98	60.96	68.28	1901.7
C3437	106.70	171.60	84.73	92.96	1087.1
C3456	21.33	97.53	14.02	14.02	1226.0
C3461	108.20		101.50	101.50	698.5
C3466	41.10		37.80	37.80	832.2
C3470	36.58	117.35	32.00	29.87	830.1
C3506	22.55	103.32	10.36	9.60	1990.4
C3526	67.00		55.16	55.16	2229.8
C3609	37.80		35.35	35.35	1884.7
C3651	54.86		44.80	44.80	1455.2
C3692	39.62		39.62	39.62	1840.4
C3833	38.10		12.16	12.16	1946.8
C3855	21.64		10.71	10.71	1249.3
C3868	13.70	91.44	9.28	9.28	830.7
C3869	40.00		36.00	36.00	1232.0
C4417	33.00	66.00	28.60	31.30	1228.7
C4449					
C4722	30.00	132.00	30.00	15.90	1984.1
C4780	12.00	64.00	6.60	6.65	2083.4
C4838	5.00	96.00	4.00	4.00	1109.6
C5069	20.00	128.00	0.00	1.95	2030.0
C5072					
C5170	28.00	58.00	18.70	18.40	1401.6
C5333	10.00		10.00	10.00	950.0
C5349	8.00		7.00	7.00	933.0
C5370	37.00	42.00		30.00	1370.0
C5487	8.00	26.00	10.00	10.00	1060.0
C6362	48.00	50.00		12.00	968.0
C6363	93.00	97.00		10.20	1039.8

BOREHOLE	Initial Strike (m)	Final Strike (m)	Initial Rest Level (m)	Final Rest Level (m)	Rest Water Altitude (m)
C6364	105.50		85.70	85.70	819.3
C6365	42.00		22.20	22.20	957.8
C6970	106.00		34.00	34.00	1976.0
C7122	76.00		13.00	13.00	1197.0
D1	111.25	126.49		106.00	1074.0
D2					
D3					
D4a	48:15				
D4b	53.34		50.29	50.29	1269.7
D5	91.40				
D7	39.62		27.43	27.43	1207.6

BOREHOLE	Test Pump Rate (m**3/h)	Production Test Duration (hours)	Final Pumping W.L (m)	Yield (m**3/d)	Specific Capacity (m**3/d/m)
C0342	0.000			326.880	
C0444	0.377	11.0		9.360	
C0479	0.409	4.5		9.816	
C0611	13.630			327.120	
C0913	0.000			66.240	
C1018	4.670	3.0	138.40	112.080	4.830
C1237	2.270	12.0		54.480	
C1397	2.000	12.0		48.000	
C1473	2.000	46.0		48.000	
C1505	0.730	174.0		17.520	
C1553	0.680	168.0		16.320	
C1613	3.180	207.0		76.320	
C1639	4.310	148.0		103.440	
C1723	5.000	99.0		12.000	
C1785	4.310	29.5	135.33	103.680	1.550
C1833	2.270	24.0	179.80	54.480	0.777
C1845	0.000			98.160	
C1882	4.560	35.0	167.60	109.440	1.484
C1895	0.000			21.600	
C1896	11.360	6.0	73.15	272.640	5.590
C1921	0.000			151.200	
C2144	0.000			21.600	
C2318	13.200	12.0		316.800	
C2345	11.520	30.0	88.39	276.480	18.142
C2434	2.500	24.0	176.78	60.000	1.969
C2727	0.000			90.720	
C2844	6.800	4.0	158.50	163.200	8.908
C2847	2.090	24.0	174.34	50.160	0.484
C2972	1.200	12.0	176.80	28.800	0.226
C3055	14.230	12.0	28.95	341.520	224.680
C3119	5.590	5.0	164.60	134.160	1.393
C3437	9.090	24.0		218.160	
C3456	3.540	20.0	146.30	85.200	0.642
C3461	4.360	24.0	127.70	104.640	3.993
C3466	12.720	24.0		305.280	
C3470	9.090	6.0	92.35	218.160	3.492
C3506	13.600	48.0	25.90	59.760	16.100
C3526					
C3609	6.130	9.5		147.360	
C3651	5.540	24.0		132.960	
C3692	0.340				
C3833	2.230	24.0	120.55	53.520	0.494
C3855	1.800		132.47	43.200	0.355
C3868	9.850	24.0	59.93	236.640	4.300
C3869	1.360	24.0	92.00	32.640	0.582
C4417		16.0	104.30		
C4449	0.000	0.0		0.000	
C4722	17.191	13.0	29.12	422.160	31.171
C4780	13.500	21.0	23.10	324.000	19.696
C4838	11.070	24.0	7.91	265.680	67.949
C5069	0.000			236.640	
C5072					
C5170	9.917		26.85	288.000	28.167
C5333				24.000	
C5349	5.542		8.26	1056.000	105.562
C5370	3.542		46.07	48.000	5.290
C5487	6.000		12.80	480.000	51.429
C6362	0.750	24.0	29.30	18.144	1.600
C6363	45.000	24.0	23.85	1088.600	79.121

BOREHOLE	Test Pump Rate (m**3/h)	Production Test Duration (hours)	Final Pumping W.L (m)	Yield (m**3/d)	Specific Capacity (m**3/d/m)
C6364	2.510	24.0	100.00	60.480	9.220
C6365	1.500	24.0	27.83	36.240	3.030
C6970					
C7122	0.500				
D1	4.800		106.76	115.200	151.579
D2	0.000			0.000	
D3	0.000			0.000	
D4a	13.090			314.160	
D4b	32.700	2.0			
D5				4.800	
D7	32.700			784.800	

BOREHOLE	Pumping T (m**2/d)	Recovery T (m**2/d)	Average T (m**2/d)	Predicted T (m**2/d)	T Data Source
C0342					
C0444					
C0479					
C0611					
C0913					
C1018				2.3	
C1237					
C1397					
C1473					
C1505					
C1553					
C1613					
C1639					
C1723					
C1785				0.6	
C1833		0.1	0.1	0.1	RECOVERY ANALYSIS
C1845					
C1882				0.6	
C1895					
C1896				2.7	
C1921					
C2144					
C2318					
C2345				10.8	
C2434				0.8	
C2727					
C2844				4.7	
C2847				0.2	
C2972				0.1	
C3055				207.7	
C3119				0.5	
C3437					
C3456				0.2	
C3461				1.8	
C3466					
C3470	4.0		4.0	4.0	WRAP DATA
C3506	8.0		8.0	8.0	WRAP DATA
C3526					
C3609					
C3651					
C3692					
C3833		0.3	0.3	0.3	RECOVERY ANALYSIS
C3855		0.1	0.1	0.1	RECOVERY ANALYSIS
C3868		5.4	5.4	5.4	RECOVERY ANALYSIS
C3869		0.3	0.3	0.3	RECOVERY ANALYSIS
C4417					
C4449					
C4722		25.2	25.2	25.2	RECOVERY ANALYSIS
C4780		4.2	4.2	4.2	RECOVERY ANALYSIS
C4838		22.1	22.1	22.1	RECOVERY ANALYSIS
C5069					
C5072					
C5170		36.3	36.3	36.3	WRAP DATA
C5333					
C5349	110.0	81.0	95.5	95.5	WRAP DATA
C5370	1.5	3.4	2.5	2.5	WRAP DATA
C5487	9.4	13.9	11.7	11.7	WRAP DATA
C6362	1.8	1.2	1.5	1.5	WRAP TEST
C6363		76.6	76.6	76.6	RECOVERY ANALYSIS

BOREHOLE	Pumping T (m**2/d)	Recovery T (m**2/d)	Average T (m**2/d)	Predicted T (m**2/d)	T Data Source
C6364	6.6	6.5	6.6	6.6	WRAP TEST
C6365	2.1	2.6	2.4	2.4	WRAP TEST
C6970					
C7122					
D1				130.8	
D2					
D3					
D4a					
D4b					
D5					
D7					

BOREHOLE	Discharge Temperature (Centigrade)
C0342	
C0444	
C0479	
C0611	
C0913	
C1018	
C1237	
C1397	
C1473	
C1505	
C1553	
C1613	
C1639	
C1723	
C1785	
C1833	
C1845	
C1882	
C1895	
C1896	
C1921	
C2144	
C2318	
C2345	
C2434	
C2727	
C2844	
C2847	
C2972	
C3055	
C3119	
C3437	30.2 C
C3456	
C3461	
C3466	Hot Water
C3470	37.7 C
C3506	23 C
C3526	
C3609	
C3651	
C3692	
C3833	27 C
C3855	26 C
C3868	36.2 C
C3869	Normal
C4417	29 C
C4449	
C4722	22 C
C4780	
C4838	
C5069	
C5072	
C5170	
C5333	
C5349	25 C
C5370	
C5487	
C6362	45 C
C6363	36.2 C

BOREHOLENO	Discharge Temperature (Centigrade)
C6364	34 C
C6365	45 C
C6970	
C7122	
D1	36 C
D2	
D3	
D4a	28 C
D4b	28 C
D5	
D7	28 C

Appendix 7 - Sample Details

APPENDIX 7 SAMPLE DETAILS

SITE NO.	BGS HYDROCHEM REF	SITE NAME	GRID REF	SAMPLE SOURCE
45	88/2685	Lorusio	AM788 387	Spring, 81°
48a-c	88/2686-88	Kapedo	AM776 299	Springs, 0°
50	88/2689	Kapedo	AM778 293	Spring, 28°
69	88/2690	Bogoria	AM750 290	Spring, 96°
71a-c	88/2691-93	Ol Kokwe	AL75306952	Springs, 94°
131	88/2694	Kampi Ya Samaki	AL68606815	B/h, ambient
132	88/2695	Chesirimion	AL687 925	B/h, ambient
133	88/2696	Tangulbei	AL95258990	B/h, 30°
134	88/2697	Kokwo Toto	AL99409900	B/h, 28°
135	88/2698	Orus (solar)	BM00500605	B/h, 28°
136	88/2699	Orus (h.p.)	BM00400580	B/h, 28°
137	88/2700	Katangora	AL93409750	B/h, 36°
138	88/2701	Ngin.-Kap.conf.	AM76952925	Spring, 30°
139	88/2702	Churo	BL11408570	Spring, 28°
140	88/2703	Ebirisat	AL936 675	Spring, 38°
141	88/2704	Ndau	ZR324 591	River
142	88/2705	Tigeri	ZR305 510	River
143	88/2706	Molo	AL661 486	River
144	88/2707	Arabel	AL79905710	River
145	88/2708	Itwa	AL90706985	River
146	88/2709	Kabarmel	AL96608290	River
147	88/2710	Mukutan	AL808 721	River
148a-c	88/2711	Nginyang	AM67550505	River
149	88/2712	Cheptopokwo	AM67551025	River
150	88/2713	Baringo	AL71506900	Lake
151a,b	88/2714	Tilam	AL79409470	Lake, dam
152	88/2715	Ol Kokwe OK1	AL75306925	Fumarole, 90°
153	88/2716	Korosi KR10	AL791 869	Fumarole, 86°
154	88/2717	Korosi KR12	AL792 857	Fumarole, 96°
155	88/2718	Korosi KR16	AL88179362	Fumarole, 94°
156	88/2719	Korosi KR18	AL87379330	Fumarole, 96°
157	88/2720	Korosi KR19	AL87419342	Fumarole, 96°
158	88/2721	Korosi KR21	AL80059115	Fumarole, 90°
159	88/2722	Korosi KR23	AL76858935	Fumarole, 95°
160	88/2723	Korosi KR24	AL76948990	Fumarole, 83°
161	88/2724	Korosi KR32	AL76858840	Fumarole, 92°
162	88/2725,6	Korosi KR34	AL67907375	Fumarole, 92°
163	88/2727	Paka PK1a	AM868 016	Fumarole, 96°
164	88/2728	Paka PK1b	AM868 017	Fumarole, 91°
165	88/2729	Paka PK1c	AM868 021	Fumarole, 91°
166	88/2730	Paka PK4a	AM86750355	Fumarole, 95°
167	88/2731	Paka PK4b	AM86750355	Fumarole, 96°
168	88/2732	Paka PK7a	AM891 010	Fumarole, 94°
169	88/2733	Paka PK7b	AM885 014	Fumarole, 92°
170	88/2734	Paka PK7c	AM886 011	Fumarole, 92°

APPENDIX 7 Cont'd

SITE NO.	BGS HYDROCHEM REF	SITE NAME	GRID REF	SAMPLE SOURCE
171	88/2735	Paka PK7d	AM890 012	Fumarole, 92°
172	89/162	Korosi KR27	AL775 899	Fumarole, 92°
173	89/163	Paka PK3	AM864 037	Fumarole, 95°
174	89/164	Paka PK6e	AM867 026	Fumarole, 95°
175	89/165	Paka PK7e	AM890 013	Fumarole, 94°
176	89/166	Paka PK20a	AM884 034	Fumarole, 94°
177	89/167	Paka PK20b	AM885 035	Fumarole, 92°
178	89/168	Paka PK23	AM893 028	Fumarole, 92°
179	89/169	Paka PK31	AM889 032	Fumarole, 94°
180	89/170	Paka PK39	AM873 053	Fumarole, 93°
181	89/171	Paka PK42	AM876 048	Fumarole, 96°
182	89/172	Paka PK49	AM902 035	Fumarole, 94°
183	89/1869	SL 26/2	AM17831312	Spring, 45°
184	89/1870	SL 27/5	AM17951318	Spring, 45°
185	89/1871	SV 3a	AM19741776	Spring, 68°
186	89/1872	SV 3b	AM19741776	Spring, 64°
187	89/1873	Kamuge	BM19551862	Spring, 50°
188	89/1874	Kageinya	BM21401897	Spring, 68°
189	89/1875	Namarunu	BN21972194	Spring, 66°
190	89/1876	Logipi	AP22652503	Spring, 61°
191	89/1878	Nangarwa	BL20610894	Spring, amb.
192	89/1879	Amaya	BL21980894	Spring, amb.
193	89/1880	N. Samburu Gates	BN22132000	Spring, amb.
194	89/1881	Kachurkolh	BM21401268	Spring, 31°
195	89/1882	Kalnangi	AM19321445	Spring, 32°
196	89/1883	Amakat pool	AM19651545	Spring, amb.
197	89/1884	S. Nangarabat	BM20831846	Spring, 31°
198a	89/1885	Napeiton	AM17121862	Springs, 33°
198b	89/1886	Napeiton H/P	AM17151865	Well
199	89/1887	Nasaken	AM17571807	Spring, 31°
200	89/1889	Kositei project	ZS82751026	Well, amb.
201	89/1890	Kositei mission	ZS82751026	Well, amb.
202	89/1891	Kositei pumped	ZS82751026	B/h, 35°
203	89/1892	Nginyang School	AM16711051	B/h
204	89/1893	Nginyang Poly.	AM16771045	B/h, 36°
205	89/1894	Chemolingot	ZS83211089	B/h, 38°
206	89/1895	Suguta River 1	BM20631912	River
207	89/1896	Suguta River 2	AM19101600	River
208	89/1897	Suguta River 3	AM19741776	River
209	89/1898	Suguta River 4	AM19641776	River
210	89/1899	Suguta Trib.	AM19371586	River
211	89/1900	Gerau	BM21751269	River
212	89/1901	Amaya	BL211 099	River
213	89/1902	Namarangule	BM220 189	River
214	89/1903	Naliyo	BM22141787	River
215	89/1904	Turkana	AR23662666	Lake
216	89/1905	Baringo, N.	AL173 174	Lake
217	89/1906	Baringo, S.	AL174 164	Lake

APPENDIX 7 Cont'd

SITE NO.	BGS HYDROCHEM REF	SITE NAME	GRID REF	SAMPLE SOURCE
218	89/1909	Silali SL4	AM19101256	Fumarole, 97°
219	89/1910	Silali SL7	AM19251263	Fumarole, 95°
220	89/1911	Silali SL11	AM19601255	Fumarole, 94°
221	89/1912	Silali SL14	AM19101273	Fumarole, 96°
222	89/1913	Silali SL15	AM19231271	Fumarole, 97°
223	89/1914	Silali SL16/16	AM19361275	Fumarole, 96°
224	89/1915	Silali SL19	AM19181304	Fumarole, 96°
225	89/1916	Silali SL22	AM19511266	Fumarole, 92°
226	89/1917	Emuruan G. EM7	BM20411667	Fumarole, 91°
227	89/1918	Emuruan G. EM9/23	BM20341667	Fumarole, 93°
228	89/1919	Emuruan G. EM9/27	BM20341667	Fumarole, 95°
229	89/1920	Emuruan G. EM9/40	BM20341667	Fumarole, 91°
230	89/1921	Emuruan G. EM16/2a	BM20981662	Fumarole, 90°
231	89/1922	Emuruan G. EM16/2b	BM20981662	Fumarole, 90°
232	89/1923	Emuruan G. EM20a	BM20641657	Fumarole, 96°
233	89/1924	Emuruan G. EM20b	BM20641657	Fumarole, 95°
234	89/1925	Emuruan G. EM20c	BM20641657	Fumarole, 92°
235	89/1926	Barrier BR1	AP23102567	Fumarole, 96°